

Washington University in St. Louis
Washington University Open Scholarship

Engineering and Applied Science Theses &
Dissertations

McKelvey School of Engineering

Spring 5-15-2015

Statistical Nested Sensor Array Signal Processing

Keyong Han
Washington University in St. Louis

Follow this and additional works at: https://openscholarship.wustl.edu/eng_etds



Part of the [Engineering Commons](#)

Recommended Citation

Han, Keyong, "Statistical Nested Sensor Array Signal Processing" (2015). *Engineering and Applied Science Theses & Dissertations*. 95.
https://openscholarship.wustl.edu/eng_etds/95

This Dissertation is brought to you for free and open access by the McKelvey School of Engineering at Washington University Open Scholarship. It has been accepted for inclusion in Engineering and Applied Science Theses & Dissertations by an authorized administrator of Washington University Open Scholarship. For more information, please contact digital@wumail.wustl.edu.

Washington University in St. Louis
School of Engineering and Applied Science
Department of Electrical & Systems Engineering

Dissertation Examination Committee:
Arye Nehorai, Chair
I. Norman Katz
Nan Lin
Hiro Mukai
Heinz Schaettler

Statistical Nested Sensor Array Signal Processing
by
Keyong Han

A dissertation presented to the Graduate School of Arts and Sciences
of Washington University in partial fulfillment of the
requirements for the degree of

Doctor of Philosophy

May 2015
Saint Louis, Missouri

© 2015, Keyong Han

Contents

| | |
|---|-------------|
| List of Figures | v |
| List of Tables | viii |
| Acknowledgments | ix |
| Abstract | xi |
| 1 Introduction | 1 |
| 1.1 Contributions of this work | 3 |
| 1.2 Organization of the dissertation | 4 |
| 1.3 Notations | 5 |
| 2 Nested Array Processing: Review | 7 |
| 2.1 Uniform linear array | 7 |
| 2.1.1 Signal model | 7 |
| 2.1.2 Source number detection | 11 |
| 2.1.3 DOA estimation using MUSIC | 13 |
| 2.2 Nested array | 13 |
| 2.2.1 Signal model | 14 |
| 2.2.2 Difference co-array perspective | 14 |
| 2.2.3 Spatial smoothing | 17 |
| 2.3 Co-prime array | 19 |
| 2.4 Summary | 19 |
| 3 Wideband Gaussian Source Processing | 20 |
| 3.1 Introduction | 20 |
| 3.2 Signal model | 21 |
| 3.3 Array processing for wideband sources | 23 |
| 3.3.1 Spatial smoothing | 23 |
| 3.3.2 Source number detection | 24 |
| 3.3.3 Direction-of-arrival estimation | 26 |
| 3.3.4 Wideband sample covariance for array processing | 26 |
| 3.4 Numerical examples | 27 |
| 3.4.1 Source number detection | 28 |

| | | |
|----------|--|-----------|
| 3.4.2 | MUSIC spectra for DOA estimation | 28 |
| 3.4.3 | Impact of the choice of I | 29 |
| 3.5 | Summary | 30 |
| 4 | Nested Array Processing for Distributed Sources | 31 |
| 4.1 | Introduction | 31 |
| 4.2 | Signal model | 32 |
| 4.3 | Spatial smoothing | 35 |
| 4.4 | Numerical examples | 39 |
| 4.4.1 | MUSIC spectral | 40 |
| 4.4.2 | RMSE versus SNR | 41 |
| 4.4.3 | Source number detection | 42 |
| 4.5 | Summary | 42 |
| 5 | Calibrating Nested Sensor Arrays with Model Errors | 44 |
| 5.1 | Introduction | 44 |
| 5.2 | Signal model | 45 |
| 5.3 | Gain error estimation | 47 |
| 5.4 | Direction-of-arrival estimation | 49 |
| 5.4.1 | Without phase error | 49 |
| 5.4.2 | With phase error | 51 |
| 5.4.3 | Cramér-Rao bound | 54 |
| 5.5 | Nonuniform linear arrays | 55 |
| 5.5.1 | General case | 55 |
| 5.5.2 | Co-prime arrays | 56 |
| 5.6 | Numerical examples | 58 |
| 5.6.1 | Robustness to model errors | 58 |
| 5.6.2 | Estimation performance with only gain errors | 58 |
| 5.6.3 | Estimation performance with both gain and phase errors | 61 |
| 5.6.4 | Co-prime array | 63 |
| 5.6.5 | Arbitrary nonuniform linear array | 65 |
| 5.7 | Summary | 67 |
| 6 | Nested Vector-Sensor Array Processing via Tensor Modeling | 68 |
| 6.1 | Introduction | 68 |
| 6.2 | Signal model | 70 |
| 6.2.1 | Matrix-based vector-sensor array | 70 |
| 6.2.2 | Tensor-based vector-sensor array | 72 |
| 6.2.3 | Tensor-based nested vector-sensor array | 73 |
| 6.3 | Source detection and DOA estimation | 76 |
| 6.3.1 | Spatial smoothing | 76 |
| 6.3.2 | Higher-order singular value decomposition | 78 |

| | | |
|-------------------|--|------------|
| 6.3.3 | Source number detection using SORTE | 79 |
| 6.3.4 | DOA estimation using tensor-MUSIC | 79 |
| 6.4 | Numerical examples | 81 |
| 6.4.1 | MUSIC spectral for the EM case | 82 |
| 6.4.2 | Detection performance for the EM case | 86 |
| 6.4.3 | Nested acoustic vector-sensor array | 87 |
| 6.5 | Summary | 89 |
| 7 | Improved Detection and Estimation Using Jackknifing | 91 |
| 7.1 | Introduction | 91 |
| 7.2 | Source number detection | 92 |
| 7.3 | Jackknifing array processing | 93 |
| 7.3.1 | Source number detection using jackknifing | 94 |
| 7.3.2 | DOA estimation using jackknifing | 97 |
| 7.4 | Numerical examples | 98 |
| 7.4.1 | Source number detection | 100 |
| 7.4.2 | DOA estimation | 105 |
| 7.5 | Summary | 106 |
| 8 | Conclusions and Future Work | 109 |
| 8.1 | Summary and conclusions | 109 |
| 8.2 | Future directions | 110 |
| References | | 112 |
| Appendix A | Derivation of (5.40) | 120 |
| Appendix B | Derivation of (6.15) | 122 |
| Appendix C | Derivation of Equation (6.16) | 124 |
| Appendix D | Internal analysis of $\mathcal{A}_{(3)}^H \odot \mathcal{A}$ | 127 |
| Appendix E | Generating $\bar{\mathcal{A}}$ | 129 |
| Appendix F | Derivation of Equation (6.20) | 130 |
| Appendix G | Proof of Theorem 7.1 | 131 |
| Vita | | 135 |

List of Figures

| | | |
|-----|---|----|
| 2.1 | The uniform linear array | 10 |
| 2.2 | A 2-level nested array with N_1 sensors in the inner ULA, and N_2 sensors in the outer ULA. | 14 |
| 2.3 | A co-prime array with co-prime integers M_1 and M_2 , with $M_1 < M_2$ | 19 |
| 3.1 | Detection accuracy comparison of SORTES, VTRS, SORTEC, and the combined ensemble method with a 6-sensor nested array, $K = 7$, $I = 41$, $Q = 100$ | 29 |
| 3.2 | MUSIC spectrum using the spatial smoothing technique, as a function of the DOA, $N = 6$, $K = 7$, $I = 41$, $Q = 100$, SNR = 0 dB. The red dash lines are the true DOAs. | 30 |
| 4.1 | MUSIC spectrum of the proposed method for two sets of ρ , as a function of θ , using a 6-sensor nested array. | 40 |
| 4.2 | RMSE of estimates of θ versus SNR, using both the PP-MUSIC and WPP-MUSIC with a 6-sensor nested array. | 41 |
| 4.3 | Detection probability of the proposed method versus SNR, with a 6-sensor ULA, a 6-sensor nested array, and a 12-sensor ULA: $K = 2$, $T = 1000$, and $\rho = 0.9$ | 42 |
| 5.1 | MUSIC spectra for a ULA (a) with model errors and (b) without model errors, $N = 6$, $K = 3$, and SNR = 0 dB. The blue lines are the spectra, whereas the red circled stems are the true DOAs. The vertical axis is the normalized spectra, and the horizontal axis is DOAs ($\times\pi$). | 59 |
| 5.2 | MUSIC spectra for a nested array (a) with model errors and (b) without model errors, $N = 6$, $K = 3$, and SNR = 0 dB. The blue lines are the spectra, whereas the red circled stems are the true DOAs. The vertical axis is the normalized spectra, and the horizontal axis is DOAs ($\times\pi$). | 59 |
| 5.3 | MUSIC spectra of a nested array with model errors for four scenarios. $N = 6$, $K = 7$, and SNR = 0 dB. The blue lines are the spectra, whereas the red circled stems are the true DOAs. The vertical axis is the normalized spectra, and the horizontal axis is DOAs ($\times\pi$). | 60 |
| 5.4 | Spatial spectra with respect to direction angles for a nested array, using the STLS approach and without calibration, $N = 6$, $K = 8$, SNR = 0 dB. | 61 |
| 5.5 | Performance of MUSIC and sparse recovery, and CRB versus SNR, with $K = 1$, $T = 500$ | 62 |

| | | |
|------|---|----|
| 5.6 | Performance of MUSIC and sparse recovery, and CRB versus sample number, with $K = 1$, SNR = 0dB. | 62 |
| 5.7 | Performance with calibration by STLS, without calibration, and CRB versus sample number, with $K = 1$, SNR = 0dB. | 63 |
| 5.8 | MUSIC spectra of a co-prime array with model errors for four scenarios. $M_1 = 4$, $M_2 = 5$, $K = 17$, and SNR = 0 dB. The blue lines are the spectra, whereas the red circled stems are the true DOAs. The vertical axis is the normalized spectra, and the horizontal axis is DOAs ($\times\pi$). | 64 |
| 5.9 | Spatial spectra with respect to direction angles ($\times\pi$), using the STLS approach and without calibration, $M_1 = 4$, $M_2 = 5$, $K = 17$, and SNR = 0 dB. | 65 |
| 5.10 | MUSIC spectra with respect to DOAs for a nonuniform linear array with gain errors only. The blue lines are the spectra, whereas the red circled stems are the true DOAs. The vertical axis is the normalized spectra, and the horizontal axis is DOAs ($\times\pi$). | 66 |
| 5.11 | Spatial spectra with respect to DOAs ($\times\pi$) for a nonuniform linear array with both gain and phase errors. | 66 |
| 6.1 | The structure of the $N \times N_c \times K$ tensor \mathcal{A} | 73 |
| 6.2 | MUSIC spectrum using a nested EM vector-sensor array with 6 sensors, as a function of elevation angle θ , $K = 6$, $T = 1000$, SNR = 21.97dB. The horizontal axis is the elevation angle, whereas the vertical axis is the MUSIC spectrum. (a) 6-sensor nested array, (b) 6-sensor ULA. | 82 |
| 6.3 | MUSIC spectrum using a nested EM vector-sensor array with 6 sensors using the proposed algorithm, as a function of azimuth ϕ and elevation angles θ , $K = 2$, $T = 1000$, SNR = 21.97dB, and true directions $\boldsymbol{\theta} = [0.18, 0.26]$, $\boldsymbol{\phi} = [0.3, 0.5]$ | 84 |
| 6.4 | MUSIC spectrum using a ULA with 6 EM vector sensors, as a function of azimuth ϕ and elevation angles θ , $K = 2$, $T = 1000$, SNR = 21.97dB, and true directions $\boldsymbol{\theta} = [0.18, 0.26]$, $\boldsymbol{\phi} = [0.3, 0.5]$ | 84 |
| 6.5 | MUSIC spectrum using a nested EM vector-sensor array with 6 sensors using the HOEVD-based algorithm, as a function of azimuth ϕ and elevation angles θ , $K = 2$, $T = 1000$, SNR = 21.97dB, and true directions $\boldsymbol{\theta} = [0.18, 0.26]$, $\boldsymbol{\phi} = [0.3, 0.5]$ | 85 |
| 6.6 | MUSIC spectrum using a nested EM vector-sensor array with 6 sensors, as a function of polarization parameters γ and η , $K = 1$, $T = 1000$, SNR = 0dB, and true polarization parameters $\eta = \pi/6$, $\gamma = \pi/6$ | 85 |
| 6.7 | Probability of detection versus SNR using a nested array with 6 EM vector sensors and ULAs with 6 and 12 EM vector sensors, $K = 2$, $T = 1000$, and true directions $\boldsymbol{\theta} = [0.18, 0.26]$, $\boldsymbol{\phi} = [0.3, 0.7]$ | 86 |
| 6.8 | MUSIC spectrum using a nested vector-sensor array with 6 acoustic sensors, as a function of elevation angle θ , $K = 6$, $T = 1000$, SNR = 0dB. | 87 |

| | | |
|------|---|-----|
| 6.9 | MUSIC spectrum using a nested acoustic vector-sensor array with 6 sensors, as a function of azimuth ϕ and elevation angles θ , $K = 2$, $T = 1000$, SNR = 21.97dB, and true directions $\boldsymbol{\theta} = [-0.05, -0.1]$, $\boldsymbol{\phi} = [0.08, 0.15]$ | 88 |
| 6.10 | MUSIC spectrum using a ULA with 6 acoustic vector sensors, as a function of azimuth ϕ and elevation angles θ , $K = 2$, $T = 1000$, SNR = 21.97dB, and true directions $\boldsymbol{\theta} = [-0.05, -0.1]$, $\boldsymbol{\phi} = [0.08, 0.15]$ | 88 |
| 6.11 | Probability of detection versus SNR using a nested array with 6 acoustic vector sensors and ULAs with 6 and 12 acoustic vector sensors, $K = 2$, $T = 1000$, and true directions $\boldsymbol{\theta} = [0.18, 0.26]$, $\boldsymbol{\phi} = [0.3, 0.7]$ | 89 |
| 7.1 | Performance comparison of four methods with ULA using 1000 samples for $\boldsymbol{\theta}_1 = [-60^0, 0^0, 30^0]$: the blue-star line is the performance with jackknifing, and the red-circle line without jackknifing. The vertical axis represents the detection accuracy, while the horizontal axis represents the SNR. | 101 |
| 7.2 | Performance comparison of four methods with ULA using 1000 samples for $\boldsymbol{\theta}_2 = [10^0, 20^0, 35^0]$: the blue-star line is the performance with jackknifing, and the red-circle line without jackknifing. The vertical axis represents the detection accuracy, while the horizontal axis represents the SNR. | 102 |
| 7.3 | Performance comparison of SORTE and VTRS with a nested array using 2000 samples. | 103 |
| 7.4 | Detection accuracy of SORTE and VTRS for different percentage values, with a nested array at an SNR of -24 dB using $T = 1000$ snapshots. | 104 |
| 7.5 | SORTE performance comparison of a 6-sensor nested array, a 6-sensor ULA, and a 12-sensor ULA using 1000 samples for $\boldsymbol{\theta}_1 = [-60^0, 0^0]$, with and without jackknifing. | 105 |
| 7.6 | SORTE performance comparison of a 6-sensor nested array, a 6-sensor ULA, and a 12-sensor ULA using 1000 samples for $\boldsymbol{\theta}_2 = [0^0, 10^0]$, with and without jackknifing. | 106 |
| 7.7 | DOA estimation using a nested array with 6 sensors: the top figure is the estimation accuracy versus SNR, and the bottom figure shows the RMSE versus SNR. | 107 |

List of Tables

| | | |
|-----|--|-----|
| 3.1 | MSE versus different numbers of I | 29 |
| 5.1 | Weight function: $N_1 = 3, N_2 = 3$ | 52 |
| 5.2 | Weight function: $N_1 = 4, N_2 = 2$ | 53 |
| 5.3 | DOA estimation of nonuniform linear arrays with model errors | 56 |
| 5.4 | Weight function for a co-prime array: $M_1 = 4, M_2 = 5$ | 57 |
| 6.1 | Algorithm for Source Number Detection Using SORTE with a 2-level Nested Vector-sensor Array | 80 |
| 6.2 | Algorithm for DOA Estimation Using Tensor MUSIC with a 2-level Nested Vector-sensor Array | 81 |
| 7.1 | Algorithm for Source Detection Using Jackknifing | 95 |
| 7.2 | MUSIC for DOA Estimation Using Jackknifing | 98 |
| 7.3 | Computation time ($\times 10^{-4}s$) for various methods based on an 8-sensor ULA with or without jackknifing, where $T = 1000, Z = 20$ | 101 |
| 7.4 | Computation time ($\times 10^{-4}s$) for SORTE and VTRS based on a 6-sensor nested array with or without jackknifing, where $T = 1000, Z = 20$ | 103 |
| 7.5 | Best percentage values for different number of snapshots using SORTE with a nested array, at an SNR of -24 dB. | 104 |

Acknowledgments

I would like to express my sincere gratitude to my advisor, Dr. Arye Nehorai, for his guidance, support, and encouragement during my research and life at Washington University. Without them, this thesis work would not have been possible.

Sincere thanks are also extended to my dissertation defense committee members, Dr.I. Norman Katz, Dr. Nan Lin, Dr. Hiro Mukai, and Dr. Heinz Schaettler, who contributed their time, knowledge and expertise.

I further thank my friends and labmates Gongguo, Sandeep, Phani, Vanessa, Tao, Peng, Xiaoxiao, Elad, Alex, Zhao, Jichuan, Mengxue, Mianzhi, and Prateek, for their help and encouragement.

The members of my family have always been the strongest support in my life. I would like to express my gratitude to my parents and old brother, who have always been there for me throughout my good and bad times, always encouraged me and made me who I am. My deep gratitude goes to my dear wife Jingyao for her encouragement and love, whenever I needed them the most.

Finally, I would like to express my special thanks to Mr. James Ballard at the Engineering Communication Center, Washington University in St. Louis, who sat with me for hours to polish the English of my papers many times.

Keyong Han

*Washington University in Saint Louis
May 2015*

To my parents, my brother, and my wife.

ABSTRACT OF THE DISSERTATION

Statistical Nested Sensor Array Signal Processing

by

Keyong Han

Doctor of Philosophy in Electrical Engineering

Washington University in St. Louis, 2015

Professor Arye Nehorai, Chair

Source number detection and direction-of-arrival (DOA) estimation are two major applications of sensor arrays. Both applications are often confined to the use of uniform linear arrays (ULAs), which is expensive and difficult to yield wide aperture. Besides, a ULA with N scalar sensors can resolve at most $N - 1$ sources. On the other hand, a systematic approach was recently proposed to achieve $O(N^2)$ degrees of freedom (DOFs) using $O(N)$ sensors based on a nested array, which is obtained by combining two or more ULAs with successively increased spacing.

This dissertation will focus on a fundamental study of statistical signal processing of nested arrays. Five important topics are discussed, extending the existing nested-array strategies to more practical scenarios. Novel signal models and algorithms are proposed.

First, based on the linear nested array, we consider the problem for wideband Gaussian sources. To employ the nested array to the wideband case, we propose effective strategies to apply nested-array processing to each frequency component, and combine all the spectral

information of various frequencies to conduct the detection and estimation. We then consider the practical scenario with distributed sources, which considers the spreading phenomenon of sources.

Next, we investigate the self-calibration problem for perturbed nested arrays, for which existing works require certain modeling assumptions, for example, an exactly known array geometry, including the sensor gain and phase. We propose corresponding robust algorithms to estimate both the model errors and the DOAs. The partial Toeplitz structure of the covariance matrix is employed to estimate the gain errors, and the sparse total least squares is used to deal with the phase error issue.

We further propose a new class of nested vector-sensor arrays which is capable of significantly increasing the DOFs. This is not a simple extension of the nested scalar-sensor array. Both the signal model and the signal processing strategies are developed in the multidimensional sense. Based on the analytical results, we consider two main applications: electromagnetic (EM) vector sensors and acoustic vector sensors.

Last but not least, in order to make full use of the available limited valuable data, we propose a novel strategy, which is inspired by the jackknifing resampling method. Exploiting numerous iterations of subsets of the whole data set, this strategy greatly improves the results of the existing source number detection and DOA estimation methods.

Chapter 1

Introduction

Array signal processing deals with signals carried by propagating waves, including electromagnetic waves and acoustic waves [1]. Sensor arrays perform spatial sampling of impinging waves to conduct estimation and detection of the source signals. Direction-of-arrival (DOA) estimation and source number detection are two major applications of sensor arrays. However, both have been mostly confined to the case of uniform linear arrays (ULAs) [2].

Source number detection is often a prerequisite for DOA estimation. The use of a ULA for source number detection has received a considerable amount of attention in the last three decades [3]-[11]. Various methods have been proposed according to different mathematical criteria. The most commonly used techniques are based on information theoretic criteria, such as the Akaike information criterion (AIC) [6], the Kullback-Leibler information criterion (KIC) [7], and Rissanen's minimum description length (MDL) [8] principle. These methods conduct detection by combining eigenvalue decomposition, the maximum likelihood function, and penalty functions. Another eigenvalue-based method, called the second order statistic of eigenvalues (SORTE) [9], is based on a gap measure of the eigenvalues. A predicted eigen-threshold (ET) approach was proposed by Chen [10], which detects the number of sources by setting an upper bound on the eigenvalues and then implementing a hypothesis testing procedure. All the aforementioned methods are based on eigenvalues of the sample covariance matrix. Eigenvectors can also be used for the determination of sources. Jiang and Ingram [11] proposed an eigenvector-based method by exploiting the property of the variance of the rotational submatrix (VTRS).

The DOA of a source signal is basically estimated by using sensor or antenna arrays [12]. Various theories and techniques have been developed for array signal processing related

to DOA estimation [13]. Generally, DOA techniques can be broadly classified into two categories: spectral-based methods and parametric methods. The spectral-based methods can be further classified into beamforming techniques [14] and subspace-based methods, including the multiple signal classification (MUSIC) algorithm [15] and the estimation of signal parameters via the rotational invariance technique (ESPRIT) [16]. However, their performances are generally not satisfactory under high-resolution scenarios. To address these issues, references [17]-[20] introduce and develop the concept of sparse optimization in DOA estimation.

A ULA with N sensors can resolve at most $N - 1$ sources using conventional subspace-based methods such as MUSIC. A systematic approach to achieve $O(N^2)$ degrees of freedom (DOFs) using $O(N)$ sensors based on a nested array was recently proposed in [21], where DOA estimation and beamforming were studied. The nested arrays are obtained by combining two or more ULAs with successively increased spacing. Owing to the property of nonuniformity, the resulting difference co-array has significantly more DOF than the original sparse array, which makes it possible for the nested array to detect more sources than the number of sensors. Pal *et al.* [22], [23] extended the one-dimensional nested array to the two-dimensional case, assuming the sensors to be present on lattices, and providing thorough analysis about the geometrical considerations and applications. Another similar nonuniform array, called the co-prime array, was proposed and developed in [24]-[26], using $M_1 + M_2$ sensors to obtain $O(M_1 M_2)$ DOF for DOA estimation, where M_1 and M_2 are co-prime.

Both nested arrays and co-prime arrays are nonuniform linear arrays. A sparse recovery strategy based on LASSO was proposed for these nonuniform linear arrays [27]. In [28], the authors showed that compressed sensing can improve the DOFs from $O(N)$ to $O(N^2)$ by using correlation-aware techniques. The mismatch problem was further investigated in [29].

However, all these strategies were based on strict assumptions, variously including narrowband sources, point sources, fully calibrated arrays, and scalar sensors. These assumptions make the existing strategies difficult to apply to practical problems. In this dissertation, we consider more general cases of both nested arrays and co-prime arrays, and propose effective algorithms to conduct statistical signal processing accordingly.

1.1 Contributions of this work

In this dissertation, we first present the background of array signal processing and then discuss basic schemes for both nested arrays and co-prime arrays. Next we extend the strategies to more practical scenarios, including wideband sources, distributed sources, models with errors, and vector sensors. We summarize the main contributions as follows.

Wideband Gaussian source processing: For narrowband sources, theories are well established and a large body of literature exists. Owing to the narrowband property, the array model can be greatly simplified. Numerous methods exist for source number detection and DOA estimation. For wideband sources, however, the literature is less abundant. Based on the linear nested array, we consider the problem for wideband Gaussian sources. To employ the nested array for the wideband case, we propose effective strategies to apply nested-array processing to each frequency component, and combine all the spectral information of various frequencies to conduct the detection and estimation. In particular, for source detection, we propose a novel approach employing the idea of ensemble, used in machine learning and statistics.

Distributed source processing: We consider the problem of using linear nested arrays to estimate DOAs of distributed sources and to detect the source number, where we have more sources than actual physical sensors. Angular spread, caused by the multipath nature of the distributed sources, makes the commonly used point-source assumption challenging. We establish the signal model for distributed sources, using a nested array. Due to the characteristics of distributed sources, the regular spatial smoothing technique, which is used to exploit the increased DOFs provided by the co-array, no longer works. We thus propose a novel spatial smoothing approach to circumvent this problem. Based on the analytical results, we construct the corresponding DOA estimation and source number detection methods.

Calibrating nested sensor arrays with model errors: We consider the problem of DOA estimation based on the nonuniform linear nested array. Both subspace-based and sparsity-based algorithms require certain modeling assumptions, for example, exactly known array geometry, including sensor gain and phase. In practice, however, the actual sensor gain and phase are often perturbed from their nominal values, which disrupts the existing DOA estimation algorithms. Here, we investigate the self-calibration problem for perturbed nested

arrays, proposing corresponding robust algorithms to estimate both the model errors and the DOAs. The partial Toeplitz structure of the covariance matrix is employed to estimate the gain errors, and the sparse total least squares is used to deal with the phase error issue.

Nested vector-sensor array processing via tensor modeling: We propose a new class of nested vector-sensor arrays. This is not a simple extension of the nested scalar-sensor array, but a novel signal model. The structure is obtained by systematically nesting two or more uniform linear arrays with vector sensors. By using one component's information of the interspectral tensor, which is equivalent to the higher-dimensional second-order statistics of the received data, the proposed nested vector-sensor array can provide $O(N^2)$ DOFs with only N physical sensors. To utilize the increased DOFs, a novel spatial smoothing approach is proposed, which needs multilinear algebra in order to preserve the data structure and avoid reorganization. Thus, the data is stored in a higher-order tensor. Both the signal model of the nested vector-sensor array and the signal processing strategies, which include spatial smoothing, source number detection, and DOA estimation, are developed in the multidimensional sense. Based on the analytical results, we consider two main applications: electromagnetic (EM) vector sensors and acoustic vector sensors.

Improved detection and estimation using jackknifing: In order to make full use of the available limited valuable data, we propose a novel strategy, which is inspired by the jackknifing resampling method. Exploiting numerous iterations of subsets of the whole data set, this strategy greatly improves the results of the existing source number detection and DOA estimation methods. With the assumption that the subsets of the data set contain enough information, we theoretically prove that the improvement of detection or estimation performance, compared with the original performance without jackknifing, is guaranteed when the detection or estimation accuracy is greater than or equal to 50%.

1.2 Organization of the dissertation

The rest of the dissertation is organized as follows. Chapter 2 presents the background of array signal processing and then discusses basis schemes for both nested arrays and coprime arrays. In Chapter 3 we develop strategies for the wideband Gaussian source scenario. The distributed source case is discussed in Chapter 4. Next, we investigate the calibration of

nested arrays with model errors in Chapter 5. Extension from scalar sensors to vector sensors is considered in Chapter 6, and jackknifing strategies to improve detection and estimation are considered in Chapter 7. We finally summarize the dissertation in Chapter 8, and point out potential future directions.

1.3 Notations

We use lower-case italic symbols to denote scalars (a), bold lower-case italic symbols to denote vectors (\mathbf{a}), bold upper-case italic symbols to denote matrices (\mathbf{A}), and calligraphic symbols to denote tensors (\mathcal{A}). We use a_i or $(\mathbf{a})_i$ to denote the i th element of vector \mathbf{a} , \mathbf{a}_i or $(\mathbf{A})_i$ to denote the i th column of matrix \mathbf{A} , $a_{i,j}$ or $(\mathbf{A})_{i,j}$ to denote the (ij) th element of matrix \mathbf{A} , $a_{i,j,k}$ or $(\mathbf{A})_{i,j,k}$ to denote the (ijk) th element of tensor \mathcal{A} .

We use $\|\cdot\|_p$ to denote the ℓ_p norm, $\|\cdot\|_F$ to denote the Frobenius norm, superscript * to denote complex conjugate, T to denote transpose, H to denote complex conjugate transpose, and $E(\cdot)$ to denote expectation. We list some notational conventions as follows.

- $\mathcal{A}_{(2)}$: mode-2 matrix unfolding of tensor $\mathcal{A} \in \mathbb{C}^{I_1 \times I_2 \times I_3}$, with dimension $I_2 \times I_3 I_1$, defined as $(\mathcal{A}_{(2)})_{i_2, (i_1-1)I_3 + i_3} = (\mathcal{A})_{i_1 i_2 i_3}$
- $\mathcal{A}_{(3)}$: mode-3 matrix unfolding of tensor $\mathcal{A} \in \mathbb{C}^{I_1 \times I_2 \times I_3}$, with dimension $I_3 \times I_1 I_2$, defined as $(\mathcal{A}_{(3)})_{i_3, (i_2-1)I_1 + i_1} = (\mathcal{A})_{i_1 i_2 i_3}$
- $\mathbf{A} \otimes \mathbf{B}$: Kronecker product of \mathbf{A} and \mathbf{B}
- $\mathbf{a} \circledast \mathbf{b}$: convolution operation between \mathbf{a} and \mathbf{b}
- $\mathbf{A} \odot \mathbf{B}$: Khatri-Rao product of \mathbf{A} and \mathbf{B}
- $\mathbf{A} \bullet \mathbf{B}$: Hadamard product of \mathbf{A} and \mathbf{B}
- $\mathcal{A} \circ \mathcal{B}$: outer product of $\mathcal{A} \in \mathbb{C}^{I_1 \times I_2}$ and $\mathcal{B} \in \mathbb{C}^{J_1 \times J_2}$, defined as $(\mathcal{A} \circ \mathcal{B})_{i_1 i_2 j_1 j_2} = a_{i_1 i_2} b_{j_1 j_2}$
- $\mathcal{A} \times_3 \mathcal{B}$: 3-mode product of $\mathcal{A} \in \mathbb{C}^{I_1 \times I_2 \times I_3}$ and $\mathcal{B} \in \mathbb{C}^{I_3 \times J}$, defined as $(\mathcal{A} \times_3 \mathcal{B})_{i_1 i_2 j} = \sum_{i_3} a_{i_1 i_2 i_3} b_{i_3 j}$

- $\mathcal{A} \dot{\times}_3 \mathcal{B}$: mode-3 inner product of $\mathcal{A} \in \mathbb{C}^{I_1 \times I_2 \times I_3}$ and $\mathcal{B} \in \mathbb{C}^{J_1 \times J_2 \times I_3}$, defined as $(\mathcal{A} \dot{\times}_3 \mathcal{B})_{i_1 i_2 j_1 j_2} = \sum_{i_3} a_{i_1 i_2 i_3} b_{j_1 j_2 i_3}$
- $\mathcal{A} \odot \mathcal{B}$: extended Khatri-Rao product of $\mathcal{A} \in \mathbb{C}^{J \times I_3}$ and $\mathcal{B} \in \mathbb{C}^{I_1 \times I_2 \times I_3}$, with dimension $I_1 J \times I_2 \times I_3$, defined as $(\mathcal{A} \odot \mathcal{B})_{(i_1 + (j-1)I_1), i_2, i_3} = a_{j, i_3} b_{i_1, i_2, i_3}$

Chapter 2

Nested Array Processing: Review

We first present the background of uniform linear arrays, including the signal model and signal processing strategies. Then we introduce schemes for nested arrays and co-prime arrays.

2.1 Uniform linear array

In this section, we consider the problem of locating K sources by using a ULA with N passive sensors. The emitted energy from the sources may be acoustic, electromagnetic (EM), and so on, and the sensors may be EM antennas, hydrophones, seismometers, etc.

2.1.1 Signal model

The development of the array model in this section is based on the following assumptions [30]:

- The sources are situated in the far field of the array.
- Both the sources and sensors in the array are in the same plane and the sources are point emitters.
- The propagation medium is homogeneous (i.e., not dispersive) so that the waves arriving at the array can be considered to be planar.

- The sensors' transfer characteristics as well as their locations are known. Namely the array is assumed to be calibrated.

We begin by considering the case of a single source. Once we establish a model of the array for this case, the general model for the multiple case is simply obtained by the superposition principle.

Let $x(t)$ denote the value of the signal waveform as measured at some reference point, at time t . Let τ_n denote the time needed for the wave to travel from the reference point to sensor n ($n = 1, \dots, m$). Then the output of sensor n can be written as

$$\tilde{y}_n(t) = \tilde{h}_n(t) \circledast s(t - \tau_n) + \tilde{e}_n(t), \quad (2.1)$$

where $\tilde{h}_n(t)$ is the impulse response of the n th sensor, and $\tilde{e}_n(t)$ is an additive noise. $h_n(t)$ is assumed known and the signal $s(t)$ as well as the delay τ_k are unknown. The parameters characterizing the source location enter in (2.1) through $\{\tau_n\}$. The frequency form of (2.1) is

$$\tilde{Y}_n(\omega) = \tilde{H}_n(\omega)S(\omega)e^{-i\omega\tau_n} + \tilde{E}_n(\omega). \quad (2.2)$$

For a general class of physical signals, the energy spectral density of $s(t)$ is bandpass. The physical signal $s(t)$ is real-valued and hence its spectrum $|S(\omega)|^2$ should be even. Suppose the baseband signal of $s(t)$ is $x(t)$, then we have

$$S(\omega) = X(\omega - \omega_c) + X^*(-(\omega + \omega_c)). \quad (2.3)$$

Let $\bar{y}_n(t)$ denote the demodulated signal:

$$\bar{y}_n(t) = \tilde{y}_n(t)e^{-i\omega_c t}. \quad (2.4)$$

The fourier transform of $\tilde{y}_n(t)$ is given by

$$\bar{Y}_n(\omega) = \tilde{H}_n(\omega + \omega_c)[X(\omega) + X^*(-\omega - 2\omega_c)]e^{-i(\omega+\omega_c)\tau_n} + \tilde{E}_n(\omega + \omega_c). \quad (2.5)$$

When $\bar{y}_n(t)$ is passed through a lowpass filter with bandwidth matched to $X(\omega)$, the component in (2.5) centered at $\omega = -2\omega_c$ is eliminated along with all the other frequency components that fall in the stopband of the lowpass filter. Hence, we obtain

$$Y_n(\omega) = H_n(\omega + \omega_c)X(\omega)e^{-i(\omega+\omega_c)\tau_n} + E_n(\omega + \omega_c), \quad (2.6)$$

where $H_n(\omega + \omega_c)$ and $E_n(\omega + \omega_c)$ denote the parts of $\tilde{H}_n(\omega + \omega_c)$ and $\tilde{E}_n(\omega + \omega_c)$ that fall within the lowpass filter's passband.

As we have assumed, the received signals are narrowband, so that $|X(\omega)|$ decreases rapidly with increasing $|\omega|$. Thus, (2.6) reduces (in an approximate way) to the following equation:

$$Y_n(\omega) = H_n(\omega_c)X(\omega)e^{-i\omega_c\tau_n} + E_n(\omega + \omega_c), \quad (2.7)$$

The time domain counterpart of (2.7) is the following:

$$y_n(t) = H_n(\omega_c)e^{-i\omega_c\tau_n}x(t) + e_n(t). \quad (2.8)$$

We define the array transfer vector (also known as array steering vector):

$$\mathbf{a}(\theta) = [H_1(\omega_c)e^{-i\omega_c\tau_1}, \dots, H_N(\omega_c)e^{-i\omega_c\tau_N}]^T, \quad (2.9)$$

where θ denotes the source's DOA, and N is the sensor number. We rewrite (2.8) as

$$\mathbf{y}(t) = \mathbf{a}(\theta)x(t) + \mathbf{e}(t), \quad (2.10)$$

where

$$\begin{aligned} \mathbf{y}(t) &= [y_1(t), \dots, y_N(t)]^T, \\ \mathbf{e}(t) &= [e_1(t), \dots, e_N(t)]^T. \end{aligned}$$

It should be noted that θ enters in (2.9) not only through $\{\tau_n\}$ but also through $H_n(\omega_c)$.

We assume that the sensors are omnidirectional over the DOA range of interest, then $\{H_n(\omega_c)\}_{n=1}^N$ are independent of θ . Then by redefining the signal $H(\omega_c)x(t)$ as $x(t)$ and

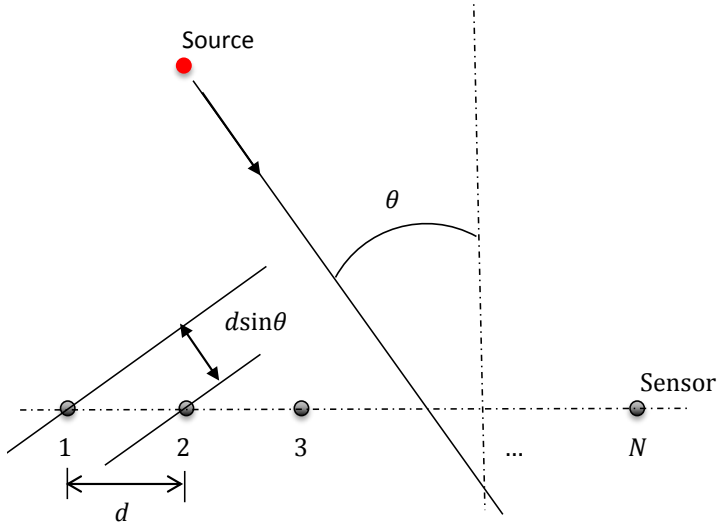


Figure 2.1: The uniform linear array

selecting the first sensor as the reference point, the expression (2.9) can be simplified to the following form:

$$\mathbf{a}(\theta) = [1, e^{-i\omega_c \tau_2}, \dots, e^{-i\omega_c \tau_N}]^T. \quad (2.11)$$

For multiple sources, a direct application of the superposition principle leads to the following model of the array:

$$\mathbf{y}(t) = \mathbf{A}\mathbf{x}(t) + \mathbf{e}(t), \quad (2.12)$$

where $\mathbf{A} = [\mathbf{a}(\theta_1), \dots, \mathbf{a}(\theta_K)]$, and $\mathbf{x}(t) = [x_1(t), \dots, x_K(t)]^T$, with K sources. Matrix \mathbf{A} is called array steering matrix or manifold matrix.

Suppose we have T snapshots. Stacking all the measurements together, we rewrite (2.12) as

$$\mathbf{Y} = \mathbf{A}\mathbf{X} + \mathbf{E}, \quad (2.13)$$

where

- $\mathbf{Y} = [\mathbf{y}(1), \mathbf{y}(2), \dots, \mathbf{y}(T)]$, an $N \times T$ matrix,
- $\mathbf{X} = [\mathbf{x}(1), \mathbf{x}(2), \dots, \mathbf{x}(T)]$, an $K \times T$ matrix, and
- $\mathbf{E} = [\mathbf{e}(1), \mathbf{e}(2), \dots, \mathbf{e}(T)]$, an $N \times T$ matrix.

Consider the array of N identical sensors uniformly spaced on a line, depicted in Fig. 2.1. With the planar wave hypothesis and the assumption that the first sensor in the array is chosen as the reference point, we get

$$\tau_n = (n - 1) \frac{d \sin(\theta)}{c}. \quad (2.14)$$

Inserting (2.14) into (2.11) gives

$$\mathbf{a}(\theta) = [1, e^{-i\omega_c d \sin(\theta)/c}, \dots, e^{-i\omega_c (N-1) d \sin(\theta)/c}]^T. \quad (2.15)$$

Let λ denote the signal wavelength: $\lambda = c/f_c$, $f_c = \omega_c/2\pi$. Define the spatial frequency: $\omega_s = 2\pi f_s$, $f_s = f_c \frac{d \sin \theta}{c} = \frac{d \sin \theta}{\lambda}$. With these notations, the transfer vector (2.15) can be rewritten as

$$\mathbf{a}(\theta) = [1, e^{-i\omega_s}, \dots, e^{-i(N-1)\omega_s}]^T. \quad (2.16)$$

The vector $\mathbf{a}(\theta)$ is uniquely defined (i.e., there is no ‘‘spatial aliasing’’) if and only if ω_s is constrained as $|\omega_s| \leq \pi$. We can further get that $d \leq \lambda/2$. We may think of the ULA as performing a uniform spatial sampling of the wavefield, the above condition simply says that the spatial sampling period d should be smaller than half of the signal wavelength.

2.1.2 Source number detection

As mentioned in Chapter 1, source number detection is a prerequisite for DOA estimation. There have been numerous strategies for source number detection. In this section, we consider only an eigenvalue-based approach: SORTE [9]. We suppose the source signals $\mathbf{x}(t)$ are all independent of each other. The noise $\mathbf{e}(t)$ is assumed to be temporally and spatially white, and uncorrelated with the sources. Based on these assumptions, the source covariance matrix is diagonal: $\mathbf{R}_x = \text{diag}\{\sigma_1^2, \dots, \sigma_K^2\}$. Then the covariance matrix of the received signal is

$$\mathbf{R}_y = \mathbf{A} \mathbf{R}_x \mathbf{A}^H + \sigma_e^2 \mathbf{I}, \quad (2.17)$$

where σ_e^2 is the noise power, and \mathbf{I} is the identity matrix.

The sample covariance matrix is a key element for source detection. Considering a uniform linear array, based on model (2.13), the sample covariance matrix is

$$\hat{\mathbf{R}}_y = \frac{1}{T} \mathbf{Y} \mathbf{Y}^H. \quad (2.18)$$

We do eigenvalue decomposition:

$$\text{EVD}(\hat{\mathbf{R}}_y) = \mathbf{U} \Lambda \mathbf{U}^H, \quad (2.19)$$

where

$$\Lambda = \text{diag}(\lambda_1, \lambda_2, \dots, \lambda_N) \quad (2.20)$$

are the eigenvalues and

$$\mathbf{U} = [\mathbf{u}_1, \mathbf{u}_2, \dots, \mathbf{u}_N] \quad (2.21)$$

is the corresponding eigenvector matrix. Suppose the eigenvalues are sorted decreasingly:

$$\lambda_1 \geq \lambda_2 \geq \dots \geq \lambda_K > \lambda_{K+1} = \dots = \lambda_N. \quad (2.22)$$

Researchers have been developing numerous detection methods based on different techniques, including eigenvalues, eigenvectors, and information theory. SORTE is an eigenvalue-based approach. A gap measure is defined:

$$\text{SORTE}(k) = \begin{cases} \frac{\text{var}(\{\nabla \lambda_i\}_{i=k+1}^{N-1})}{\text{var}(\{\nabla \lambda_i\}_{i=k}^{N-1})}, & \text{var}(\{\nabla \lambda_i\}_{i=k}^{N-1}) \neq 0 \\ +\infty & \text{var}(\{\nabla \lambda_i\}_{i=k}^{N-1}) = 0 \end{cases} \quad (2.23)$$

where $k = 1, \dots, N-2$, $\nabla \lambda_i = \lambda_i - \lambda_{i+1}$ and

$$\text{var}(\{\nabla \lambda_i\}_{i=k}^{N-1}) = \frac{1}{N-k} \sum_{i=k}^{N-1} (\nabla \lambda_i - \frac{1}{N-k} \sum_{j=k}^{N-1} \nabla \lambda_j)^2. \quad (2.24)$$

Then the source number is

$$\hat{K} = \arg \min_k \text{SORTE}(k). \quad (2.25)$$

2.1.3 DOA estimation using MUSIC

DOA estimation is based on the condition that we already know, or have already estimated the source number. MUSIC [15] is one of the earliest proposed subspace-based algorithms for DOA estimation.

Suppose we know the source number K . Then the noise subspace is formed by a matrix containing the noise eigenvectors:

$$\mathbf{U}_e = [\mathbf{u}_{K+1}, \mathbf{u}_{K+2}, \dots, \mathbf{u}_N]. \quad (2.26)$$

The cornerstone of MUSIC is the remarkable observation that the steering vectors corresponding to signal components are orthogonal to the noise subspace eigenvectors:

$$\{\mathbf{a}(\theta_1), \dots, \mathbf{a}(\theta_K)\} \perp \{\mathbf{u}_{K+1}, \mathbf{u}_{K+2}, \dots, \mathbf{u}_N\}. \quad (2.27)$$

Therefore, $\mathbf{a}(\theta)^H \mathbf{U}_e \mathbf{U}_e^H \mathbf{a}(\theta) = 0$ for $\theta = \theta_i$, corresponding to the i th incoming signal. We define the MUSIC spectrum as

$$S_{\text{MUSIC}}(\theta) = \frac{1}{\mathbf{a}(\theta)^H \mathbf{U}_e \mathbf{U}_e^H \mathbf{a}(\theta)}. \quad (2.28)$$

Then, to obtain the DOA estimates, we conduct an exhaustive search over the impinging direction space, compute the MUSIC spectrum for all direction angles, and find the K largest peaks.

2.2 Nested array

In comparison to ULAs, nested arrays [21] are nonuniform arrays. We assume there is a nonuniform linear nested array with N sensors, consisting of two concatenated ULAs. Suppose the inner ULA has N_1 sensors with intersensor spacing d_I and the outer ULA has N_2 sensors with intersensor spacing $d_O = (N_1 + 1)d_I$, as shown in Fig. 2.2.

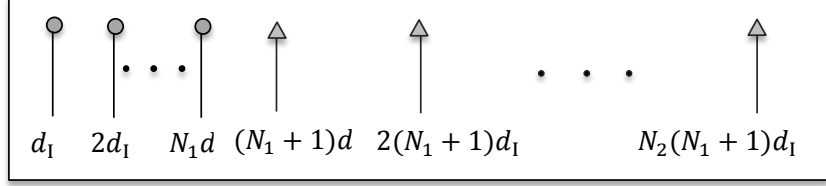


Figure 2.2: A 2-level nested array with N_1 sensors in the inner ULA, and N_2 sensors in the outer ULA.

2.2.1 Signal model

With the same assumptions as for the N -sensor ULA, we can get the similar signal model as (2.12):

$$\mathbf{y}(t) = \mathbf{A}_{\text{na}} \mathbf{x}(t) + \mathbf{e}(t), \quad (2.29)$$

where the matrix $\mathbf{A}_{\text{na}} = [\mathbf{a}_{\text{na}}(\theta_1), \mathbf{a}_{\text{na}}(\theta_2), \dots, \mathbf{a}_{\text{na}}(\theta_K)]$. The difference from \mathbf{A} in the N -sensor ULA is that the i th element of the steering vector $\mathbf{a}_{\text{na}}(\theta_k)$ is $e^{j(2\pi/\lambda)d_i \sin \theta_k}$, with d_i being the integer multiple of the basic spacing d_{I} or d_{O} . Thus, the autocorrelation matrix of the received signal for nested array is

$$\mathbf{R}_y = \mathbf{A}_{\text{na}} \mathbf{R}_x \mathbf{A}_{\text{na}}^H + \sigma_e^2 \mathbf{I}. \quad (2.30)$$

Vectorizing \mathbf{R}_y , we get

$$\mathbf{v} = (\mathbf{A}_{\text{na}}^* \odot \mathbf{A}_{\text{na}}) \mathbf{p} + \sigma_e^2 \mathbf{1}_e, \quad (2.31)$$

where $\mathbf{p} = [\sigma_1^2, \sigma_2^2, \dots, \sigma_K^2]^T$, and $\mathbf{1}_e = [\mathbf{e}_1^T, \mathbf{e}_2^T, \dots, \mathbf{e}_N^T]^T$, with \mathbf{e}_i being a vector of all zeros except a 1 at the i th position. We can view vector \mathbf{v} in (2.31) as some new longer received signals with the new manifold matrix $\mathbf{A}_{\text{na}}^* \odot \mathbf{A}_{\text{na}}$, and the new source signals \mathbf{p} .

2.2.2 Difference co-array perspective

In this section, we will revisit the signal model (2.31) from the difference co-array [31]-[33] perspective.

Definition 2.1. (*Difference co-array*): Let us consider an array of N sensors, with d_i denoting the position of the i th sensor. Define the set

$$D = \{d_i - d_j\}, \quad \forall i, j = 1, 2, \dots, N. \quad (2.32)$$

In our definition of the set D , we allow repetition of its elements. We also define the set D_u which consists of the distinct elements of the set D . Then the difference co-array of the given array is defined as the array which has sensors located at positions given in the set D_u .

To denote the number of repetition of each element in set D , we define the weight function.

Definition 2.2. Define an integer valued function $w : D_u \rightarrow \mathbb{N}^+$ such that $w(d) = \text{no. of occurrences of } d \text{ in } D$, $d \in D_u$, where \mathbb{N}^+ is the set of positive integers. The weight function $w(d)$ denotes the number of times d occurs.

It is to be noted that the cardinality of D_u for a given array gives the DOFs that can be obtained from the difference co-array associated with that array. We will show in the following that if we use the second-order statistics (2.30), then, by exploiting the DOF of the difference co-array, there is a possibility that we can get $O(N^2)$ DOFs using only $O(N)$ physical elements.

To calculate the weight function, we define a function $c(n)$, which takes a value of 1 if there is a real sensor located at nd_I , and 0 otherwise. Then the weight function $w(n)$ can be computed as the convolution:

$$w(n) = (\mathbf{c} \circledast \mathbf{c}^-)(n), \quad (2.33)$$

where $c^-(n) = c(-n)$. Since $w(n)$ is symmetric around 0, we consider only the case of $n \geq 0$.

Now, we consider the virtual steering matrix $\mathbf{A}_{\text{na}}^* \odot \mathbf{A}_{\text{na}}$ in model (2.31). The distinct rows of $\mathbf{A}_{\text{na}}^* \odot \mathbf{A}_{\text{na}}$ behave like the manifold of a longer array whose sensor locations are given by the distinct values in the set $\{d_i - d_j, 1 \leq i, j \leq N\}$ where d_i denotes the position of the i th sensor of the original array. This array is precisely the difference co-array of the original

array. Instead of (2.29), we apply source number detection and DOA estimation to the data in (2.31) and work with the difference co-array instead of the original array.

Example 2.1. Consider a 2-level nested array with 6 sensors, $N_1 = 3$, and $N_2 = 3$.

- *Sensor positions:* $\mathbf{d} = [1, 2, 3, 4, 8, 12]d$ (d is the minimal distance between sensors)
- *Indication function* $\mathbf{c} = \{c(n)|n = 1, \dots, 12\} = [1, 1, 1, 1, 0, 0, 0, 1, 0, 0, 0, 1]$
- *Difference co-array sensor set (positive values):*

$$D = \{0, 0, 0, 0, 0, 0, 1, 1, 1, 2, 2, 3, 4, 4, 5, 6, 7, 8, 9, 10, 11\}$$

The virtual ULA has elements at $D_u = \{0, 1, 2, 3, 4, 5, 6, 7, 8, 9, 10, 11\}$

- Then the weight function

$$\mathbf{w} = \{w(n)|n = 0, \dots, 11\} = [6, 3, 2, 1, 2, 1, 1, 1, 1, 1, 1],$$

$$\text{where } w(n) = (\mathbf{c} \circledast \mathbf{c}^-)(n) = \sum_{m=-\infty}^{+\infty} c(m)c^-(n-m).$$

For the two-level nested array in Fig. 2.2, we have the sensor locations:

$$\begin{aligned} S_I &= \{n_1 d_I, n_1 = 1, 2, \dots, N_1\} \text{ and} \\ S_O &= \{n_2(N_1 + 1)d_I, n_2 = 1, 2, \dots, N_2\}. \end{aligned}$$

We can observe that the difference co-array of the nested array is a filled ULA with $2N_2(N_1 + 1) - 1$ elements whose positions are:

$$S_{ca} = \{nd_I, n = -M, \dots, M, M = N_2(N_1 + 1) - 1\}. \quad (2.34)$$

Thus, for a two-level nested array, we can obtain $2N_2(N_1 + 1) - 1$ DOFs in the co-array using only $N_1 + N_2$ elements.

For a nested array, we can always get a consecutive virtual ULA without any holes. However, this is not always true for other nonuniform linear arrays, such as the co-prime array in section 2.3.

2.2.3 Spatial smoothing

In this section, we apply spatial smoothing to exploit the increased DOFs offered by the co-array. Note that, we consider a two-level nested array with N sensors, and $N/2$ sensors in each level.

We remove the repeated rows from $\mathbf{A}_{\text{na}}^* \odot \mathbf{A}_{\text{na}}$ and also sort them so that the i th row corresponds to the sensor location $(-N^2/4 - N/2 + i)d$ in the difference co-array of the 2-level nested array, giving a new vector:

$$\mathbf{z}_1 = \mathbf{A}_1 \mathbf{p} + \sigma_n^2 \bar{\mathbf{e}}, \quad (2.35)$$

where $\bar{\mathbf{e}} \in \mathbb{R}^{((N^2-2)/2+N) \times 1}$ is a vector of all zeros except a 1 at the $(N^2/4 + N/2)$ th position.

The difference co-array of this 2-level nested array has sensors located from $(-N^2/4 - N/2 + 1)d$ to $(N^2/4 + N/2 - 1)d$. We divide this co-array into $N^2/4 + N/2$ overlapping subarrays, each with $N^2/4 + N/2$ elements, where the i th subarray has sensors located at

$$\left\{ (-i + 1 + n)d, \quad n = 0, 1, \dots, \frac{N^2}{4} + \frac{N}{2} - 1 \right\}. \quad (2.36)$$

The i th subarray corresponds to the $(N^2/4 + N/2 - i + 1)$ th to $(N^2 - 2)/2 + N - i + 1$ th rows of \mathbf{z}_1 , denoted as

$$\mathbf{z}_{1i} = \mathbf{A}_{1i} \mathbf{p} + \sigma_n^2 \bar{\mathbf{e}}_i. \quad (2.37)$$

We can check that

$$\mathbf{z}_{1i} = \mathbf{A}_{11} \Phi^{i-1} \mathbf{p} + \sigma_n^2 \bar{\mathbf{e}}_i, \quad (2.38)$$

where

$$\Phi = \begin{pmatrix} e^{-j\pi \sin \theta_1} & & & \\ & e^{-j\pi \sin \theta_2} & & \\ & & \ddots & \\ & & & e^{-j\pi \sin \theta_K} \end{pmatrix}. \quad (2.39)$$

Define

$$\mathbf{R}_i \triangleq \mathbf{z}_{1i} \mathbf{z}_{1i}^H. \quad (2.40)$$

Taking the average of \mathbf{R}_i over all i , we get

$$\mathbf{R}_{ss} \triangleq \frac{1}{\left(\frac{N^2}{4} + \frac{N}{2}\right)} \sum_{i=1}^{N^2/4+N/2} \mathbf{R}_i. \quad (2.41)$$

We call the matrix \mathbf{R}_{ss} as the spatially smoothed matrix and it enables us to perform DOA estimation of $O(N^2)$ sources with N sensors. We can further show that

$$\mathbf{R}_{ss} = \hat{\mathbf{R}}^2, \quad (2.42)$$

where

$$\hat{\mathbf{R}} = \frac{1}{\left(\frac{N^2}{4} + \frac{N}{2}\right)} (\mathbf{A}_{11} \boldsymbol{\Lambda} \mathbf{A}_{11}^H + \sigma_n^2 \mathbf{I}), \quad (2.43)$$

$$\mathbf{A}_{11}^H = \begin{pmatrix} 1 & \nu_1 & \dots & \nu_1^{(N^2/4+N/2-1)} \\ 1 & \nu_2 & \dots & \nu_2^{(N^2/4+N/2-1)} \\ \vdots & \vdots & \vdots & \vdots \\ 1 & \nu_K & \dots & \nu_K^{(N^2/4+N/2-1)} \end{pmatrix} \quad (2.44)$$

$$(2.45)$$

with $\nu_i^n = e^{-j\frac{2\pi}{\lambda}nd\sin(\theta_i)}$, and

$$\boldsymbol{\Lambda} = \begin{pmatrix} \sigma_1^2 & & & \\ & \sigma_2^2 & & \\ & & \ddots & \\ & & & \sigma_K^2 \end{pmatrix}. \quad (2.46)$$

The matrix $\hat{\mathbf{R}}$ has the same form as the conventional covariance matrix used in subspace based DOA estimation technique when applied on a ULA with $N^2/4 + N/2$ sensors whose array manifold is represented by \mathbf{A}_{11} .

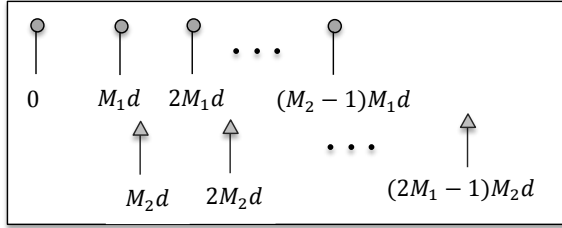


Figure 2.3: A co-prime array with co-prime integers M_1 and M_2 , with $M_1 < M_2$.

2.3 Co-prime array

The co-prime array [24] is another class of non-uniform linear array. Similar to the nested array, it increases DOFs by employing the idea of difference co-array. Since the strategies are the same, we introduce only the structures.

Consider a linear array with $2M_1 + M_2 - 1$ sensors, where M_1 and M_2 are co-prime integers, and $M_1 < M_2$. These sensors are located at

$$\{m_1 M_2 d, m_2 M_1 d, 0 \leq m_1 \leq 2M_1 - 1, 0 \leq m_2 \leq M_2 - 1\}. \quad (2.47)$$

Fig. 2.3 illustrates the co-prime array. Note that the two sets of sensors are linearly placed. It has been shown that we can obtain a virtual hole-free ULA with sensors located at

$$\{nd, -M_1 M_2 \leq n \leq M_1 M_2\}. \quad (2.48)$$

2.4 Summary

In this chapter we presented the background of linear sensor array processing, including the signal model, source number detection, and DOA estimation. Then we briefly introduced the basic strategies of nested arrays and co-prime arrays. By employing the concept of the difference co-array, they increase the DOFs from $O(N)$ to $O(N^2)$. To employ the increased DOFs, spatial smoothing is used to build up the ranks. Finally, we obtained an equivalent virtual non-hole ULA, which is used to conduct signal processing.

Chapter 3

Wideband Gaussian Source Processing

In this chapter, we consider nested array processing for wideband Gaussian sources.¹

3.1 Introduction

For narrowband sources, theories are well established and a large body of literature exists [13]. Owing to the narrowband property, the array model can be greatly simplified. For wideband sources, however, the literature is less abundant. Wax *et al.* are among the earlier researchers in this field [34], decomposing the incoherent wideband signal into many narrowband signals, and using discrete Fourier transform (DFT) along the temporal domain. Wang and Kaveh [35] considered the case of coherent wideband sources. In this chapter, we consider uncorrelated sources.

Most existing strategies are confined to the ULA case. Here, we consider the nested array as presented in Section 2.2. Note that the application of nested microphone array is not new in the processing of acoustic and speech signals [36]. However, they usually do not examine the analytical aspects of the nested array.

¹This chapter is based on K. Han and A. Nehorai, “Wideband Gaussian source processing using a linear nested array,” IEEE Signal Processing Letters, Vol. 20, pp. 1110-1113, Nov. 2013. © IEEE 2013.

In this chapter, we propose two algorithms for wideband source number detection based on SORTE. Further we propose a combined method, employing the idea of ensemble [37], used in machine learning and statistics. In addition, we construct a combined MUSIC spectrum to exploit all the spectral information from different frequency analyses. Simulations are provided to demonstrate the advantages of our strategies.

3.2 Signal model

We assume there is a 2-level nested array with N sensors, as shown in Fig. 2.2. We assume K wideband sources are in the surveillance region, impinging on this linear array from directions $\{\theta_k, k = 1, \dots, K\}$. Suppose that the incident wideband signals have a common bandwidth B with center frequency f_c .

Let $s_k(t)$ denote the k th baseband signal. Then the observed bandpass signal $\bar{x}_k(t)$ at a reference point can be written as

$$\bar{x}_k(t) = s_k(t)e^{j2\pi f_c t}. \quad (3.1)$$

If we observe the signal over the time interval $[t_1, t_2]$, then the baseband signal can be written as [38]

$$s_k(t) = \sum_{i=1}^I S_k(f_i) e^{j2\pi f_i t}, \quad t_1 \leq t \leq t_2, \quad (3.2)$$

where $S_k(f_i)$ are the Fourier coefficients

$$S_k(f_i) = \frac{1}{t_2 - t_1} \int_{t_1}^{t_2} s_k(t) e^{-j2\pi f_i t} dt, \quad (3.3)$$

with $f_i = f_l + (i-1)B/(I-1)$, $i = 1, \dots, I$. f_l denotes the lowest frequency included in the bandwidth B , and I is the number of frequency components. We choose f_l and I so that the frequencies are symmetric about 0 Hz. By considering the propagation delay $\tau_{k,n}$ of the k th signal at the n th sensor, the modulated bandpass signal at the reference point can be

presented as

$$\bar{x}_k(t + \tau_{k,n}) = \sum_{i=1}^I S_k(f_i) e^{j2\pi(f_c+f_l)(t+\tau_{k,n})}, \quad (3.4)$$

where $\tau_{k,n} = nd_I \sin(\theta_k)/C$, $k = 1, \dots, K$, and $n = 1, \dots, N$, with C being the propagation speed.

The demodulated signal can be expressed as

$$x_k(t, \tau_{k,n}) = \bar{x}_k(t + \tau_{k,n}) e^{-j2\pi f_c t}. \quad (3.5)$$

Stacking $\{x_k(t, \tau_{k,n})\}_{n=1}^N$ according to sensor number, we get the $N \times 1$ vector $\mathbf{x}_k(t)$. Let $\mathbf{a}(\theta_k, f_c + f_i)$ denote the $N \times 1$ steering vector of the k th source and the i th frequency component:

$$\mathbf{a}(\theta_k, f_i) = [e^{j2\pi(f_c+f_i)\tau_{k,1}}, \dots, e^{j2\pi(f_c+f_i)\tau_{k,N}}]^T. \quad (3.6)$$

Then the received data vector has the form

$$\mathbf{x}(t) = \sum_{k=1}^K \mathbf{x}_k(t) = \sum_{i=1}^I [\mathbf{A}(\boldsymbol{\theta}, f_i) \mathbf{S}(f_i) + \mathbf{E}(f_i)] e^{j2\pi f_i t}, \quad (3.7)$$

where $\mathbf{A}(\boldsymbol{\theta}, f_i) = [\mathbf{a}(\theta_1, f_i), \dots, \mathbf{a}(\theta_K, f_i)]$, $\mathbf{S}(f_i) = [S_1(f_i), \dots, S_K(f_i)]^T$ is the $K \times 1$ signal vector, and $\mathbf{E}(f_i) = [E_1(f_i), \dots, E_N(f_i)]^T$ is the $N \times 1$ noise Fourier coefficient vector. Define

$$\mathbf{y}(i) \triangleq \mathbf{A}(\boldsymbol{\theta}, f_i) \mathbf{S}(f_i) + \mathbf{E}(f_i), \quad i = 1, \dots, I. \quad (3.8)$$

Then $\{\mathbf{y}(i)\}$ are by definition the $N \times 1$ Fourier coefficient vectors of $\mathbf{x}(t)$.

We assume the source signals follow Gaussian distributions, $S_k(f_i) \sim \mathcal{N}(0, \sigma_{k,i}^2)$, and that they are all independent of each other. The noise $\mathbf{E}(f_i)$ is assumed to be white Gaussian and uncorrelated with sources. Based on our assumption, the source autocorrelation matrix $\mathbf{R}_{\mathbf{s}_i}$ is diagonal: $\mathbf{R}_{\mathbf{s}_i} = \text{diag}(\sigma_{1,i}^2, \sigma_{2,i}^2, \dots, \sigma_{K,i}^2)$. We use \mathbf{A}_i to represent $\mathbf{A}(\boldsymbol{\theta}, f_i)$ for brevity. Then the autocorrelation matrix of $\{\mathbf{y}(i)\}$ is $\mathbf{R}_{\mathbf{y}_i} = \mathbf{A}_i \mathbf{R}_{\mathbf{s}_i} \mathbf{A}_i^H + \sigma_E^2 \mathbf{I}$, where σ_E^2 is the noise power, and \mathbf{I} is the identity matrix. Vectorizing $\mathbf{R}_{\mathbf{y}_i}$ [21], similar to (2.31), we get

$$\mathbf{v}_i = (\mathbf{A}_i^* \odot \mathbf{A}_i) \mathbf{p}_i + \sigma_E^2 \mathbf{1}_e, \quad (3.9)$$

where $\mathbf{p}_i = [\sigma_{1,i}^2, \dots, \sigma_{K,i}^2]^T$, and $\mathbf{1}_e = [\mathbf{e}_1^T, \mathbf{e}_2^T, \dots, \mathbf{e}_N^T]^T$, with \mathbf{e}_i being a vector of all zeros except a 1 at the i th position. We can view vector \mathbf{v}_i in (3.9) as some new longer received signals with the new manifold matrix $\mathbf{A}_i^* \odot \mathbf{A}_i$, and the new source signals \mathbf{p}_i .

3.3 Array processing for wideband sources

We will use the nested array mentioned above to conduct source number detection and DOA estimation. First, we will present the corresponding spatial smoothing for wideband sources, which is a variation of that in Section 2.2.3. Then we propose two algorithms based on SORTE, and further propose a novel strategy employing the idea of ensemble for source number detection. Third, we will provide a novel strategy for wideband source estimation using MUSIC.

3.3.1 Spatial smoothing

To exploit the increased DOFs provided by the co-array, we need to apply spatial smoothing. We remove the repeated rows from $\mathbf{A}_i^* \odot \mathbf{A}_i$ and also sort them so that the j th row corresponds to the sensor location $(-N^2/4 - N/2 + j)d_I$ in the difference co-array of the 2-level nested array, giving a new vector: $\bar{\mathbf{v}}_i = \bar{\mathbf{A}}_i \mathbf{p}_i + \sigma_E^2 \bar{\mathbf{e}}$, where $\bar{\mathbf{e}} \in \mathbb{R}^{((N^2-2)/2+N) \times 1}$ is a vector of all zeros except a 1 at the center position. The difference co-array of this 2-level nested array has sensors located at

$$(-N^2/4 - N/2 + 1)d_I, \dots, -d_I, 0, d_I, \dots, (N^2/4 + N/2 - 1)d_I. \quad (3.10)$$

We now divide these $N^2/2 + N - 1$ sensors into $N^2/4 + N/2$ overlapping subarrays, where the l th subarray has sensors located at $\{(-l + 1 + n)d_I, n = 0, 1, \dots, \frac{N^2}{4} + \frac{N}{2} - 1\}$. The l th subarray corresponds to the $(N^2/4 + N/2 - l + 1)$ th to $(N^2 + N - l)$ th rows of $\bar{\mathbf{v}}_i$, denoted as $\bar{\mathbf{v}}_i^l = \bar{\mathbf{A}}_i^l \mathbf{p}_i + \sigma_E^2 \mathbf{e}_l$. We can check that $\bar{\mathbf{v}}_i^l = \bar{\mathbf{A}}_i^1 \Phi^{l-1} \mathbf{p}_i + \sigma_E^2 \mathbf{e}_l$, where Φ is same as in (2.39). Viewing $\bar{\mathbf{v}}_i^l$ as a newly received vector, we get the equivalent covariance matrix $\mathbf{R}_i^l = \bar{\mathbf{v}}_i^l \bar{\mathbf{v}}_i^{lT}$.

Taking the average of \mathbf{R}_i^l yields

$$\mathbf{R}_i^{\text{avg}} = \frac{1}{\left(\frac{N^2}{4} + \frac{N}{2}\right)} \sum_{l=1}^{N^2/4+N/2} \mathbf{R}_i^l. \quad (3.11)$$

The spatially smoothed matrix $\mathbf{R}_i^{\text{avg}}$ enables us to identify up to $N^2/4 + N/2 - 1$ sources with N sensors. This is same as discussed in Section 2.2.3.

3.3.2 Source number detection

As mentioned in the introduction, we consider a narrowband decomposition for the wideband case. Considering the spatial smoothing matrix $\mathbf{R}_i^{\text{avg}}$ for the i th frequency, f_i , we do eigenvalue decomposition: $\text{EVD}(\mathbf{R}_i^{\text{avg}}) = \mathbf{U}_i \boldsymbol{\Lambda}_i \mathbf{U}_i^T$, where $\boldsymbol{\Lambda}_i = \text{diag}(\lambda_i^1, \lambda_i^2, \dots, \lambda_i^{N^2/4+N/2})$ are the eigenvalues, and $\mathbf{U}_i = [\mathbf{u}_i^1, \mathbf{u}_i^2, \dots, \mathbf{u}_i^{N^2/4+N/2}]$ is the corresponding eigenvector matrix. We suppose the eigenvalues are sorted decreasingly:

$$\lambda_i^1 \geq \lambda_i^2 \geq \dots \geq \lambda_i^K > \lambda_i^{K+1} = \dots = \lambda_i^{N^2/4+N/2}. \quad (3.12)$$

We denote $\tilde{N} \triangleq N^2/4 + N/2$. According to the SORTE method, as presented in Section 2.1.2, we define the corresponding gap with respect to the i th frequency:

$$\text{SORTE}_i(k) = \begin{cases} \frac{\text{var}(\{\nabla \lambda_i^j\}_{j=k+1}^{\tilde{N}-1})}{\text{var}(\{\nabla \lambda_i^j\}_{j=k}^{\tilde{N}-1})}, & \text{var}(\{\nabla \lambda_i^j\}_{j=k}^{\tilde{N}-1}) \neq 0 \\ +\infty & \text{var}(\{\nabla \lambda_i^j\}_{j=k}^{\tilde{N}-1}) = 0 \end{cases}, \quad (3.13)$$

where $k = 1, \dots, \tilde{N} - 2$, $\nabla \lambda_i^j = \lambda_i^j - \lambda_i^{j+1}$, and

$$\text{var}(\{\nabla \lambda_i^j\}_{j=k}^{\tilde{N}-1}) = \frac{1}{\tilde{N} - k} \sum_{j=k}^{\tilde{N}-1} (\nabla \lambda_i^j - \frac{1}{\tilde{N} - k} \sum_{j=k}^{\tilde{N}-1} \nabla \lambda_i^j)^2. \quad (3.14)$$

Then the source number is $K_i = \arg \min_k \text{SORTE}_i(k)$.

Note that the number $K_i \in \{1, 2, \dots, \tilde{N} - 1\}$ is based on the information of frequency f_i . To exploit all the frequency information, we propose the following two algorithms.

- SORTEC

Based on the detected source number K_i for each frequency, we count the occurrence of distinct numbers N_k , $k = 1, \dots, \tilde{N} - 1$. Then we find the source number:

$$K = \arg \max_k N_k. \quad (3.15)$$

- SORTES

Based on the gaps for each frequency, we take the summation first rather than conduct detection. Then we decide the source number using the summation:

$$K = \arg \min_k \sum_i^I \text{SORTE}_i(k). \quad (3.16)$$

Existing literature investigates source number detection by using various methods singly. The idea of ensemble, used in machine learning and statistics, inspires us to conduct source detection by combining multiple methods. Typically, more computation is required to evaluate the ensemble's performance than for a single method.

- Ensemble

Suppose we have M detection methods in total: $\mathcal{D}_1, \mathcal{D}_2, \dots, \mathcal{D}_M$, each with detection accuracy p . Then we obtain the detected source number K_1, K_2, \dots, K_M based on each method. Next, we count the occurrence of each distinct number, denoted as N_k , $k = 1, \dots, \tilde{N} - 1$, with summation M . The final source number is chosen as the one that occurs most frequently:

$$K = \arg \max_k N_k. \quad (3.17)$$

When the detection accuracy p for each method is greater than or equal to 50%, the improvement of the ensemble is guaranteed [39].

3.3.3 Direction-of-arrival estimation

For this section, we assume the source number has been correctly detected, and we use the MUSIC strategy as discussed in Section 2.1.3. We write the noise subspace as

$$\mathbf{U}_i^E = [\mathbf{u}_i^{K+1}, \mathbf{u}_i^{K+2}, \dots, \mathbf{u}_i^{\tilde{N}}], \quad (3.18)$$

which consists of the last $\tilde{N} - K$ eigenvectors corresponding to the smallest $\tilde{N} - K$ eigenvalues. The estimated DOA can be found through an exhaustive search over all the direction space of the MUSIC spectrum:

$$M_i(\theta) = \frac{1}{(\mathbf{a}_i^\theta)^H \mathbf{U}_i^E (\mathbf{U}_i^E)^H \mathbf{a}_i^\theta}, \quad (3.19)$$

where $\mathbf{a}_i^\theta = [1, a_i^\theta, \dots, (\mathbf{a}_i^\theta)^{\tilde{N}-1}]$, with $a_i^\theta = e^{-j2\pi(f_c+f_i)d_I \sin(\theta)/c}$. Combining the resulting measurements for all the different frequencies, we consider the new combined MUSIC spectrum:

$$M(\theta) = \frac{1}{\frac{1}{I} \sum_{i=1}^I (\mathbf{a}_i^\theta)^T \mathbf{U}_i^E (\mathbf{U}_i^E)^T \mathbf{a}_i^\theta}. \quad (3.20)$$

Then the estimated DOAs correspond to the K largest values of the spectrum $M(\theta)$.

3.3.4 Wideband sample covariance for array processing

According to Section 3.2, our observed data is $\mathbf{x}(t)$ in (3.7), and our problem of interest is to detect the source number and estimate the DOAs from the Fourier coefficients $\mathbf{y}(i)$, $i = 1, \dots, I$ in (3.8). Suppose our total observation time is T_0 , and we divide it into Q segments, with each segment $t_0 = t_2 - t_1$. We assume that there are I samples within each segment. Therefore, we have $I \cdot Q$ samples:

$$\hat{\mathbf{X}} = [\hat{\mathbf{x}}(1), \hat{\mathbf{x}}(2), \dots, \hat{\mathbf{x}}(I \cdot Q)]_{N \times (I \cdot Q)}. \quad (3.21)$$

We will investigate the impact of I and Q on the performance through numerical examples. For each segment q , we employ DFT to get the $N \times I$ corresponding frequency coefficient matrix:

$$\hat{\mathbf{Y}}_q = [\hat{\mathbf{y}}_q(1), \dots, \hat{\mathbf{y}}_q(i), \dots, \hat{\mathbf{y}}_q(I)], \quad q = 1, \dots, Q. \quad (3.22)$$

Considering all the segments, we can get the $N \times Q$ coefficient matrix for each frequency index i :

$$\hat{\mathbf{Y}}^i = [\hat{\mathbf{y}}_1(i), \dots, \hat{\mathbf{y}}_q(i), \dots, \hat{\mathbf{y}}_Q(i)], \quad i = 1, \dots, I. \quad (3.23)$$

The resulting sample covariance matrix for frequency index i can be written as

$$\hat{\mathbf{R}}_{\mathbf{y}_i} = \frac{1}{Q} \hat{\mathbf{Y}}^i (\hat{\mathbf{Y}}^i)^H. \quad (3.24)$$

Following the spatial smoothing technique in subsection A, we can get the sample spatial smoothing matrix $\hat{\mathbf{R}}_i^{\text{avg}}$. Accordingly, we can conduct source detection and DOA estimation based on this sample covariance matrix.

3.4 Numerical examples

In this section, we use numerical examples to show the effectiveness of our proposed strategies for wideband source detection and DOA estimation with a linear nested array.

In the examples, we consider a 2-level nested array with $N = 6$ sensors, with both the inner and outer ULAs having three sensors. The interspacing d_I is chosen as half of the shortest wavelength of the wideband signals, which ensures that there is no spatial aliasing. d_O is equal to $4d_I$. Suppose there are $K = 7$ wideband sources impinging from directions $\boldsymbol{\theta} = [-60^\circ, -35^\circ, -15^\circ, 5^\circ, 30^\circ, 45^\circ, 60^\circ]$. It is impossible for us to use a 6-sensor ULA to detect seven sources. However, the spatial smoothing matrix $\mathbf{R}_i^{\text{avg}}$ in (3.11) helps a nested array obtain this goal. Suppose the wideband sources have the same center frequency, $f_c = 100$ Hz, and the same bandwidth, $B = 40$ Hz. Further suppose the sources follow zero mean Gaussian random processes with equal power, independent of each other. We choose equal power for simplicity here, but our method works also for different powers. The noises are white Gaussian, and uncorrelated with the sources.

3.4.1 Source number detection

The array output is decomposed into $I = 41$ narrowband components via DFT. The selection of proper value of I will be explained next. We choose the segment number to be $Q = 100$. Therefore we use a total of $I \times Q = 4100$ samples.

To employ the ensemble strategy, we considered three methods: SORTEC, SORTES, and one that utilizes the variance of transformed rotational submatrix (VTRS) [11]. The VTRS method as used here applies a strategy similar to SORTEC. Fig. 3.1 shows the results of the aforementioned three methods and the combined ensemble method. It describes the detection accuracy with respect to the signal-to-noise ratio (SNR), defined below:

$$\text{SNR} = 10\log_{10}\frac{\mathbb{E}[x^2]}{\mathbb{E}[e^2]}. \quad (3.25)$$

The detection accuracy is defined as F_K/F , where F is the trial number, and F_K is the number of times that the true source number K is detected. We can see that the ensemble method outperforms all of the three separate methods, and achieves great improvement. Note that the detection accuracy is almost always above 0.5 for different SNRs, which guarantees the improvement of the ensemble, as discussed in the previous section. SORTES performs much better than SORTEC, which is reasonable because SORTES determines the source number based on a combined gap of different frequencies.

We also investigated the performance with respect to various numbers of snapshots: with $I = 41$, the effectiveness of the ensemble can be guaranteed with over 2500 snapshots.

3.4.2 MUSIC spectra for DOA estimation

Fig. 3.2 shows the representative MUSIC spectra using the spatial smoothing technique, with respect to various angles at a SNR of 0 dB. We can see that the proposed method can resolve the seven wideband sources sufficiently well.

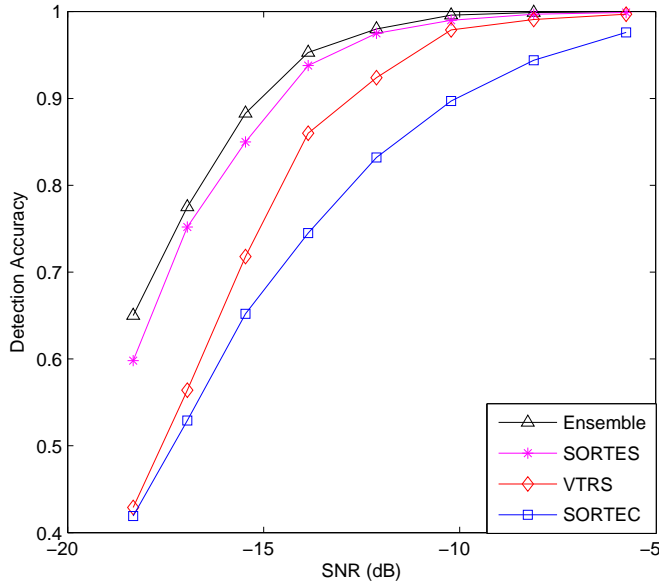


Figure 3.1: Detection accuracy comparison of SORTES, VTRS, SORTEC, and the combined ensemble method with a 6-sensor nested array, $K = 7$, $I = 41$, $Q = 100$.

3.4.3 Impact of the choice of I

To investigate the impact on the estimation performance of the choice of I , we fixed the sample number at 4000. For different numbers of I , Table 3.1 shows the MSE results for estimation of a wideband source with $\theta = 30^0$. We can see that a moderate I guarantees good performance. When I is too small, it will lose information on most frequencies. On the other hand, when I is too large, the fusion process will perform badly.

Table 3.1: MSE versus different numbers of I

| I | 2 | 4 | 8 | 10 | 20 |
|-----|-------|-------|------|-------|-------|
| MSE | 1.253 | 0.198 | 0.1 | 0.099 | 0.087 |
| I | 40 | 50 | 100 | 160 | 200 |
| MSE | 0.093 | 0.097 | 0.12 | 0.129 | 0.147 |

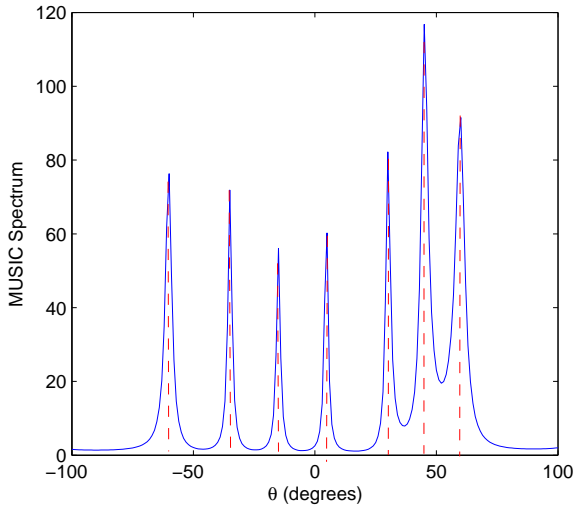


Figure 3.2: MUSIC spectrum using the spatial smoothing technique, as a function of the DOA, $N = 6$, $K = 7$, $I = 41$, $Q = 100$, SNR = 0 dB. The red dash lines are the true DOAs.

3.5 Summary

In this chapter [40], we proposed novel strategies for wideband source detection and DOA estimation with a nested array. This approach can estimate a number of wideband sources that is greater than the number of sensors, and obtain good estimation performance. Simulations demonstrate the effectiveness of our strategy. One thing to note is that the assumptions of this strategy are relatively restrictive, and the strategy is not suitable for correlated sources.

Chapter 4

Nested Array Processing for Distributed Sources

In the previous chapter, we considered the scenario of wideband sources. In this chapter, we consider the more practical problem of distributed sources.²

4.1 Introduction

Most existing results about antenna arrays are based on signal and noise models which assume that the signals are propagated from point sources. However, in practice, signal sources may often be transmitted by reflection, causing angular spread. Besides, the reflective medium may often be dispersive, and thus making the point-source assumption questionable. In this chapter, we will concentrate on distributed sources.

Distributed sources have received a considerable amount of attention in the last two decades [41]-[46]. Distributed source modeling and DOA estimation were explored in [41] and [42], where MUSIC-based method was used to estimate the DOAs. One robust approach using array geometry has been developed for DOA estimation using ESPRIT [45]. In [44], an estimation strategy based on ML was proposed. One computationally attractive method based on covariance matching was investigated in [43]. Recently, Lee, Joung, and Kim [46] proposed a method based on the conventional beamforming approach.

²This chapter is based on K. Han and A. Nehorai, “Nested array processing for distributed sources,” IEEE Signal Processing Letters, Vol. 21, pp. 1111-1114, Sep. 2014. © IEEE 2014.

Most existing strategies, for both point and distributed sources, are confined to the case of ULA [2]. In this chapter, we establish the signal model for distributed sources using a nested array. To exploit the increased DOFs provided by the difference co-array, we propose a novel spatial smoothing approach with *a priori* knowledge of the angular spreading parameters. Based on the analytical results, we will construct corresponding source number detection and DOA estimation methods.

4.2 Signal model

Again, we consider the linear nested array in Fig. 2.2. Further suppose the sensor positions are $\mathbf{r} \triangleq \mathbf{z}d_{\text{I}}$, where

$$\begin{aligned}\mathbf{z} &\triangleq \{z_i, i = 1, \dots, N\} \\ &= [1, 2, \dots, N_1, N_1 + 1, 2(N_1 + 1), \dots, N_2(N_1 + 1)]\end{aligned}\quad (4.1)$$

is an integer vector containing the sensors' position information.

First, consider the 1-dimensional impinging source directions $\{\theta_k, k = 1, \dots, K\}$. Then, the signal model can be written as

$$\mathbf{y}(t) = \mathbf{A}\mathbf{x}(t) + \mathbf{e}(t), \quad (4.2)$$

where $\mathbf{y}(t) = [y_1(t), y_2(t), \dots, y_N(t)]^T$ is the received signal vector at the N sensors at time t . Note that we have replaced \mathbf{A}_{ra} in (2.29) with \mathbf{A} . Let $\mathbf{a}(\theta_k)$ be the $N \times 1$ steering vector, $\mathbf{a}(\theta_k) = \{e^{jz_id_{\text{I}}(\pi/\lambda)\sin\theta_k} | n = 0, \dots, N-1\}$, where λ denotes the carrier wavelength. Then the manifold matrix can be expressed as

$$\mathbf{A} = [\mathbf{a}(\theta_1), \mathbf{a}(\theta_2), \dots, \mathbf{a}(\theta_K)]. \quad (4.3)$$

$\mathbf{x}(t) = [x_1(t), x_2(t), \dots, x_K(t)]^T$ is the source vector. We suppose the source signals follow Gaussian distributions, $x_k \sim \mathcal{N}(0, \sigma_k^2)$, and they are all independent of each other. The noise signal $\mathbf{e}(t) = [e_1(t), e_2(t), \dots, e_N(t)]^T$ is assumed to be white Gaussian with power σ_e^2 , and uncorrelated with the sources.

Next, we consider the case of the distributed source, which is a generalization of the collection of K -point sources [42]. Such a source is usually described by a distributed source density that indicates the amount of source power coming from each direction. Denoting the distributed source density by $x(\theta, t)$, we have

$$x(\theta, t) = \sum_{m=1}^{\infty} c_m(t) e^{jm\theta}, \quad (4.4)$$

where $c_m(t)$ is a function of the signal envelope and unknown parameters. We consider one class of distributed sources employed in [42], for which

$$c_m(t) = \sum_{k=1}^K x_k(t) \rho_k^m e^{-jm\theta_k}, \quad (4.5)$$

with $0 \leq \rho_k < 1$ and $0 \leq \theta_k \leq 2\pi$. Then the output can be expressed as

$$\mathbf{y}(t) = \sum_{k=1}^K \mathbf{b}(\theta_k, \rho) x_k(t) + \mathbf{e}(t). \quad (4.6)$$

If we write the steering vector as

$$\mathbf{a}(\omega_k) = [e^{jz_1\omega_k}, e^{jz_2\omega_k}, \dots, e^{jz_N\omega_k}]^T, \quad (4.7)$$

with $d_I = \lambda/2$, and $\omega_k = \pi \sin \theta_k$, following the analysis in [42] we can obtain

$$\begin{aligned} \mathbf{b}(\omega_k, \boldsymbol{\rho}_k) &= \boldsymbol{\rho}_k \bullet \mathbf{a}(\omega_k) \\ &= [\rho_k^{z_1} e^{jz_1\omega_k}, \rho_k^{z_2} e^{jz_2\omega_k}, \dots, \rho_k^{z_N} e^{jz_N\omega_k}]^T, \end{aligned} \quad (4.8)$$

where $\boldsymbol{\rho}_k = [\rho_k^{z_1}, \rho_k^{z_2}, \dots, \rho_k^{z_N}]^T$.

Therefore, for distributed sources, the output of the nested array can be written as

$$\mathbf{y}(t) = \mathbf{B}\mathbf{x}(t) + \mathbf{e}(t), \quad (4.9)$$

with $\mathbf{B} = [\mathbf{b}(\omega_1, \rho_1), \mathbf{b}(\omega_2, \rho_2), \dots, \mathbf{b}(\omega_K, \rho_K)]$. The covariance matrix of $\mathbf{y}(t)$ is

$$\mathbf{R}_y = \mathbf{B}\mathbf{R}_x\mathbf{B}^H + \sigma_e^2\mathbf{I}. \quad (4.10)$$

Vectorizing \mathbf{R}_y in (4.10), we get a long vector

$$\mathbf{u} = (\mathbf{B}^* \odot \mathbf{B})\mathbf{s} + \sigma_e^2\mathbf{1}_e, \quad (4.11)$$

where $\mathbf{s} = [\sigma_1^2, \sigma_2^2, \dots, \sigma_K^2]^T$, and $\mathbf{1}_e = [\mathbf{e}_1^T, \mathbf{e}_2^T, \dots, \mathbf{e}_N^T]^T$, with \mathbf{e}_i being a vector of all zeros except for a 1 at the i th position. We can view the vector \mathbf{u} as representing new longer received signals with the new manifold matrix $\mathbf{B}^* \odot \mathbf{B}$, and new source signals \mathbf{s} . The distinct rows of $\mathbf{B}^* \odot \mathbf{B}$ behave like the manifold of a longer array whose sensors are located at positions given by distinct values in the set $\{(z_i - z_j)d_I, 1 \leq i, j \leq N\}$.

We write $\mathbf{B}^* \odot \mathbf{B}$ as

$$\mathbf{B}^* \odot \mathbf{B} = [\bar{\mathbf{b}}(\omega_1, \rho_1), \bar{\mathbf{b}}(\omega_2, \rho_2), \dots, \bar{\mathbf{b}}(\omega_K, \rho_K)]_{N^2 \times K}, \quad (4.12)$$

with

$$\bar{\mathbf{b}}(\omega_k, \rho_k) = [\mathbf{b}^*(\omega_k, \rho_k) \odot \mathbf{b}(\omega_k, \rho_k)]_{N^2 \times 1} \triangleq \{b_{i,k} \mid i = 1, \dots, N^2, k = 1, \dots, K\}. \quad (4.13)$$

To obtain the expression of $b_{i,k}$, we first define two operations between two vectors. Employing the integer vector \mathbf{z} , we define Khatri-Rao addition \oplus as

$$\dot{\mathbf{z}} = \mathbf{z} \oplus \mathbf{z} \triangleq \{\dot{z}_i \mid i = 1, \dots, N^2\}, \quad (4.14)$$

with element $\dot{z}_{(i-1)N+j} = z_i + z_j$, and Khatri-Rao difference \ominus as

$$\ddot{\mathbf{z}} = \mathbf{z} \ominus \mathbf{z} \triangleq \{\ddot{z}_i \mid i = 1, \dots, N^2\}, \quad (4.15)$$

with element $\ddot{z}_{(i-1)N+j} = z_i - z_j$. Based on $\dot{\mathbf{z}}$ and $\ddot{\mathbf{z}}$, we can get

$$b_{i,k} = \rho_k^{z_i} e^{j\ddot{z}_i \omega_k}. \quad (4.16)$$

Recall that the element of $\mathbf{A}_{\text{na}}^* \odot \mathbf{A}_{\text{na}}$ in model (2.31) is $e^{j\tilde{z}_i \omega_k}$, which is equal to $b_{i,k}$ with $\rho_k = 1$. Therefore, we can see that $\mathbf{B}^* \odot \mathbf{B}$ is a weighted version of $\mathbf{A}_{\text{na}}^* \odot \mathbf{A}_{\text{na}}$, with weights being related to the scattering parameters ρ_k of the distributed sources.

4.3 Spatial smoothing

To exploit the increased DOFs offered by the difference co-array, we propose to apply the spatial smoothing technique in a new fashion based on what is presented in Section 2.2.3, where the point source model is employed. Since the strategy is not suitable for distributed sources, as presented in this section, we thus propose a new fashion of spatial smoothing by exploiting *a priori* knowledge of the spreading parameters.

Considering $\mathbf{B}^* \odot \mathbf{B}$ in model (4.11), we remove the repeated rows from $\mathbf{B}^* \odot \mathbf{B}$ and also sort them so that the i th row corresponds to the sensor location $(-\bar{N} + i)d_l$ in the difference co-array of the 2-level nested array, with $\bar{N} = N^2/4 + N/2$, giving a new vector:

$$\tilde{\mathbf{u}} = \tilde{\mathbf{B}}\mathbf{s} + \sigma_e^2 \tilde{\mathbf{e}}, \quad (4.17)$$

where $\tilde{\mathbf{e}} \in \mathbb{R}^{(2\bar{N}-1) \times 1}$ is a vector of all zeros except for a 1 at the center position. Denote

$$\tilde{\mathbf{B}} = \{\tilde{\mathbf{b}}(\omega_1, \rho_1), \tilde{\mathbf{b}}(\omega_2, \rho_2), \dots, \tilde{\mathbf{b}}(\omega_K, \rho_K)\} \quad (4.18)$$

and

$$\tilde{\mathbf{b}}(\omega_k, \rho_k) = \{\tilde{b}_{i,k} \mid i = 1, 2, \dots, 2\bar{N} - 1\}. \quad (4.19)$$

Then we can obtain $\tilde{b}_{i,k} = \rho_k^{\tilde{z}_i} e^{j\tilde{z}_i \omega_k}$. The integer set

$$\tilde{\mathbf{z}} \triangleq \{\tilde{z}_i = i - \bar{N} \mid i = 1, 2, \dots, 2\bar{N} - 1\}, \quad (4.20)$$

and \tilde{z}_i is the corresponding integer exponent of ρ_k when \tilde{z}_i is fixed. We denote $\tilde{\mathbf{z}} \triangleq \{\tilde{z}_i \mid i = 1, 2, \dots, 2\bar{N} - 1\}$.

As for point sources, according to the analysis in Section 2.2.3, we can get the corresponding vector $\tilde{\mathbf{v}}$ by vectorizing the covariance matrix:

$$\tilde{\mathbf{v}} = \tilde{\mathbf{A}}\mathbf{s} + \sigma_e^2\tilde{\mathbf{e}}, \quad (4.21)$$

with $\tilde{\mathbf{A}} = \{\tilde{a}_{i,k} = e^{j\tilde{z}_i\omega_k}\}$. We can see that the point source model is a special case with $\rho_k = 1$. Additionally, the point source model has a Vandermonde array manifold with unit circle entries, whereas the distributed source model produces a Vandermonde array manifold with non-unit circle entries. This makes the typical point-source strategy unsuitable for distributed sources. Thus, we will propose a novel strategy by exploiting *a priori* knowledge of the spreading parameters. First we consider a special case when all the sources have the same distribution parameter, denoted as ρ . This assumption is reasonable when the sources are similar.

Observing the structures of $\tilde{\mathbf{B}}$ and $\tilde{\mathbf{A}}$, we can verify that $\tilde{\mathbf{B}} = \Psi\tilde{\mathbf{A}}$, where

$$\Psi = \text{diag}(\rho^{\tilde{z}_1}, \rho^{\tilde{z}_2}, \dots, \rho^{\tilde{z}_{2\bar{N}-1}}). \quad (4.22)$$

Thus we have

$$\tilde{\mathbf{u}} = \Psi\tilde{\mathbf{A}}\mathbf{s} + \sigma_e^2\tilde{\mathbf{e}}. \quad (4.23)$$

The difference co-array of this 2-level nested array has sensors located at

$$(-\bar{N} + 1)d_{\text{I}}, \dots, -d_{\text{I}}, 0, d_{\text{I}}, \dots, (\bar{N} - 1)d_{\text{I}}. \quad (4.24)$$

We now divide these $2\bar{N} - 1$ sensors into \bar{N} overlapping subarrays, each with \bar{N} elements, where the i th subarray has sensors located at $\{(-i + 1 + n)d_{\text{I}}, n = 0, 1, \dots, \bar{N} - 1\}$. The i th subarray corresponds to the $(\bar{N} - i + 1)$ th to $(2\bar{N} - i)$ th rows of $\tilde{\mathbf{u}}$, denoted as

$$\begin{aligned} \tilde{\mathbf{u}}_i &= \tilde{\mathbf{B}}_i\mathbf{s} + \sigma_e^2\mathbf{e}_i \\ &= \Psi_i\tilde{\mathbf{A}}_i\mathbf{s} + \sigma_e^2\mathbf{e}_i \\ &= \Psi_i\tilde{\mathbf{A}}_1\Phi^{i-1}\mathbf{s} + \sigma_e^2\mathbf{e}_i, \end{aligned} \quad (4.25)$$

where

$$\Psi_i = \text{diag}(\rho^{\tilde{z}_{\bar{N}-i+1}}, \dots, \rho^{\tilde{z}_{2\bar{N}-i}}), \quad (4.26)$$

$$\Phi = \text{diag}(e^{-j\omega_1}, e^{-j\omega_2}, \dots, e^{-j\omega_K}) \quad (4.27)$$

and $\tilde{\mathbf{A}}_i$ is the corresponding i th submatrix of $\tilde{\mathbf{A}}$. Specifically, the first submatrix

$$\tilde{\mathbf{A}}_1 = \{a_{n,k} = e^{-j(n-1)\omega_k} | n = 1, \dots, \bar{N}, k = 1, \dots, K\}. \quad (4.28)$$

Provided *a priori* knowledge about the spreading parameter ρ , we can conduct the following transformation:

$$\tilde{\mathbf{u}}_i = \Psi_i^{-1} \tilde{\mathbf{u}}_i = \tilde{\mathbf{A}}_1 \Phi^{i-1} \mathbf{s} + \Psi_i^{-1} \sigma_e^2 \mathbf{e}_i. \quad (4.29)$$

Recall that for point sources, we have the i th subarray vector

$$\tilde{\mathbf{v}}_i = \tilde{\mathbf{A}}_i \mathbf{s} + \sigma_e^2 \mathbf{e}_i = \tilde{\mathbf{A}}_1 \Phi^{i-1} \mathbf{s} + \sigma_e^2 \mathbf{e}_i. \quad (4.30)$$

Comparing $\tilde{\mathbf{u}}_i$ with $\tilde{\mathbf{v}}_i$, we can see that the difference is the noise term, from $\sigma_e^2 \mathbf{e}_i$ to $\Psi_i^{-1} \sigma_e^2 \mathbf{e}_i$. We will show that the resulting noise term, which contains the distributed source parameters, would not affect the estimation and detection performance of nested arrays.

Based on (4.29), we can obtain the spatially smoothed matrix for distributed sources:

$$\tilde{\mathbf{R}}_{\text{avg}} = \frac{1}{\bar{N}} \sum_{i=1}^{\bar{N}} \tilde{\mathbf{R}}_i, \quad (4.31)$$

where $\tilde{\mathbf{R}}_i = \tilde{\mathbf{u}}_i \tilde{\mathbf{u}}_i^H$. $\tilde{\mathbf{R}}_{\text{avg}}$ enables us to perform DOA estimation of $O(N^2)$ distributed sources with N sensors, as proved by the following theorem:

Theorem 4.1. *The spatially smoothed matrix $\tilde{\mathbf{R}}_{\text{avg}}$ in (4.31) can be expressed as $\tilde{\mathbf{R}}_{\text{avg}} = \tilde{\mathbf{R}}^2$ where*

$$\tilde{\mathbf{R}} = \frac{1}{\sqrt{\bar{N}}} (\tilde{\mathbf{A}}_1 \mathbf{R}_x \tilde{\mathbf{A}}_1^H + \rho^{-\tilde{z}_{\bar{N}}} \sigma_e^2 \mathbf{I}). \quad (4.32)$$

Proof. First, we consider

$$\begin{aligned}
\tilde{\mathbf{R}}_i &= \bar{\mathbf{u}}_i \bar{\mathbf{u}}_i^H \\
&= (\tilde{\mathbf{A}}_1 \Phi^{i-1} \mathbf{s} + \Psi_i^{-1} \sigma_e^2 \mathbf{e}_i) (\tilde{\mathbf{A}}_1 \Phi^{i-1} \mathbf{s} + \Psi_i^{-1} \sigma_e^2 \mathbf{e}_i)^H \\
&= \tilde{\mathbf{A}}_1 \Phi^{i-1} \mathbf{s} \mathbf{s}^H (\Phi^{i-1})^H \tilde{\mathbf{A}}_1^H + \sigma_e^2 \tilde{\mathbf{A}}_1 \Phi^{i-1} \mathbf{s} \mathbf{e}_i^H \Psi_i^{-1} \\
&\quad + \sigma_e^2 \Psi_i^{-1} \mathbf{e}_i \mathbf{s}^H (\Phi^{i-1})^H \tilde{\mathbf{A}}_1^H + \sigma_e^4 \Psi_i^{-1} \mathbf{e}_i \mathbf{e}_i^H \Psi_i^{-1}.
\end{aligned}$$

Note that Ψ_i^{-1} is a real diagonal matrix, so $(\Psi_i^{-1})^H = \Psi_i^{-1}$.

Since \mathbf{e}_i is a vector with all zeros except a 1 at the i th position, and

$$\Psi_i^{-1} = \text{diag}(\rho^{-\tilde{z}_{\bar{N}-i+1}}, \dots, \rho^{-\tilde{z}_{2\bar{N}-i}}), \quad (4.33)$$

we can calculate that

$$\Psi_i^{-1} \sigma_e^2 \mathbf{e}_i = \rho^{-\tilde{z}_{\bar{N}}} \sigma_e^2 \mathbf{e}_i, \quad (4.34)$$

where $\rho^{-\tilde{z}_{\bar{N}}}$ is the (i, i) th element of Ψ_i^{-1} . Therefore, we have

$$\begin{aligned}
\tilde{\mathbf{R}}_i &= \tilde{\mathbf{A}}_1 \Phi^{i-1} \mathbf{s} \mathbf{s}^H (\Phi^{i-1})^H \tilde{\mathbf{A}}_1^H + \rho^{-\tilde{z}_{\bar{N}}} \sigma_e^2 \tilde{\mathbf{A}}_1 \Phi^{i-1} \mathbf{s} \mathbf{e}_i^H \\
&\quad + \rho^{-\tilde{z}_{\bar{N}}} \sigma_e^2 \mathbf{e}_i \mathbf{s}^H (\Phi^{i-1})^H \tilde{\mathbf{A}}_1^H + \rho^{-2\tilde{z}_{\bar{N}}} \sigma_e^4 \mathbf{e}_i \mathbf{e}_i^H.
\end{aligned} \quad (4.35)$$

Then, we can calculate [21]:

$$\begin{aligned}
\tilde{\mathbf{R}}_{\text{avg}} &= \frac{1}{\bar{N}} \sum_{i=1}^{\bar{N}} \tilde{\mathbf{R}}_i \\
&= \frac{1}{\bar{N}} [\tilde{\mathbf{A}}_1 \Xi \Xi^H \tilde{\mathbf{A}}_1^H + \rho^{-\tilde{z}_{\bar{N}}} \sigma_e^2 \tilde{\mathbf{A}}_1 \Xi \\
&\quad + \rho^{-\tilde{z}_{\bar{N}}} \sigma_e^2 \Xi^H \tilde{\mathbf{A}}_1^H + \rho^{-2\tilde{z}_{\bar{N}}} \sigma_e^4 \mathbf{I}],
\end{aligned} \quad (4.36)$$

with $\boldsymbol{\Xi} = \mathbf{R}_x \tilde{\mathbf{A}}_1^H$. Finally we can get

$$\begin{aligned}
\tilde{\mathbf{R}}_{\text{avg}} &= \frac{1}{\bar{N}} [\tilde{\mathbf{A}}_1 \mathbf{R}_x \tilde{\mathbf{A}}_1^H \tilde{\mathbf{A}}_1 \mathbf{R}_x \tilde{\mathbf{A}}_1^H + \\
&\quad 2\rho^{-\tilde{z}_{\bar{N}}} \sigma_e^2 \tilde{\mathbf{A}}_1 \mathbf{R}_x \tilde{\mathbf{A}}_1^H + \rho^{-2\tilde{z}_{\bar{N}}} \sigma_e^4 \mathbf{I}] \\
&= \frac{1}{\bar{N}} (\tilde{\mathbf{A}}_1 \mathbf{R}_x \tilde{\mathbf{A}}_1^H + \rho^{-\tilde{z}_{\bar{N}}} \sigma_e^2 \mathbf{I})^2 \\
&= \tilde{\mathbf{R}}^2,
\end{aligned} \tag{4.37}$$

with $\tilde{\mathbf{R}} = \frac{1}{\sqrt{\bar{N}}} (\tilde{\mathbf{A}}_1 \mathbf{R}_x \tilde{\mathbf{A}}_1^H + \rho^{-\tilde{z}_{\bar{N}}} \sigma_e^2 \mathbf{I})$. \square

As mentioned before, the effect of the distributed source model is to produce a Vandermonde array manifold with non-unit circle entries, which contributes to the noise variance in $\tilde{\mathbf{R}}$ with spreading parameters. $\tilde{\mathbf{R}}$ has the same form as the conventional covariance matrix of the signal received by a longer ULA consisting of \bar{N} sensors. The equivalent array manifold is represented by $\tilde{\mathbf{A}}_1$. Thus, we can apply subspace based methods like MUSIC to identify up to $\bar{N} - 1$ sources.

The above analysis is based on the same spreading parameter ρ for all sources. When the parameters are different, we cannot easily find the equivalent matrix Ψ_i in (4.25). Thus, we will not be able to obtain the simple form (4.29), and further we cannot achieve results similar to those in **Theorem 1**. Nevertheless, to investigate its performance with different ρ , we propose to use the average of ρ_k , $k = 1, \dots, K$ to replace the ρ in Ψ_i . We will demonstrate its effectiveness through numerical examples.

4.4 Numerical examples

In this section, we use numerical examples to show the effectiveness of our proposed strategy. The nested array we use contains $N = 6$ sensors, with $N_1 = 3$ and $N_2 = 3$.

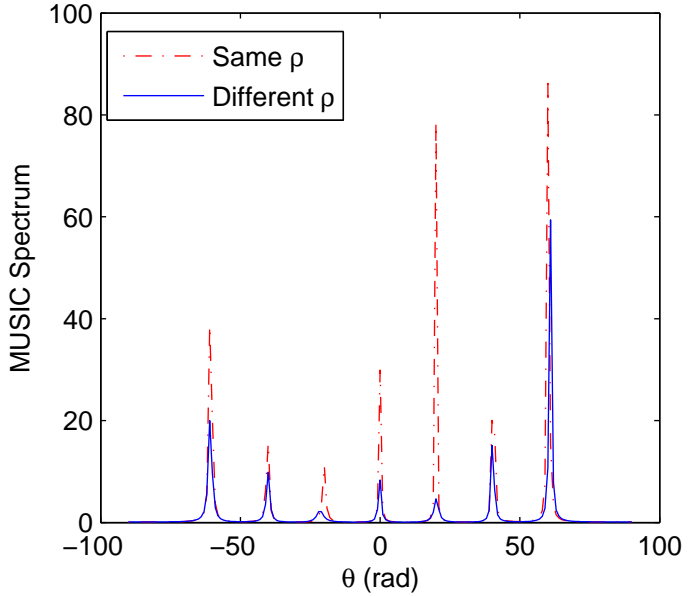


Figure 4.1: MUSIC spectrum of the proposed method for two sets of ρ , as a function of θ , using a 6-sensor nested array.

4.4.1 MUSIC spectral

We consider $K = 7$ sources with impinging directions $\boldsymbol{\theta} = [-60^\circ, -40^\circ, -20^\circ, 0^\circ, 20^\circ, 40^\circ, 60^\circ]$, using a nested array. Two classes of distributed sources are investigated: one with the same spreading parameter $\rho = 0.8$, the other with different values

$$\boldsymbol{\rho} = [0.8, 0.7, 0.75, 0.85, 0.78, 0.83, 0.8].$$

Note that we have more sources than sensors. Fig. 4.1 shows the MUSIC spectrum after applying the proposed spatial smoothing technique. We use a total of $T = 1000$ snapshots at a signal-to-noise ratio (SNR) of 0 dB. As can be seen, the proposed strategy can resolve the seven distributed sources for both cases. The case with the same ρ performs better, as expected. Note that it is not always the case that all the sources can be resolved. With smaller SNRs, fewer samples, or smaller spreading parameters, the probability of false estimation becomes larger. This validates our former analysis that the regular spatial smoothing technique obscures the beautiful structure of $\bar{\mathbf{R}}_{\text{avg}}$, which is of the same form as a conventional longer array. Thus, the subspace based approach, MUSIC, no longer works.

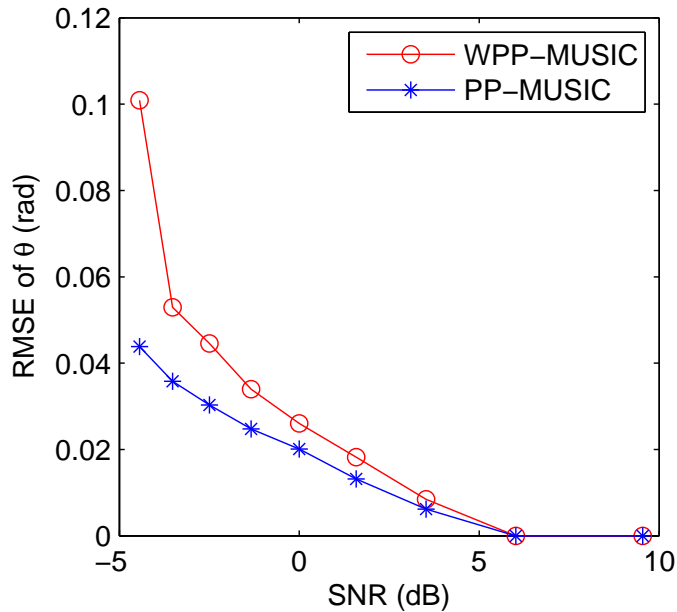


Figure 4.2: RMSE of estimates of θ versus SNR, using both the PP-MUSIC and WPP-MUSIC with a 6-sensor nested array.

4.4.2 RMSE versus SNR

In this section, we consider one source $\theta = 35^\circ$ with spreading parameter $\rho = 0.8$. We compare our proposed ‘‘prior processing’’ MUSIC (PP-MUSIC) with the regular ‘‘without prior processing’’ MUSIC (WPP-MUSIC) [21], by studying the root mean squared error (RMSE) of the DOA estimates versus SNR, which is defined in (3.25). Fig. 4.2 shows the RMSE of both methods as a function of SNR for $T = 1000$ snapshots, averaged over 1000 Monte Carlo simulations. We can see that the performance of both methods improves with increasing SNR, and our proposed method performs better than the regular method.

Note that we fix the spreading parameter at $\rho = 0.8$ in the above example. With different ρ , the estimation performance will improve with increasing ρ . In addition, the PP-MUSIC and WPP-MUSIC will merge at $\rho = 1$, which is identical to the point source model. This is also true for source detection.

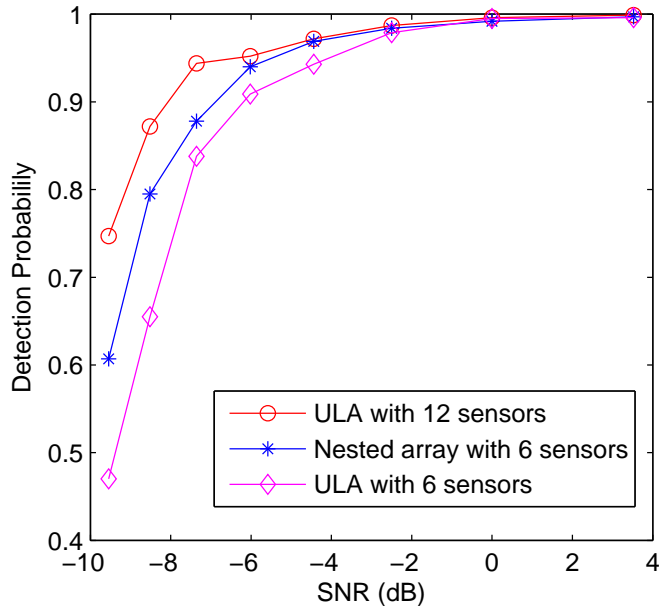


Figure 4.3: Detection probability of the proposed method versus SNR, with a 6-sensor ULA, a 6-sensor nested array, and a 12-sensor ULA: $K = 2$, $T = 1000$, and $\rho = 0.9$.

4.4.3 Source number detection

In this section, suppose that we have $K = 2$ sources, but this number is unknown and we need to detect it. We compare the detection performance of a 6-sensor ULA, a 6-sensor nested array, and a 12-sensor ULA. The detection probability versus SNR is depicted in Fig. 4.3. The detection probability is defined as F_K/F , where F is the trial number and F_K is the number of times that K is detected. We can see that the two-level nested array outperforms the corresponding ULA with same number of sensors and performs close to the much longer ULA.

4.5 Summary

In this chapter [47], we considered distributed source processing using the recently proposed linear nested arrays. Based on the conventional ULA signal model for distributed sources and the nested array signal model for point sources, we established the nested array model

for distributed sources. To employ the increased DOFs provided by the difference co-array, we proposed an improved spatial smoothing strategy based on *a priori* knowledge of the spreading parameter, and analytically proved its effectiveness. The spatial smoothing strategy enables a nested array with N sensors to detect $O(N^2)$ distributed sources, as in the case of point sources. Next, we developed the corresponding source number detection and DOA estimation approaches for the proposed strategies. The results were verified through numerical examples.

Chapter 5

Calibrating Nested Sensor Arrays with Model Errors

The previous two chapters focused on signal processing with fully calibrated nested arrays. In practice, however, the actual sensor gain and phase are often perturbed from their nominal values, which disrupts the existing DOA estimation algorithms. In this chapter, we investigate the self-calibration problem for perturbed nested arrays.³

5.1 Introduction

Strategies in most references require exact knowledge of the array's sensor gain and phase. Nevertheless, typically, the actual sensor gain and phase are perturbed from their assumed nominal values. DOA estimation using ULAs with model errors has been well studied in the past two decades [48]-[52]. Self-calibration algorithms have been proposed based on various strategies, including the Toeplitz structure of the covariance matrix [51] and a subspace-based scheme [48]. Performance analysis was conducted for MUSIC algorithms in [49]-[50], and [52]. All these strategies were proposed for ULAs. The calibration problem for circular arrays was investigated in [53].

In this chapter, we consider the model-error problem for nested arrays, and further, the general case of nonuniform linear arrays. To the authors' knowledge, this is the first attempt

³This chapter is based on K. Han, P. Yang, and A. Nehorai, "Calibrating nested sensor arrays with model errors," Proc. 48th Asilomar Conf. Signals, Syst. Comput., Pacific Grove, CA, Nov. 2014. © IEEE 2014.

to investigate the calibration problem for nonuniform linear arrays. Due to their nonuniform structures, the traditional methods for ULAs may become inapplicable. We propose a corresponding gain-error estimation method based on the structure of nested arrays. For phase errors, rather than estimating the phase error parameters, we directly estimate the DOAs by constructing a sparse total least squares (STLS) problem, which was first investigated in [19]. Additionally, we will also investigate another class of nonuniform linear arrays: co-prime arrays, as presented in Section 2.3.

5.2 Signal model

We consider a nonuniform linear nested array with N sensors, whose sensor positions are $\mathbf{d} \triangleq \mathbf{z}d_{\text{I}}$, where $\mathbf{z} \triangleq [z_1, \dots, z_N]^T$ is an integer vector containing the sensors' position information. d_{I} is the smallest sensor interspacing. Also, we denote $\mathbf{d} = [d_1, \dots, d_N]^T$. We assume K narrowband sources are in the surveillance region, impinging on this linear array from directions $\{\theta_k, k = 1, \dots, K\}$, with powers $\{\sigma_i^2, i = 1, \dots, K\}$. We can obtain the received signal as

$$\mathbf{y}(t) = \mathbf{A}\mathbf{x}(t) + \mathbf{e}(t), \quad (5.1)$$

where $\mathbf{y}(t) = [y_1(t), y_2(t), \dots, y_N(t)]^T$ is the received signal vector at the N sensors at time t . Let $\mathbf{a}(\theta_k)$ be the $N \times 1$ steering vector, and the i th element of $\mathbf{a}(\theta_k)$ be $e^{j(2\pi/\lambda)d_i \sin \theta_k}$, where λ denotes the carrier wavelength. Then the manifold matrix can be expressed as

$$\mathbf{A} = [\mathbf{a}(\theta_1), \mathbf{a}(\theta_2), \dots, \mathbf{a}(\theta_K)]. \quad (5.2)$$

We suppose the source signals $\mathbf{x}(t)$ are all independent of each other. The noise $\mathbf{e}(t)$ is assumed to be temporally and spatially white, and uncorrelated with the sources. Based on these assumptions, the source covariance matrix is diagonal: $\mathbf{R}_x = \text{diag}\{\sigma_1^2, \dots, \sigma_K^2\}$. Then the covariance matrix of the received signal is

$$\mathbf{R}_y = \mathbf{A}\mathbf{R}_x\mathbf{A}^H + \sigma_e^2\mathbf{I}, \quad (5.3)$$

where σ_e^2 is the noise power, and \mathbf{I} is the identity matrix.

In the presence of gain and phase errors, (5.1) becomes

$$\mathbf{y}(t) = \Psi \Phi \mathbf{A} \mathbf{x}(t) + \mathbf{e}(t), \quad (5.4)$$

where $\Psi = \text{diag}(\psi_1, \psi_2, \dots, \psi_N)$ and $\Phi = \text{diag}(e^{j\phi_1}, e^{j\phi_2}, \dots, e^{j\phi_N})$. $\psi_i > 0$ and $\phi_i \in \mathbb{R}$ ($i = 1, \dots, N$) are gain and phase errors respectively. We assume they are deterministic unknown. The covariance matrix will become

$$\mathbf{R}_y = \Psi \Phi \mathbf{A} \mathbf{R}_x \mathbf{A}^H \Phi^H \Psi^H + \sigma_e^2 \mathbf{I}. \quad (5.5)$$

For ULA case, when the sensors have no gain or phase errors, the covariance matrix \mathbf{R}_y has Toeplitz structure [51], with element

$$r_{i,l} = \sum \sigma_k^2 e^{j(i-l)\omega_k} + \delta_{i,l} \sigma_e^2, \quad i \geq l, \quad (5.6)$$

where we assume $d_I = \lambda/2$, and $\omega_k = \pi \sin \theta_k$. $\delta_{i,l}$ is defined as

$$\delta_{i,l} = \begin{cases} 1, & i = l \\ 0, & i \neq l \end{cases}. \quad (5.7)$$

Since \mathbf{R}_y is Hermitian symmetric, we concentrate on only the lower left half of the matrix. Next, we define an indication function $\gamma_{i,l} = z_i - z_l$, which indicates the phase information of \mathbf{R}_y 's entries. Thus we have the indication matrix for a 6-sensor ULA:

$$\Gamma_y = \left(\begin{array}{cccccc} 0 & & & & & & \\ 1 & 0 & & & & & \\ 2 & 1 & 0 & & & & \\ 3 & 2 & 1 & 0 & & & \\ 4 & 3 & 2 & 1 & 0 & & \\ 5 & 4 & 3 & 2 & 1 & 0 & \end{array} \right). \quad (5.8)$$

In Γ_y , we have marked the identical entries with same colors.

Consider any two elements $r_{i,l}$, $i \geq l$ and $r_{p,q}$, $p \geq q$, where $\gamma_{i,l} = \gamma_{p,q}$. From these elements, we can construct an equation which can be used to estimate the error parameters [51]. Thus,

based on properties of the main diagonal and sub-diagonal elements of \mathbf{R}_y and Γ_y , the matrix can provide $\sum_{i=2}^N (i(i-1)/2)$ equations to estimate gain parameters, and $\sum_{i=2}^{N-1} (i(i-1)/2)$ equations to estimate the phase parameters. Note that the main diagonal entries do not contribute to the phase error parameter estimation. The solution is found by the least squares method. One deficiency is that both of the two overdetermined linear systems have low ranks: the gain error case has rank $N - 1$, whereas the phase error case has rank $N - 2$. When it comes to the nested array, the Toeplitz structure of \mathbf{R}_y would be partially destroyed due to the nonuniformity. Nevertheless, we will show that gain estimation can still be well achieved by employing the remaining Toeplitz structure. However, the phase-error estimation will be seriously deteriorated, a problem we will also address.

5.3 Gain error estimation

In this section, we assume *a priori* knowledge of the noise power σ_e^2 . For the case with unknown σ_e^2 , we can simply estimate it first according to [54]. Thus we have

$$\begin{aligned}\tilde{\mathbf{R}}_y &= \mathbf{R}_y - \sigma_e^2 \mathbf{I} \\ &\triangleq \{\tilde{r}_{i,l}\}_{i,l=1,\dots,N} \\ &= \left\{ \psi_i \psi_l \sum_{k=1}^K \sigma_k^2 e^{j(z_i - z_l) \omega_k} e^{j(\phi_i - \phi_l)} \right\}.\end{aligned}\quad (5.9)$$

We define

$$\begin{aligned}\xi_{ijpq} &\triangleq \ln \left\{ \frac{|\tilde{r}_{il}|}{|\tilde{r}_{pq}|} \right\} \\ &= \ln \left\{ \frac{\psi_i \psi_l}{\psi_p \psi_q} \cdot \frac{|\sum_{k=1}^K \sigma_k^2 e^{j(z_i - z_l) \omega_k}|}{|\sum_{k=1}^K \sigma_k^2 e^{j(z_p - z_q) \omega_k}|} \right\}.\end{aligned}\quad (5.10)$$

When $z_i - z_l = z_p - z_q$, (5.10) can be further written as

$$\xi_{ilpq} = \ln \psi_i + \ln \psi_l - \ln \psi_p - \ln \psi_q. \quad (5.11)$$

In a ULA, $z_i - z_l = z_p - z_q$ is equivalent to $i - l = p - q$, i.e., \tilde{r}_{il} and \tilde{r}_{pq} lie on the same diagonal. However, this is not true for a nested array.

Recalling the difference co-array defined in Section 2.2.2, we have the following result based on the weight functions in (2.33).

Proposition 5.1. *The number of equations applicable for gain-error estimation is*

$$\sum_{w(n) \geq 2, n \geq 0} \frac{w(n)(w(n) - 1)}{2}. \quad (5.12)$$

Proof. The proof is straightforward, according to the analysis in [51]. \square

Now we consider a two-level nested array with N sensors in Fig. 2.2. The virtual sensors of the difference co-array are located at

$$\{nd_1, (-N_2(N_1 + 1) + 1) \leq n \leq (N_2(N_1 + 1) - 1)\}. \quad (5.13)$$

For $n = 0$, we can easily get $w(0) = N_1 + N_2 = N$. If we concentrate on the positive positions ($n > 0$), we have the following result:

$$w(n) = \begin{cases} N_1 - n + 1 & \text{if } 0 < n \leq N_1 \\ N_2 - 1 & \text{if } n = N_1 + 1 \\ 1 & \text{if } n \geq N_1 + 2 \end{cases}. \quad (5.14)$$

Based on only $w(0)$, we can obtain $N(N - 1)/2$ equations. To form a nested array, the sensor number needs to satisfy $N \geq 3$. Thus we have $N \leq N(N - 1)/2$, so we can always construct an overdetermined linear system:

$$\mathbf{B}\tilde{\Psi} = \Xi, \quad (5.15)$$

where $\tilde{\Psi} = [\ln(\psi_1), \ln(\psi_2), \dots, \ln(\psi_N)]^T$, $\Xi = [\dots, \xi_{ilpq}, \dots]^T$, and \mathbf{B} is the corresponding tall coefficient matrix for $\tilde{\Psi}$. We will provide an illustration in Section 5.4.2, together with the phase error case.

Similar to the ULA case, \mathbf{B} is of rank $N - 1$, with the null space spanning vector $\boldsymbol{\mu} = [1, 1, \dots, 1]^T$. If we obtain the minimum norm least squares solution to (5.15), a general

solution can be achieved by adding $\epsilon\boldsymbol{\mu}$, where ϵ is an arbitrary scalar. This amounts to saying that we can determine the sensor gain only to within an arbitrary multiplicative constant e^ϵ . Namely, our estimated gain errors are $\bar{\boldsymbol{\Psi}} = e^\epsilon \boldsymbol{\Psi}$. We will show that this multiplicative constant does not affect the DOA estimation.

5.4 Direction-of-arrival estimation

In this section, we will estimate the DOAs for two cases: without phase error and with phase error. For the first case, we provide both MUSIC and sparse recovery approaches. For the second problem, we may find that there are not enough equations, as in the ULA case, to estimate the phase errors. Alternatively, we propose to use the sparse total least squares (STLS) [19] method to recover the DOAs.

5.4.1 Without phase error

For this case, we assume only gain errors exist. We will consider the DOA estimation based on the estimated gain errors, with the following result.

Proposition 5.2. *The multiplicative constant e^ϵ corresponding to the estimated gain errors does not affect the DOA estimation.*

Proof. With $\boldsymbol{\Phi} = \mathbf{I}$, we have $\tilde{\mathbf{R}}_y = \boldsymbol{\Psi} \mathbf{A} \mathbf{R}_x \mathbf{A}^H \boldsymbol{\Psi}^H$. Together with $\bar{\boldsymbol{\Psi}} = e^\epsilon \boldsymbol{\Psi}$, we obtain

$$\check{\mathbf{R}}_y = \bar{\boldsymbol{\Psi}}^{-1} \tilde{\mathbf{R}}_y \bar{\boldsymbol{\Psi}}^{-H} = \mathbf{A} \frac{\mathbf{R}_x}{e^{2\epsilon}} \mathbf{A}^H. \quad (5.16)$$

If we add the noise term back, we have

$$\hat{\mathbf{R}}_y = \check{\mathbf{R}}_y + \sigma_e^2 \mathbf{I} = \mathbf{A} \frac{\mathbf{R}_x}{e^{2\epsilon}} \mathbf{A}^H + \sigma_e^2 \mathbf{I}. \quad (5.17)$$

This is equivalent to the case of no gain errors, with fractional signal powers. Thus, we can apply the MUSIC approach as in [21]. Since the only difference is the source powers, the

corresponding noise subspace will not change. Thus the MUSIC spectrum will remain the same, which leads to the same DOA estimation.

On the other hand, we consider the DOA estimation by applying sparse recovery. Vectorizing (5.17), we get

$$\hat{\mathbf{v}} = (\mathbf{A}^* \odot \mathbf{A}) \frac{\mathbf{p}}{e^{2\epsilon}} + \sigma_e^2 \mathbf{1}_e, \quad (5.18)$$

where $\mathbf{p} = [\sigma_1^2, \sigma_2^2, \dots, \sigma_K^2]^T$, and $\mathbf{1}_e = [\mathbf{e}_1^T, \mathbf{e}_2^T, \dots, \mathbf{e}_N^T]^T$, with \mathbf{e}_i being a vector of all zeros except for a 1 at the i th position. Thus, we have the sparse recovery strategy:

$$\hat{\mathbf{p}}_g = \arg \min_{\mathbf{p}_g} \|(\hat{\mathbf{v}} - \sigma_e^2 \mathbf{1}_e) - \mathbf{A}_s \mathbf{p}_g\|_2^2 + \lambda \|\mathbf{p}_g\|_1, \quad (5.19)$$

where \mathbf{A}_s is a sensing matrix consisting of the searching steering vectors:

$$\mathbf{A}_s = [\mathbf{a}(\theta_1^s), \mathbf{a}(\theta_2^s), \dots, \mathbf{a}(\theta_D^s)], \quad (5.20)$$

where $\mathbf{a}(\theta_i^s) = \mathbf{a}(\theta_i^s)^* \otimes \mathbf{a}(\theta_i^s)$, and D is the searching grid size, with $D \gg K$. For the case without gain error, we have the vectorized equation:

$$\hat{\mathbf{v}} = (\mathbf{A}^* \odot \mathbf{A}) \mathbf{p} + \sigma_e^2 \mathbf{1}_e. \quad (5.21)$$

Further, we can construct the similar sparse recovery problem:

$$\hat{\mathbf{p}} = \arg \min_{\mathbf{p}} \|(\hat{\mathbf{v}} - \sigma_e^2 \mathbf{1}_e) - \mathbf{A}_s \mathbf{p}\|_2^2 + \lambda \|\mathbf{p}\|_1. \quad (5.22)$$

Comparing (5.18), (5.19) and (5.21), (5.22), we can easily obtain $\hat{\mathbf{p}}_g = e^{2\epsilon} \hat{\mathbf{p}}$. Namely, the estimated $\hat{\mathbf{p}}_g$, for the case with gain errors, has non-zero values at the same positions as in the case without gain errors, with fractional spectrum values. \square

Remark 5.1. *The above analysis is based on the assumption that we obtain the true gain errors with only a multiplicative constant. In practice, we can achieve only approximate values. The accuracy depends on the noise level and the sample size.*

5.4.2 With phase error

Next, we assume that the phase errors exist. Considering (5.9) again, we define

$$\begin{aligned}\tau_{ilpq} &\triangleq \text{angle}(\tilde{r}_{il}) - \text{angle}(\tilde{r}_{pq}) \\ &= \text{angle} \left(\sum_{k=1}^K \sigma_k^2 e^{j(z_i - z_l)\omega_k} \right) + \phi_i - \phi_l \\ &\quad - \text{angle} \left(\sum_{k=1}^K \sigma_k^2 e^{j(z_p - z_q)\omega_k} \right) - \phi_p + \phi_q.\end{aligned}\tag{5.23}$$

When $z_i - z_l = z_p - z_q$, (5.23) can be further written as

$$\tau_{ilpq} = \phi_i - \phi_l - \phi_p + \phi_q.\tag{5.24}$$

Since the main diagonal elements of $\tilde{\mathbf{R}}_y$ do not contain phase error information, we have the following result.

Proposition 5.3. *The number of equations applicable for phase-error estimation is*

$$\sum_{w(n) \geq 2, n \geq 1} \frac{w(n)(w(n) - 1)}{2}.\tag{5.25}$$

This number is quite small due to the nonuniformity of nested arrays, and in some cases is even smaller than the number of unknown phase error parameters. Typically, the more levels in a nested array, the smaller the number of available equations. Therefore, we can obtain the following linear system as in (5.15):

$$\mathbf{C}\tilde{\Phi} = \mathcal{T},\tag{5.26}$$

but it is not always overdetermined.

Example 5.1. Consider a 2-level nested array with 6 sensors, $N_1 = 3$, and $N_2 = 3$. The sensor positions are $[1, 2, 3, 4, 8, 12]d_L$. Thus, we have the indication matrix:

$$\Gamma_y = \begin{pmatrix} 0 \\ 1 & 0 \\ 2 & 1 & 0 \\ 3 & 2 & 1 & 0 \\ 7 & 6 & 5 & 4 & 0 \\ 11 & 10 & 9 & 8 & 4 & 0 \end{pmatrix} \quad (5.27)$$

Based on (5.14) in Section III, we have the weight function values in Table 5.1. If we define $\nu_g(n)$ and $\nu_p(n)$ as the number of equations provided by the n th index for gain error and phase-error estimation respectively, then $\nu_g(n) = w(n)(w(n) - 1)/2$, where $n \geq 0$, and $\nu_p(n) = w(n)(w(n) - 1)/2$, where $n \geq 1$. Its values are also shown in Table 5.1. Therefore, for gain-error estimation, we have $\sum_{n=0}^{11} \nu_g(n) = 20$ equations. As analyzed before, this number is greater than the number of gain error parameters. For phase-error estimation we have $\sum_{n=0}^{11} \nu_p(n) = 5$ equations in total, which is smaller than the number of phase error parameters. Thus, we cannot form an overdetermined system for phase-error estimation, and the least squares method becomes inapplicable.

Table 5.1: Weight function: $N_1 = 3, N_2 = 3$

| n | 0 | 1 | 2 | 3 | 4 | 5 | 6 | 7 | 8 | 9 | 10 | 11 |
|------------|----|---|---|---|---|---|---|---|---|---|----|----|
| $w(n)$ | 6 | 3 | 2 | 1 | 2 | 1 | 1 | 1 | 1 | 1 | 1 | 1 |
| $\nu_g(n)$ | 15 | 3 | 1 | 0 | 1 | 0 | 0 | 0 | 0 | 0 | 0 | 0 |
| $\nu_p(n)$ | 0 | 3 | 1 | 0 | 1 | 0 | 0 | 0 | 0 | 0 | 0 | 0 |

When the inner ULA has more sensors than the outer ULA, it is possible to achieve more equations than phase error parameters.

Example 5.2. With $N_1 = 4$, and $N_2 = 2$, we have 10 linear equations, shown in Table 5.2, which is greater than the parameter number 6. However, the corresponding linear matrix \mathbf{C} in (5.26) has at most rank $N - 2$, which is the same as the case of the ULA [51]. Thus the least squares solution again fails to provide accurate estimation of the phase errors.

Table 5.2: Weight function: $N_1 = 4, N_2 = 2$

| n | 0 | 1 | 2 | 3 | 4 | 5 | 6 | 7 | 8 | 9 |
|------------|---|---|---|---|---|---|---|---|---|---|
| $w(n)$ | 6 | 4 | 3 | 2 | 1 | 1 | 1 | 1 | 1 | 1 |
| $\nu_p(n)$ | 0 | 6 | 3 | 1 | 0 | 0 | 0 | 0 | 0 | 0 |

To circumvent the problem in Example 5.2, we propose to employ the STLS approach proposed in [19]. Instead of estimating the phase errors, we directly estimate the DOAs.

For this section, we assume that we have already estimated the gain error parameters. Then with phase errors, we have $\tilde{\mathbf{R}}_y = \Psi \Phi A \mathbf{R}_x A^H \Phi^H \Psi^H$. Together with $\bar{\Psi} = e^\epsilon \Psi$, we obtain

$$\check{\mathbf{R}}_y = \bar{\Psi}^{-1} \tilde{\mathbf{R}}_y \bar{\Psi}^{-H} = \Phi A \frac{\mathbf{R}_x}{e^{2\epsilon}} A^H \Phi^H. \quad (5.28)$$

Again, we add the noise term back and obtain

$$\hat{\mathbf{R}}_y = \check{\mathbf{R}}_y + \sigma_e^2 \mathbf{I} = \Phi A \frac{\mathbf{R}_x}{e^{2\epsilon}} A^H \Phi^H + \sigma_e^2 \mathbf{I}. \quad (5.29)$$

We denote $\phi = [\phi_1, \dots, \phi_N]^T$, and $\hat{\phi} = \text{vec}(\phi \phi^T)$. Then we vectorize $\hat{\mathbf{R}}_y$ in (5.29), obtaining

$$\hat{\mathbf{v}} = [\Pi \bullet (\mathbf{A}^* \odot \mathbf{A})] \frac{\mathbf{p}}{e^{2\epsilon}} + \sigma_e^2 \mathbf{1}_e, \quad (5.30)$$

where $\Pi = [\hat{\phi} \ \hat{\phi} \ \cdots \ \hat{\phi}]_{N^2 \times K}$. To employ STLS, we further write $\hat{\mathbf{v}}$ in (5.30) as

$$\begin{aligned} \hat{\mathbf{v}} &= [\Pi \bullet (\mathbf{A}^* \odot \mathbf{A})] \frac{\mathbf{p}}{e^{2\epsilon}} + \sigma_e^2 \mathbf{1}_e \\ &= [(\mathbf{A}^* \odot \mathbf{A}) + (\Pi - \bar{\mathbf{I}}) \bullet ((\mathbf{A}^* \odot \mathbf{A}))] \frac{\mathbf{p}}{e^{2\epsilon}} + \sigma_e^2 \mathbf{1}_e \\ &\triangleq (\bar{\mathbf{A}} + \mathbf{E}) \frac{\mathbf{p}}{e^{2\epsilon}} + \sigma_e^2 \mathbf{1}_e, \end{aligned} \quad (5.31)$$

where $\bar{\mathbf{I}}$ is an $N^2 \times K$ matrix with all elements 1, $\bar{\mathbf{A}} \triangleq \mathbf{A}^* \odot \mathbf{A}$, and $\mathbf{E} = (\Pi - \bar{\mathbf{I}}) \bullet ((\mathbf{A}^* \odot \mathbf{A}))$. Thus, we construct the STLS problem as

$$\begin{aligned} \{\hat{\mathbf{p}}_g, \hat{\mathbf{E}}\} &= \arg \min_{\mathbf{p}_g, \mathbf{E}} \|(\hat{\mathbf{v}} - \sigma_e^2 \mathbf{1}_e) - (\mathbf{A}_s + \mathbf{E}) \mathbf{p}_g\|_2^2 \\ &\quad + \|\mathbf{E}\|_F^2 + \lambda \|\mathbf{p}_g\|_1. \end{aligned} \quad (5.32)$$

We use the alternating minimization algorithm to solve the above problem. Specifically, for each iteration, $\hat{\mathbf{p}}_g$ is obtained by solving

$$\hat{\mathbf{p}}_g = \arg \min_{\mathbf{p}_g} \|(\hat{\mathbf{v}} - \sigma_e^2 \mathbf{1}_e) - (\bar{\mathbf{A}} + \mathbf{E}) \mathbf{p}_g\|_2^2 + \lambda \|\mathbf{p}_g\|_1, \quad (5.33)$$

with \mathbf{E} fixed. Then with the updated $\hat{\mathbf{p}}_g$, $\hat{\mathbf{E}}$ is found by solving

$$\hat{\mathbf{E}} = \arg \min_{\mathbf{E}} \|(\hat{\mathbf{v}} - \sigma_e^2 \mathbf{1}_e) - \bar{\mathbf{A}} \hat{\mathbf{p}}_g - \mathbf{E} \hat{\mathbf{p}}_g\|_2^2 + \|\mathbf{E}\|_F^2. \quad (5.34)$$

The multiplier $e^{2\epsilon}$ affects the estimated results $\hat{\mathbf{p}}_g$ by a multiplicative factor, but has no effect on the positions of the non-zero values, as discussed before. Steps (5.33) and (5.34) are iterated until a sub-optimal solution is achieved.

Remark 5.2. *The phase error issue here is different from the phase-mismatch issue in the sparse recovery problem [29]. The phase-mismatch issue imposes phase errors with respect to DOAs, which are the same for all the elements in one specific column of \mathbf{A} . However for the phase errors considered in this section, we are referring to errors with respect to sensors, which are the same for all the elements in one specific row of \mathbf{A} .*

5.4.3 Cramér-Rao bound

It is important to determine the robustness of the DOA estimation by the proposed strategies. Thus, we derive the Cramér-Rao bound (CRB) of the DOAs for nested arrays.

The CRB is obtained by taking the inverse of the Fisher information matrix. Based on the unconditional signal model (5.4), it has been shown that the CRB for DOAs is [55]

$$\text{CRB}(\boldsymbol{\omega}) = \frac{\sigma_e^2}{2T} \{ \text{Re}[\mathbf{H} \bullet (\mathbf{R}_x \bar{\mathbf{A}}^H \mathbf{R}_y^{-1} \bar{\mathbf{A}} \mathbf{R}_x)^T] \}^{-1}, \quad (5.35)$$

where

$$\bar{\mathbf{A}} = \Psi \Phi \mathbf{A} \triangleq [\bar{\mathbf{a}}(\omega_1), \bar{\mathbf{a}}(\omega_2), \dots, \bar{\mathbf{a}}(\omega_K)], \quad (5.36)$$

$$\mathbf{H} = \mathbf{D}^H [\mathbf{I} - \bar{\mathbf{A}}(\bar{\mathbf{A}}^H \bar{\mathbf{A}})^{-1} \bar{\mathbf{A}}^H] \mathbf{D}, \quad (5.37)$$

$$\mathbf{D} = [\mathbf{d}_1, \mathbf{d}_2, \dots, \mathbf{d}_K], \quad (5.38)$$

$$\mathbf{d}_k = \frac{d\bar{\mathbf{a}}(\omega_k)}{d\omega_k}, \quad (5.39)$$

and T is the number of snapshots. Note that the superscripts H and T are different from the matrix \mathbf{H} and snapshot number T .

In this section, we assume there is only one signal source ($K = 1$). Thus, matrix \mathbf{A} becomes vector \mathbf{a} , and \mathbf{R}_x becomes a scalar σ_s^2 . We derive the closed-form CRB for ω in the Appendix A:

$$\text{CRB}(\omega) = \frac{\sigma_e^2(\sigma_e^2 + \bar{\mathbf{a}}^H \bar{\mathbf{a}} \sigma_s^2)}{2T\sigma_s^4[\bar{\mathbf{a}}^H \bar{\mathbf{a}} \bar{\mathbf{a}}^H \mathbf{B}^H \mathbf{B} \bar{\mathbf{a}} - (\bar{\mathbf{a}}^H \mathbf{B}^H \bar{\mathbf{a}})^2]}, \quad (5.40)$$

where $\mathbf{B} = \text{diag}(d_1, d_2, \dots, d_N)$.

We will compare the DOA estimation performance of the proposed strategies with the CRB in (5.40).

5.5 Nonuniform linear arrays

Most existing works concentrate on calibrating model errors for uniform linear arrays. In Sections 5.2-5.4, we have investigated the model error problem for a nested array, which is a class of nonuniform linear arrays. In this section, we will consider the more general case, and specifically, we will consider another kind of nonuniform linear arrays: co-prime arrays.

5.5.1 General case

For any nonuniform linear array, we can always write the signal model as

$$\mathbf{y}(t) = \mathbf{A}\mathbf{x}(t) + \mathbf{e}(t). \quad (5.41)$$

Table 5.3: DOA estimation of nonuniform linear arrays with model errors

```

begin
    Obtain  $\mathbf{y}(t), t = 1, \dots, T$ , and  $\sigma_e^2$  for a given array.
    Calculate sample covariance matrix  $\mathbf{R}_y$ .
    Achieve gain error parameters  $\bar{\Psi}$  by solving (5.15).
    Formulate STLS problem (5.32) based on estimated  $\bar{\Psi}$ .
    do
        Obtain  $\hat{\mathbf{p}}_g$  according to (5.33)
        Obtain  $\hat{\mathbf{E}}$  according to (5.34)
    until A sub-optimal solution is achieved.
end

```

Different linear arrays vary in their sensor position information, namely the exponents of the elements of steering matrix \mathbf{A} . Thus, the analysis is the same as the nested array.

Further, we can obtain the covariance matrix \mathbf{R}_y . As for gain-error estimation, we can always achieve $N(N - 1)/2$ equations by employing the diagonal entries. Thus, similarly, we can construct an over-determined system. As for phase estimation, we again cannot guarantee an over-determined system. Therefore, the sparse total least squares will be exploited to estimate the DOAs. Table 5.3 shows the general algorithm to estimate DOAs and calibrate model errors for nonuniform linear arrays.

Remark 5.3. *Nonuniform linear arrays try to cover a large array aperture with a limited number of sensors. Thus the efficient use of sensors is the priority. However, spatial ambiguity exists due to sensor placement with inter-element distances larger than a half-wavelength. When calibrating model errors for nonuniform linear arrays, we need to pay attention to the sensor positions. For nested arrays, due to the hole-free property of its co-array, we do not have such an issue.*

5.5.2 Co-prime arrays

In this section, we examine co-prime arrays. Consider a linear array with $2M_1 + M_2 - 1$ sensors, where M_1 and M_2 are co-prime integers, and $M_1 < M_2$. These sensors are located

at

$$\{m_1 M_2 d, m_2 M_1 d, 0 \leq m_1 \leq 2M_1 - 1, 0 \leq m_2 \leq M_2 - 1\}. \quad (5.42)$$

Fig. 2.3 illustrates the co-prime array. Note that the two sets of sensors are linearly placed. It has been shown that we can obtain a virtual hole-free uniform linear array with sensors located at

$$\{nd_I, -M_1 M_2 \leq n \leq M_1 M_2\}. \quad (5.43)$$

Since the strategies are similar to the case of nested arrays, we provide only an illustrative example.

Example 5.3. Consider a co-prime array with $M_1 = 4$ and $M_2 = 5$, where the sensors are located at $[0, 4, 5, 8, 10, 12, 15, 16, 20, 25, 30, 35]d_I$. Then, following the steps in the nested array case, we can calculate the indication matrix Γ_y . Next, we can obtain the weight function $w(n)$ and $v_g(n)$, shown in Table 5.4. Note that we consider only the positive sensor positions from 0 to $M_1 M_2 = 20$. We can see that many more equations can be formulated than the number of unknown gain parameters. Further, we can estimate the gain error parameters and DOAs according to Table 5.3.

Table 5.4: Weight function for a co-prime array: $M_1 = 4, M_2 = 5$

| n | 0 | 1 | 2 | 3 | 4 | 5 | 6 | 7 | 8 | 9 | 10 |
|----------|----|----|----|----|----|----|----|----|----|----|----|
| $w(n)$ | 12 | 2 | 2 | 2 | 5 | 7 | 2 | 2 | 4 | 1 | 6 |
| $v_g(n)$ | 66 | 1 | 1 | 1 | 10 | 21 | 1 | 1 | 6 | 0 | 15 |
| n | 11 | 12 | 13 | 14 | 15 | 16 | 17 | 18 | 19 | 20 | — |
| $w(n)$ | 2 | 3 | 1 | 1 | 5 | 2 | 1 | 1 | 1 | 4 | — |
| $v_g(n)$ | 1 | 3 | 0 | 0 | 10 | 1 | 0 | 0 | 0 | 6 | — |

Remark 5.4. The proposed approach is suitable for any nonuniform linear arrays, not limited to the ones with non-hole or partially non-hole co-arrays, such as the nested array case in (5.13) and the co-prime array case in (5.43). The non-hole property of the co-array is necessary for spatial smoothing in MUSIC-based DOA estimation. However, the proposed calibration strategies do not depend on that. In other words, the non-hole property of the co-array of any nonuniform linear arrays affects the spatial smoothing, DOA estimation, and the number of DOFs, rather than the calibration process. We will show this in Section 5.6.5 through numerical examples.

5.6 Numerical examples

In this section, we provide numerical examples of DOA estimation with model errors. We first consider a 2-level nested array with $N = 6$ sensors, where $N_1 = 3$, and $N_2 = 3$. We will consider both MUSIC and sparse recovery methods for the case with only gain errors, and will consider the STLS method for the case with both gain and phase errors. Then, we provide numerical examples of a co-prime array with $M_1 = 4$ and $M_2 = 5$.

5.6.1 Robustness to model errors

In this example, we compare the robustness of the ULA and the nested array with the same number of sensors. Suppose ψ_i are randomly chosen from a uniform distribution with interval $[0, 2]$, and ϕ_i are randomly chosen from a uniform distribution with interval $[0, \pi/3]$. Assume there are $K = 3$ sources with impinging directions $\boldsymbol{\omega} = [-0.4, -0.2, 0]\pi$. The MUSIC spectra of the ULA with model errors and without model errors are depicted in Fig. 5.1, at an SNR of 0dB. The cases for the nested array are depicted in Fig. 5.2. We take the SNR as in (3.25). We can see that the ULA fails to estimate all the sources when there are model errors, whereas the nested array can still resolve the three sources, though with small estimation errors. Apparently, the nested array shows more robust performance than the ULA.

5.6.2 Estimation performance with only gain errors

In this section, we concentrate on the nested array. Assume there are $K = 7$ sources, with DOAs $\boldsymbol{\omega} = [-0.4, -0.25, -0.1, 0.05, 0.2, 0.35, 0.5]\pi$. Gain errors are chosen as $\boldsymbol{\Psi} = \text{diag}\{0.5, 1.3, 1.5, 3.8, 1.1, 1.4\}$, and phase errors are chosen as $\boldsymbol{\Phi} = \mathbf{I}$. We use $T = 1000$ snapshots for estimation. Both MUSIC and sparse recovery approaches are investigated, and the estimation results are shown in Fig. 5.3.

With model errors, the nested array fails to resolve the seven sources correctly with MUSIC, as shown in Fig. 5.3(a). After calibrating the sensor array by estimating gain errors, the

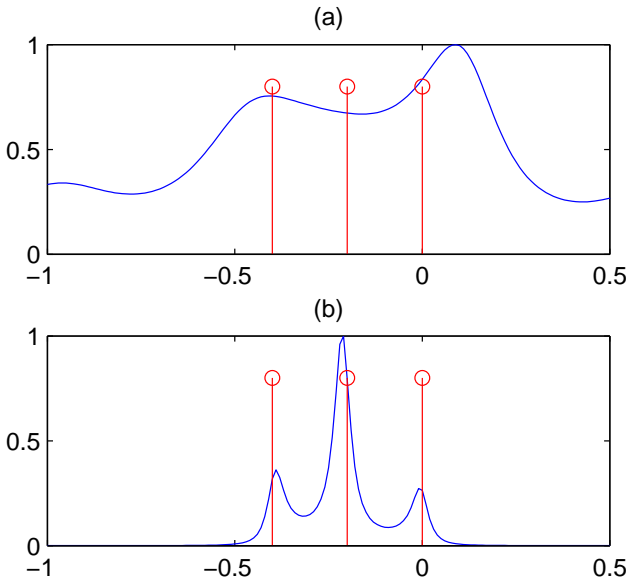


Figure 5.1: MUSIC spectra for a ULA (a) with model errors and (b) without model errors, $N = 6$, $K = 3$, and SNR = 0 dB. The blue lines are the spectra, whereas the red circled stems are the true DOAs. The vertical axis is the normalized spectra, and the horizontal axis is DOAs ($\times \pi$).

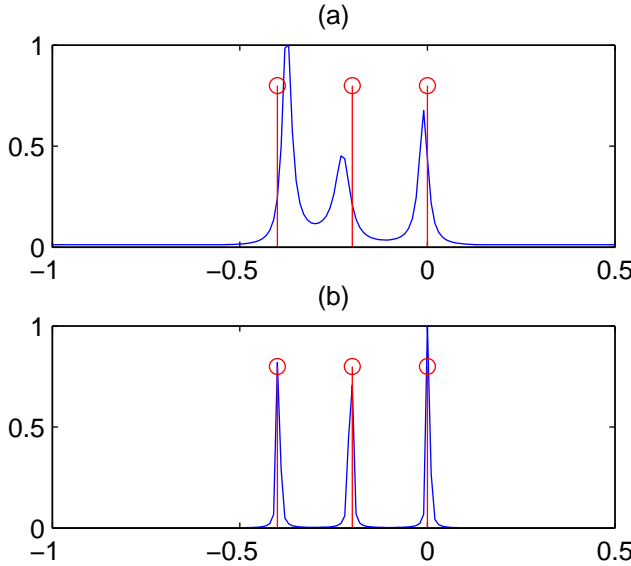


Figure 5.2: MUSIC spectra for a nested array (a) with model errors and (b) without model errors, $N = 6$, $K = 3$, and SNR = 0 dB. The blue lines are the spectra, whereas the red circled stems are the true DOAs. The vertical axis is the normalized spectra, and the horizontal axis is DOAs ($\times \pi$).

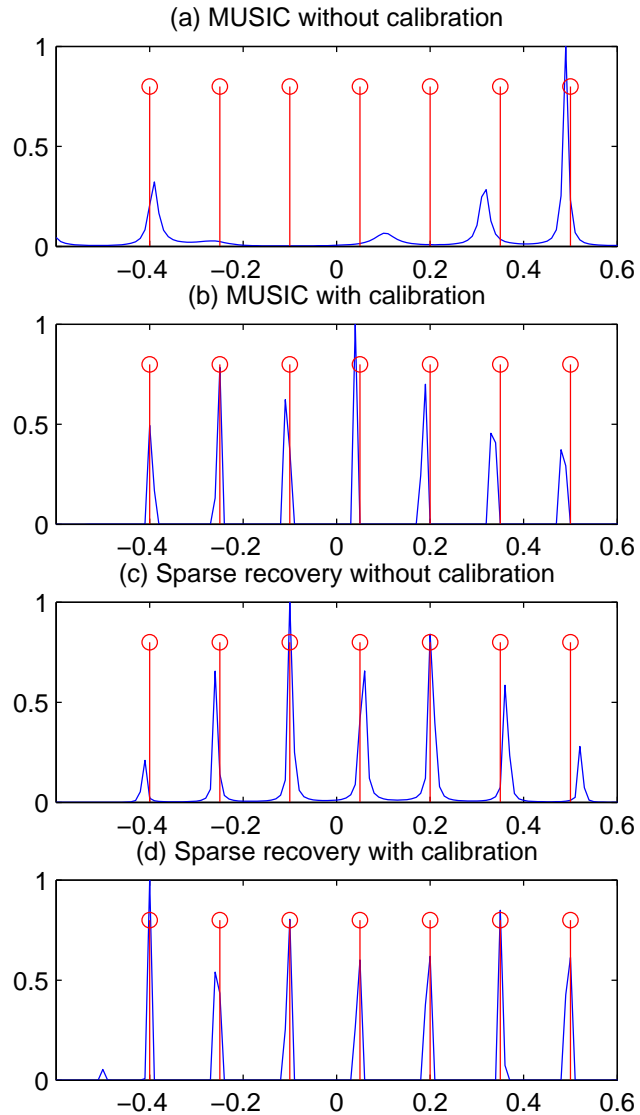


Figure 5.3: MUSIC spectra of a nested array with model errors for four scenarios. $N = 6$, $K = 7$, and SNR = 0 dB. The blue lines are the spectra, whereas the red circled stems are the true DOAs. The vertical axis is the normalized spectra, and the horizontal axis is DOAs ($\times \pi$).

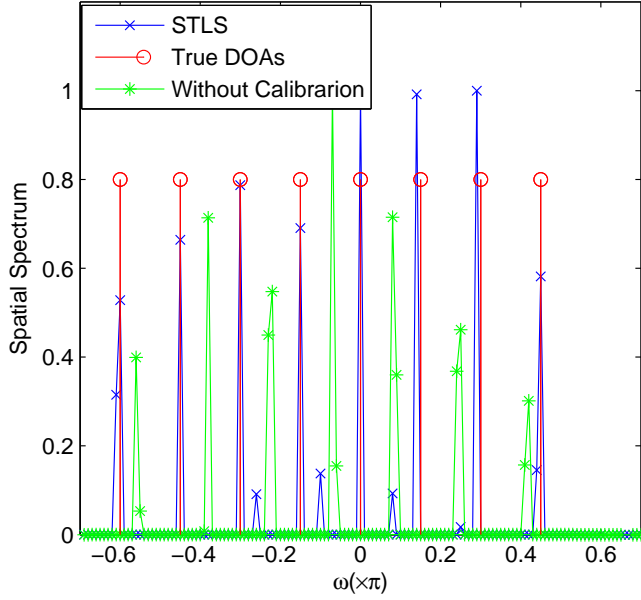


Figure 5.4: Spatial spectra with respect to direction angles for a nested array, using the STLS approach and without calibration, $N = 6$, $K = 8$, SNR = 0 dB.

MUSIC and sparse recovery methods both work well to resolve all the sources. As expected, the sparse recovery strategy performs better than MUSIC.

Next, we consider only one source with DOA $\omega = -0.22\pi$. The gain errors are same as the former example. We run 1500 Monte Carlo simulations, and plot the root mean square error (RMSE) of both MUSIC and sparse recovery, and the CRB with respect to SNR and snapshot number in Fig. 5.5 and Fig. 5.6 respectively. We can see that the performance of sparse recovery and MUSIC is similar, both approaching the CRB at high SNRs and large sample numbers.

5.6.3 Estimation performance with both gain and phase errors

We now assume that both gain and phase errors exist for the nested array, where ψ_i are randomly chosen from a uniform distribution with interval $[0, 5]$, and ϕ_i are randomly chosen from a uniform distribution with interval $[0, \pi/3]$. There are $K = 8$ sources with impinging directions $\boldsymbol{\omega} = [-0.6, -0.45, -0.3, -0.15, 0, 0.15, 0.3, 0.45]\pi$. For the STLS approach, we

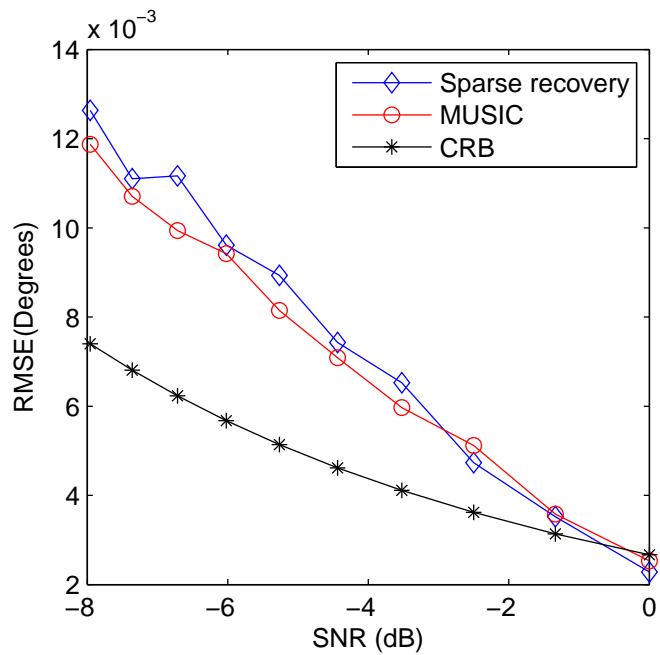


Figure 5.5: Performance of MUSIC and sparse recovery, and CRB versus SNR, with $K = 1$, $T = 500$.

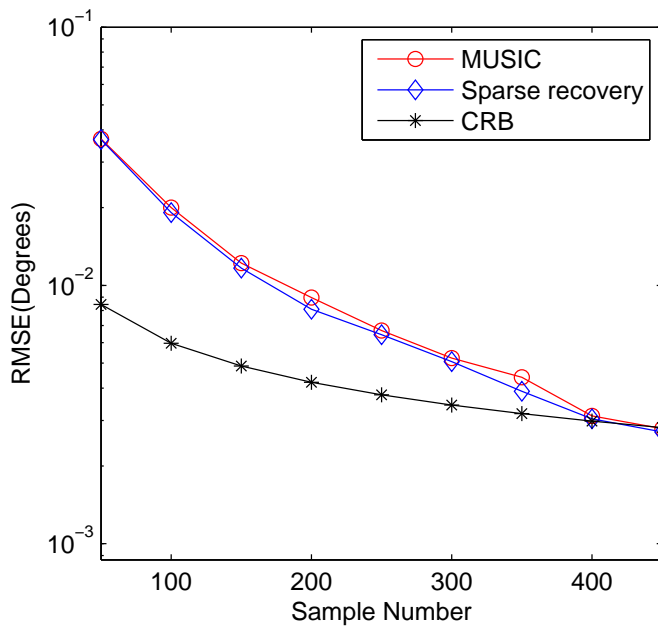


Figure 5.6: Performance of MUSIC and sparse recovery, and CRB versus sample number, with $K = 1$, $\text{SNR} = 0\text{dB}$.

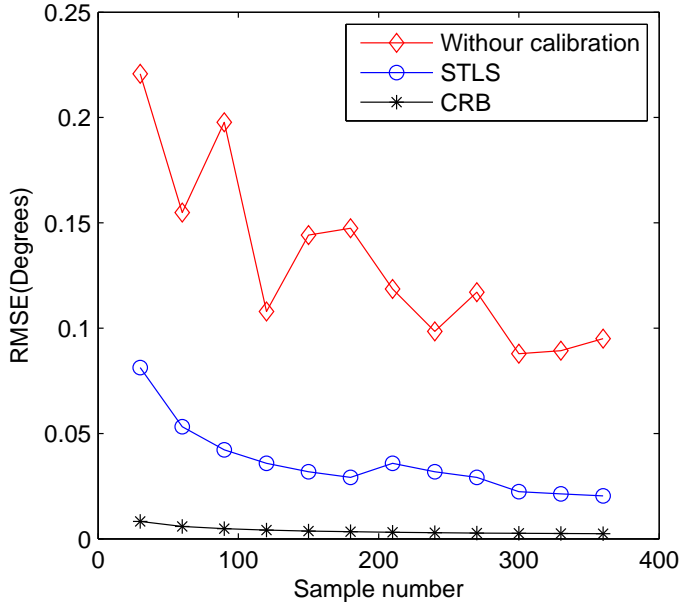


Figure 5.7: Performance with calibration by STLS, without calibration, and CRB versus sample number, with $K = 1$, SNR = 0dB.

conducted 10 iterations, and the estimation performance is shown in Fig. 5.4. The results show that our STLS method calibrates the sensor array errors well.

Additionally, we consider the performance of STLS with only one source at $\omega = -0.22\pi$, compared to the CRB. The results are shown in Fig. 5.7. We can see that STLS calibrates the model errors well, and improves the estimation performance greatly, compared to the non-calibration case. However, there is still some gap between its RMSE and the CRB.

5.6.4 Co-prime array

For co-prime arrays, we consider only two cases: one is with only gain errors, and the other is with both gain and phase errors. We expect to obtain improvements similar to those for nested arrays.

First we consider the case with only gain errors. Assume $K = 17$ sources exist, with $\sin\theta$ uniformly distributed between -0.8 and 0.9 . Gain errors are chosen as

$$\Psi = \text{diag}\{0.5, 1.3, 1.5, 3.8, 1.1, 1.4, 0.5, 1.3, 1.5, 3.8, 1.1, 1.4\},$$

and phase errors are chosen as $\Phi = \mathbf{I}$. Both MUSIC and sparse recovery approaches are investigated, and the estimation results are shown in Fig. 5.8. We can see that the results are the same as the nested array case in Fig. 5.3.

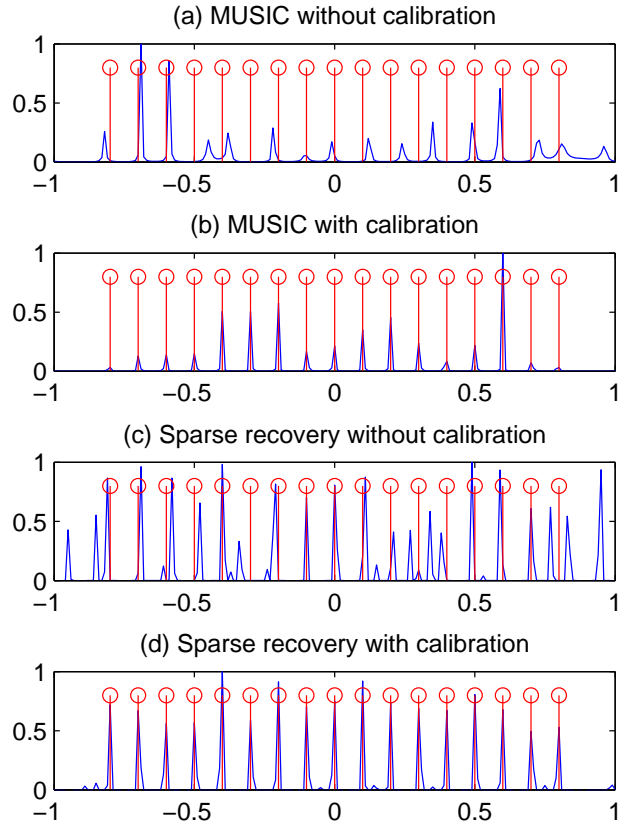


Figure 5.8: MUSIC spectra of a co-prime array with model errors for four scenarios. $M_1 = 4$, $M_2 = 5$, $K = 17$, and SNR = 0 dB. The blue lines are the spectra, whereas the red circled stems are the true DOAs. The vertical axis is the normalized spectra, and the horizontal axis is DOAs ($\times\pi$).

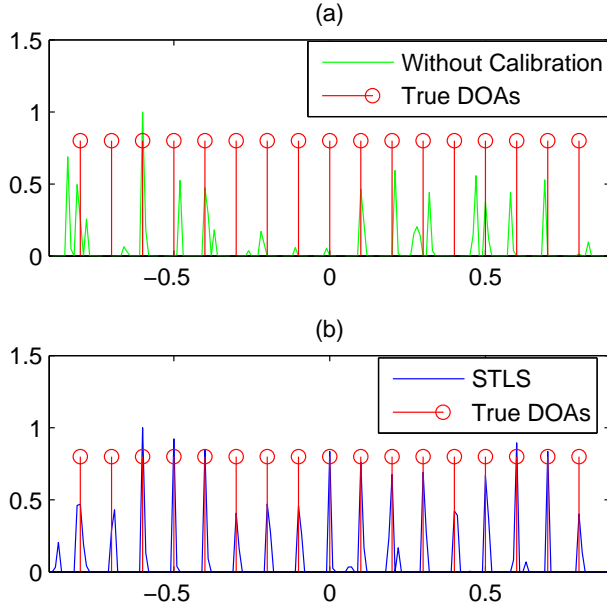


Figure 5.9: Spatial spectra with respect to direction angles ($\times \pi$), using the STLS approach and without calibration, $M_1 = 4$, $M_2 = 5$, $K = 17$, and SNR = 0 dB.

Next, we consider the case with both gain and phase errors. The results are shown in Fig. 5.9. The proposed strategy calibrates the sensor array errors well.

5.6.5 Arbitrary nonuniform linear array

To show that our proposed strategies are not confined to non-hole co-array cases, we provide examples for an arbitrary nonuniform linear array with five sensors, located at $[0, 1, 3, 5, 8]d$, with gain errors $\Psi = \text{diag}\{0.5, 1.3, 3.8, 1.5, 1.1\}$ and phase errors randomly chosen from a uniform distribution with interval $[0, \pi/6]$. Assume three sources exist, with DOAs $\omega = [-0.4, -0.25, 0.3]$. In Fig. 5.10, we show the DOA estimation based on MUSIC for the case with gain errors only. In Fig. 5.11, we show the DOA estimation based on STLS for the case with both gain and phase errors. We can see that both scenarios validate the effectiveness of our proposed methods.

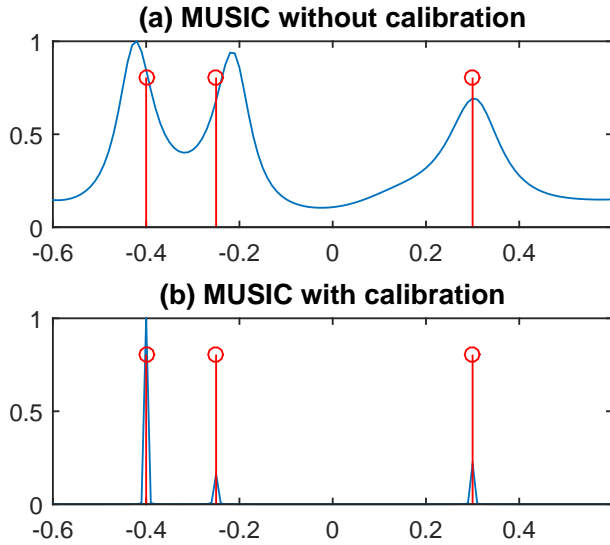


Figure 5.10: MUSIC spectra with respect to DOAs for a nonuniform linear array with gain errors only. The blue lines are the spectra, whereas the red circled stems are the true DOAs. The vertical axis is the normalized spectra, and the horizontal axis is DOAs ($\times \pi$).

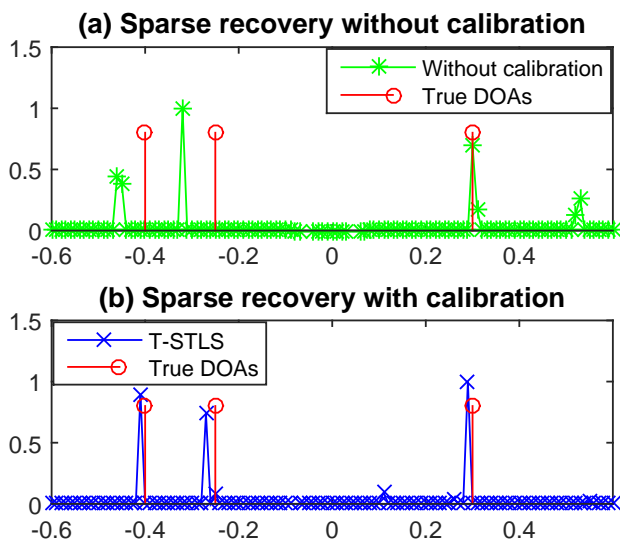


Figure 5.11: Spatial spectra with respect to DOAs ($\times \pi$) for a nonuniform linear array with both gain and phase errors.

5.7 Summary

In this chapter [56], we investigated the practical problem of DOA estimation with model errors for nested arrays, and then extended the proposed strategies to the general case of nonuniform linear arrays. We provided detailed analysis of the error effect on nested arrays, and proposed robust self-calibration algorithms to estimate the model errors and the DOAs as well. The CRB was also derived to analyze the estimation performance of the proposed strategies. The general case of nonuniform linear arrays, including co-prime arrays, has also been considered. Numerical examples demonstrated the effectiveness of our strategies. Additionally, the nested array showed more robust performance than the ULA with the same number of sensors.

Chapter 6

Nested Vector-Sensor Array Processing via Tensor Modeling

In this chapter, we extend the nested array strategy to vector sensors in a novel tensor framework⁴

6.1 Introduction

Vector sensors, which measure multiple physical components, have proven useful in electromagnetic, sonar, and seismological applications. Many array processing techniques have been developed for source localization and polarization estimation using vector sensors. An electromagnetic (EM) vector-sensor array, which consists of six spatially collocated antennas, measures the complete electric and magnetic fields induced by EM signals. The EM vector-sensor array was first introduced by Nehorai and Paldi in [57], where a cross-product based direction-of-arrival (DOA) estimation method applicable to single-source scenarios was proposed. MUSIC-based algorithms were proposed by Wong and Zoltowski [58],[59]. Different ESPRIT-based methods for DOA estimation have been developed separately in [60]-[62]. [63] and [64] investigated identifiability issues, providing some upper bounds for the number of sources identifiable. Another important vector-sensor array is the acoustic vector-sensor array, first proposed by Nehorai and Paldi [65]. The idea of using vector sensors that measure both pressure and velocity has been widely used to solve the passive DOA

⁴This chapter is based on K. Han and A. Nehorai, “Nested vector-sensor array processing via tensor modeling,” IEEE Trans. on Signal Processing, Vol. 62, pp. 2542-2553, May 2014. © IEEE 2014.

estimation problem [66]-[70]. In this chapter, we will mainly focus on applications of these two vector-sensor arrays.

Most of the previous work on DOA estimation with vector-sensor arrays uses matrix techniques directly derived from scalar-sensor array processing. Such a method is based on a long vector, which is concatenated with all components of the vector-sensor array. A method that keeps the multidimensional structures for data organization and processing was proposed in [71] using vector sensors for seismic sources, where the received measurements are represented as a multidimensional tensor. A version of the MUSIC algorithm adapted to the multilinear structure was proposed based on the higher-order eigenvalue decomposition (HOEVD) of a fourth-order tensor.

A tensor is a multidimensional array [72], [73], for which multilinear algebra provides a good framework to conserve the multidimensional structure of the information. Decompositions of higher-order tensors have been shown to be of great interest in signal processing [74]-[79]. Two main decompositions are CANDECOMP/PARAFAC (CP) [80], [81] and Higher Order Singular Value Decomposition (HOSVD) [82], both of which can be considered to be higher-order generalizations of the matrix singular value decomposition (SVD). One DOA estimation strategy based on HOSVD was proposed in [79], where the tensor structure of the data was well exploited, and the HOSVD was applied to the covariance tensor. Another estimation strategy based on HOSVD was proposed in [83], where the HOSVD was applied to the measurement tensor. Though both approaches use HOSVD, they are different strategies. Another decomposition, namely HOEVD, was defined in [73]. It uses the concept of simple orthogonality, and allows detection of an increased number of sources [71]. However, this approach was shown to be equivalent to using matrix formulism on a “long-vector” in [84]. Additionally, it has been shown that the HOSVD method in [79] is more effective than the HOEVD method. Therefore, in this chapter, we will use the HOSVD-based strategy proposed in [79].

In the existing literature, the nested-array strategy was applied only to scalar-sensor arrays, including one-dimensional and two-dimensional spatial cases. However, it is of great analytical and practical interest to consider the vector-sensor array model employing the idea of the nested array. In this chapter, we will apply the nested-array concept to the vector-sensor array. More specifically, we will provide a detailed analysis for the construction of the signal

model of the nested vector-sensor array. We will see that multilinear algebra plays an important role in the signal processing of the proposed array. Similar to the case of the nested scalar-sensor array, the nested vector-sensor array shows superior performance in terms of DOF and estimation resolution.

6.2 Signal model

In this section, we construct the signal model of the proposed nested vector-sensor array.

6.2.1 Matrix-based vector-sensor array

We assume there is a linear array with N vector sensors. The output of each vector sensor is an N_c -dimensional vector which contains all the N_c components. We assume K far-field sources are in the surveillance region, impinging on this linear array from directions $\{(\phi_k, \theta_k), k = 1, \dots, K\}$, where ϕ_k and θ_k represent the azimuth and the elevation angles of the k th signal respectively. We assume $-\pi \leq \phi \leq \pi$ and $-\pi/2 \leq \theta \leq \pi/2$. The measurement received at the array at time t can be modeled as [61]

$$\mathbf{y}(t) = \mathbf{A}\mathbf{x}(t) + \mathbf{e}(t), \quad (6.1)$$

where $\mathbf{y}(t)$ and $\mathbf{e}(t)$ are $NN_c \times 1$ complex vectors, respectively, and $\mathbf{x}(t)$ is the $K \times 1$ source vector. The $NN_c \times K$ array manifold \mathbf{A} can be expressed as

$$\mathbf{A} = [\mathbf{a}_1, \dots, \mathbf{a}_k, \dots, \mathbf{a}_K], \quad (6.2)$$

where $\mathbf{a}_k = \mathbf{d}_k \otimes \mathbf{p}_k$, with

$$\mathbf{d}_k = [e^{j2\pi \mathbf{u}_k^T \mathbf{r}_1 / \lambda}, \dots, e^{j2\pi \mathbf{u}_k^T \mathbf{r}_N / \lambda}]^T, \text{ and}$$

$$\mathbf{p}_k = [p_{k1}, p_{k2}, \dots, p_{kN_c}]^T.$$

Here, \mathbf{a}_k is the $NN_c \times 1$ steering vector of the array associated with a signal coming from the direction (ϕ_k, θ_k) . \mathbf{d}_k denotes the phase delay of the k th signal at the N sensors with respect

to the origin, λ represents the wavelength of the signals, and \mathbf{r}_n denotes the coordinates of the n th sensor. The vector $\mathbf{u}_k = [\cos\phi_k \cos\theta_k, \sin\phi_k \cos\theta_k, \sin\theta_k]^T$ is the unit vector at the sensor pointing towards the k th signal. \mathbf{p}_k , which varies for different kinds of vector sensors, is the steering vector of a single vector sensor located at the origin. Each element of \mathbf{p}_k corresponds to one component of a vector sensor. Next, we will consider applications to both EM and acoustic vector sensors. When we consider EM or acoustic vector sensors, the differences from the original signal model are the steering vectors. Thus, we will present the array steering vectors for both EM and acoustic vector-sensor arrays.

Electromagnetic vector sensors

Electromagnetic vector sensors measure the complete electromagnetic field [57]. We consider a linear array with N EM vector sensors, each having $N_c = 6$ components. Here, we consider polarized signals.

The array steering vector can be written as $\mathbf{a}_k = \mathbf{d}_k \otimes \mathbf{p}_k$, with

$$\mathbf{p}_k = \mathbf{V}_k \boldsymbol{\rho}_k, \quad (6.3)$$

where

$$\mathbf{V}_k = \begin{pmatrix} -\sin\phi_k & -\cos\phi_k \sin\theta_k \\ \cos\phi_k & -\sin\phi_k \sin\theta_k \\ 0 & \cos\theta_k \\ -\cos\phi_k \sin\theta_k & \sin\phi_k \\ -\sin\phi_k \sin\theta_k & -\cos\phi_k \\ \cos\theta_k & 0 \end{pmatrix}, \quad (6.4)$$

and

$$\boldsymbol{\rho}_k = [\cos\gamma_k \ \sin\gamma_k e^{j\eta_k}]^T. \quad (6.5)$$

Here, \mathbf{a}_k is the $6N \times 1$ steering vector of the array associated with a polarized signal coming from the direction (ϕ_k, θ_k) with polarization (γ_k, η_k) , where $\gamma_k \in [0, 2\pi]$ and $\eta_k \in (-\pi, \pi]$ are polarization parameters referred to as the auxiliary polarization angle and polarization phase difference, respectively. \mathbf{V}_k is the steering matrix of one EM vector sensor associated with the k th signal. $\boldsymbol{\rho}_k$ is the polarization vector for the k th signal.

Acoustic Vector Sensors

We assume there is a linear array with N acoustic vector sensors. The output of each vector sensor is an N_c -dimensional vector which contains $N_c = 4$ components: the acoustic pressure and the acoustic particle-velocity vector [66].

The array steering vector can be written as $\mathbf{a}_k = \mathbf{d}_k \otimes \mathbf{p}_k$, with

$$\mathbf{p}_k = [1, \mathbf{u}_k^T]^T, \quad (6.6)$$

which is the steering vector of a single vector sensor located at the origin.

6.2.2 Tensor-based vector-sensor array

In this section, we propose a tensorial model for sources impinging on a vector-sensor array based on model (6.1).

First, we consider only one source signal x_k . We set the $N \times N_c$ array manifold matrix \mathbf{A}_k for the k th source as the outer product of the phase delay vector \mathbf{d}_k and the steering vector \mathbf{p}_k :

$$\mathbf{A}_k = \mathbf{d}_k \circ \mathbf{p}_k. \quad (6.7)$$

Then, we can get the $N \times N_c$ measurement matrix at time t :

$$\mathbf{Y}_k(t) = \mathbf{A}_k x_k(t) + \mathbf{E}_k(t). \quad (6.8)$$

$\mathbf{Y}_k(t)$ and $\mathbf{E}_k(t)$ are the corresponding measurements and noise at all the components of all the sensors.

Considering K sources in the surveillance region, we can get the summed measurement matrix as

$$\mathbf{Y}(t) = \sum_{k=1}^K \mathbf{A}_k x_k(t) + \mathbf{E}_k(t). \quad (6.9)$$

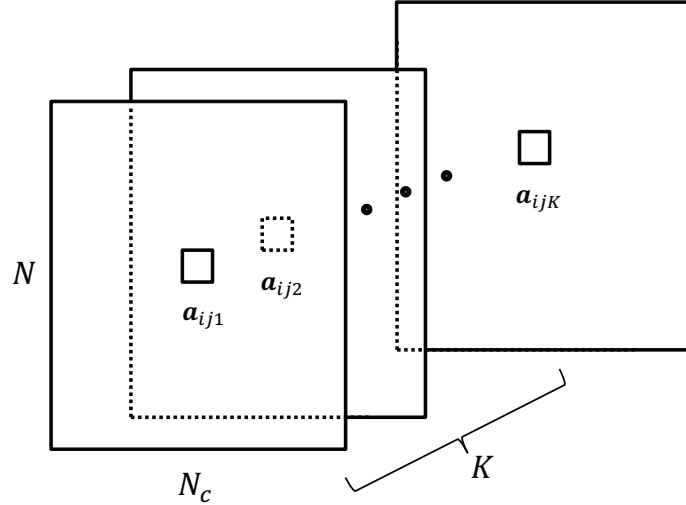


Figure 6.1: The structure of the $N \times N_c \times K$ tensor \mathcal{A} .

We further transform model (6.9) to the tensor form:

$$\mathbf{Y}(t) = \mathcal{A} \times_3 \mathbf{x}(t) + \mathbf{E}(t), \quad (6.10)$$

where \mathcal{A} is a $N \times N_c \times K$ tensor with element $a_{i,j,k} = (\mathbf{A}_k)_{i,j}$, shown in Fig. 6.1. While $\mathbf{Y}(t)$ is a matrix, it is decomposed in a tensor form to explicitly bring out the additional dimension.

Comparing models (6.1) and (6.10), we can see they contain the same amount of statistical information. In order to find the DOA of sources and the source number, we will consider the second-order statistics through a “spectral tensor”.

6.2.3 Tensor-based nested vector-sensor array

Now we consider a two-level nested vector-sensor array. Instead of N scalar vectors as in Fig. 2.2, we consider N vector sensors, where again each vector sensor has N_c elements. Suppose the sensors are located along the z -axis:

$$\begin{aligned} & \{(0, 0, d_I), (0, 0, 2d_I), \dots, (0, 0, N_1 d_I), \\ & (0, 0, (N_1 + 1)d_I), \dots, (0, 0, N_2(N_1 + 1)d_I)\}, \end{aligned}$$

where $d_I = \lambda/2$. Then the phase delay vector for the k th signal is

$$\mathbf{d}_k = [e^{j\pi\sin\theta_k} \ e^{j2\pi\sin\theta_k} \ \dots \ e^{jN_1\pi\sin\theta_k} \ e^{j(N_1+1)\pi\sin\theta_k} \\ e^{j2(N_1+1)\pi\sin\theta_k} \ \dots \ e^{jN_2(N_1+1)\pi\sin\theta_k}]^T. \quad (6.11)$$

Based on the phase delay vector, we can write the manifold matrix \mathbf{A}_k in (6.7):

$$\mathbf{A}_k = \begin{pmatrix} p_{k1}e^{j\pi\sin\theta_k} & \dots & p_{kN_c}e^{j\pi\sin\theta_k} \\ p_{k1}e^{j2\pi\sin\theta_k} & \dots & p_{kN_c}e^{j2\pi\sin\theta_k} \\ \vdots & \ddots & \vdots \\ p_{k1}e^{jN_1\pi\sin\theta_k} & \dots & p_{kN_c}e^{jN_1\pi\sin\theta_k} \\ p_{k1}e^{j(N_1+1)\pi\sin\theta_k} & \dots & p_{kN_c}e^{j(N_1+1)\pi\sin\theta_k} \\ \vdots & \ddots & \vdots \\ p_{k1}e^{jN_2(N_1+1)\pi\sin\theta_k} & \dots & p_{kN_c}e^{jN_2(N_1+1)\pi\sin\theta_k} \end{pmatrix}.$$

We suppose the source signals $\mathbf{x}(t)$ are all independent of each other. The noise $\mathbf{e}(t)$ is assumed to be temporally and spatially white, and uncorrelated with the sources. Based on model (6.10), we get the interspectral tensor \mathcal{R} , which is the fourth-order complex tensor of size $N \times N_c \times N \times N_c$, defined as the second-order automoments and crossmoments between all the components on all sensors, as follows:

$$\mathcal{R} = \mathbb{E}[\mathbf{Y} \circ \mathbf{Y}^*], \quad (6.12)$$

where the element of \mathcal{R} is given by

$$r_{i_1 i_2 i_3 i_4} = \mathbb{E}[y_{i_1 i_2} y_{i_3 i_4}^*]. \quad (6.13)$$

Note that \mathcal{R} is a tensorial version of the covariance matrix $\mathbf{R}_{\mathbf{y}}$.

Substituting (6.10) into (6.12) yields:

$$\begin{aligned}
\mathcal{R} &= \mathbb{E}[\mathbf{Y} \circ \mathbf{Y}^*] \\
&= \mathbb{E}[(\mathcal{A} \times_3 \mathbf{x} + \mathbf{E}) \circ (\mathcal{A} \times_3 \mathbf{x} + \mathbf{E})^*] \\
&= \mathbb{E}[(\mathcal{A} \times_3 \mathbf{x}) \circ (\mathcal{A} \times_3 \mathbf{x})^* + (\mathcal{A} \times_3 \mathbf{x}) \circ \mathbf{E}^* + \\
&\quad \mathbf{E} \circ (\mathcal{A} \times_3 \mathbf{x})^* + \mathbf{E} \circ \mathbf{E}^*] \\
&= \mathbb{E}[(\mathcal{A} \times_3 \mathbf{x}) \circ (\mathcal{A} \times_3 \mathbf{x})^*] + \mathbb{E}[\mathbf{E} \circ \mathbf{E}^*] \tag{6.14} \\
&= \mathcal{A} \times_3 \mathbb{E}[\mathbf{x} \circ \mathbf{x}^*] \dot{\times}_3 \mathcal{A}^* + \mathbb{E}[\mathbf{E} \circ \mathbf{E}^*], \tag{6.15}
\end{aligned}$$

where $\mathbb{E}[\mathbf{x} \circ \mathbf{x}^*] = \text{diag}(\sigma_1^2, \sigma_2^2, \dots, \sigma_K^2)$ is the covariance matrix of the sources. Equation (6.14) is due to the assumptions that sources and noise are independent, sources are zero mean Gaussian, and noise is white Gaussian. We show the derivation of (6.15) in Appendix B.

Now, we do the mode-2 matricization of tensor \mathcal{R} :

$$\begin{aligned}
\mathbf{Q} &\triangleq \mathcal{R}_{(2)}^T \\
&= (\mathcal{A}_{(3)}^H \odot \mathcal{A}) \times_3 \mathbf{s} + \sigma_e^2 \vec{\mathbf{I}}, \tag{6.16}
\end{aligned}$$

where \mathbf{Q} is a $N_c N^2 \times N_c$ matrix. Here $\mathbf{s} = [\sigma_1^2 \ \sigma_2^2 \ \dots \ \sigma_K^2]^T$ and $\vec{\mathbf{I}}$ is a $N_c N^2 \times N_c$ matrix defined as

$$\vec{\mathbf{I}} = \begin{pmatrix} \vec{\mathbf{1}} & & \\ & \vec{\mathbf{1}} & \\ & & \ddots \\ & & & \vec{\mathbf{1}} \end{pmatrix}_{N_c N^2 \times N_c}, \tag{6.17}$$

where $\vec{\mathbf{1}} = [\mathbf{e}_1^T \ \mathbf{e}_2^T \ \dots \ \mathbf{e}_N^T]^T$ with \mathbf{e}_n^T being a $N \times 1$ column vector of all zeros except for a 1 at the n th position. Following the definition of the extended Khatri-Rao product, we can see the tensor $\mathcal{A}_{(3)}^H \odot \mathcal{A}$ is of dimension $N_c N^2 \times N_c \times K$. Thus, after multiplying the third dimension by s , the tensor becomes a matrix. The derivation of (6.16) is shown in Appendix C.

Comparing (6.16) with (6.10), we can say that \mathbf{Q} in (6.16) behaves like the signal received at a longer vector-sensor array whose manifold is given by $\mathcal{A}_{(3)}^H \odot \mathcal{A}$. The equivalent source signal vector is represented by \mathbf{s} , and the noise becomes a deterministic matrix given by $\sigma_e^2 \bar{\mathbf{I}}$.

Looking deeply through the structure of tensor $\mathcal{A}_{(3)}^H \odot \mathcal{A}$, we can find there are N_c sets of horizontal slices, each corresponding to one component and containing N^2 slices. We provide the internal analysis of $\mathcal{A}_{(3)}^H \odot \mathcal{A}$ in Appendix D. Within each set, the distinct horizontal slices behave like the manifold of a longer vector-sensor array whose sensor locations are given by the distinct values in the set $\{\mathbf{r}_i - \mathbf{r}_j, 1 \leq i, j \leq N\}$. This array is precisely the difference co-array of the original array [85]. Hence, instead of model (6.10), we will apply DOA estimation and source number detection to the data in model (6.16), which provides more DOFs than a ULA.

6.3 Source detection and DOA estimation

In this section, we will conduct source number detection and DOA estimation based on the nested vector-sensor array signal model (6.16). To exploit the increased DOFs offered by the co-array, we propose to apply the spatial smoothing technique in a new fashion, as presented in [21]. Before conducting source number detection and DOA estimation, we present the higher-order singular value decomposition (HOSVD) of tensors [79].

6.3.1 Spatial smoothing

Considering one set of horizontal slices in tensor $\mathcal{A}_{(3)}^H \odot \mathcal{A}$, with $\bar{N} \triangleq N^2/4 + N/2$, we construct a new $(2\bar{N} - 1) \times N_c \times K$ tensor $\bar{\mathcal{A}}$, following the procedure in Appendix E. Equivalently, we can get a new model by removing the corresponding rows from the observation matrix \mathbf{Q} and sorting them accordingly:

$$\bar{\mathbf{Q}} = \bar{\mathcal{A}} \times_3 \mathbf{s} + \sigma_e^2 \bar{\mathbf{E}}, \quad (6.18)$$

where $\bar{\mathbf{E}} \in \mathbb{R}^{(2\bar{N}-1) \times N_c}$ is a matrix with all zeros except for a 1 at the position $(\bar{N}, 1)$. The difference co-array of this 2-level nested array has sensors located at

$$(-\bar{N} + 1)d_I, \dots, -d_I, 0, d_I, \dots, (\bar{N} - 1)d_I.$$

We now divide these $2\bar{N} - 1$ sensors into \bar{N} overlapping subarrays, where the l th subarray has sensors located at

$$\{(-l + 1 + n)d_I, n = 0, 1, \dots, \bar{N} - 1\}.$$

We can see that each subarray has \bar{N} sensors. The l th subarray corresponds to the $(\bar{N} - l + 1)$ th to $(2\bar{N} - l)$ th rows of $\bar{\mathbf{Q}}$, denoted as

$$\bar{\mathbf{Q}}_l = \bar{\mathbf{A}}_l \times_3 \mathbf{s} + \sigma_e^2 \bar{\mathbf{E}}_l, \quad (6.19)$$

where $\bar{\mathbf{E}}_l$ is a $\bar{N} \times N_c$ matrix, with all zeros except for a 1 at position $(l, 1)$. In Appendix F, we show that the l th subarray is related to the first subarray by

$$\bar{\mathbf{A}}_l = \bar{\mathbf{A}}_1 \times_3 \Phi^{l-1}, \quad (6.20)$$

where

$$\Phi = \begin{pmatrix} e^{-j\pi \sin \theta_1} & & & \\ & e^{-j\pi \sin \theta_2} & & \\ & & \ddots & \\ & & & e^{-j\pi \sin \theta_K} \end{pmatrix}. \quad (6.21)$$

Further we get

$$\bar{\mathbf{Q}}_l = \bar{\mathbf{A}}_1 \times_3 \Phi^{l-1} \mathbf{s} + \sigma_e^2 \bar{\mathbf{E}}_l. \quad (6.22)$$

We define that

$$\mathcal{R}_l \triangleq \bar{\mathbf{Q}}_l \circ \bar{\mathbf{Q}}_l^*. \quad (6.23)$$

Taking the average of \mathcal{R}_l over all l , we get

$$\mathcal{T} \triangleq \frac{1}{\bar{N}} \sum_{l=1}^{\bar{N}} \mathcal{R}_l. \quad (6.24)$$

We call the $\bar{N} \times N_c \times \bar{N} \times N_c$ tensor \mathcal{T} the spatially smoothed interspectral tensor. Note that the tensor \mathcal{T} is quite different from a fourth order cumulant. We will use it to conduct source number detection and DOA estimation. We would like to clarify that the operations defined in this section for spatial smoothing are used to exploit the increased DOFs provided by the nested array. They themselves do not contribute to the DOF. Additionally, the Vandermonde structure of the array manifold $\bar{\mathcal{A}}_l$ guarantees the unique source localization.

Note that we have N_c set of horizontal slices. Each of them corresponds to one component, and can be used to derive a spatially smoothed interspectral tensor \mathcal{T} . Without loss of generality, we will consider using the first set in the following sections. It has been shown that a 2-level nested array with N scalar sensors can provide \bar{N} DOFs. Therefore, based on \mathcal{T} , we expect to estimate up to $\bar{N} - 1$ sources as well, by using the HOSVD method presented in the next section.

6.3.2 Higher-order singular value decomposition

HOSVD, as stated in [79], efficiently exploits the tensor structure of the multidimensional data. The HOSVD of the spatially smoothed interspectral tensor \mathcal{T} can be written as

$$\mathcal{T} = \mathcal{K} \times_1 \mathbf{U}_1 \times_2 \mathbf{U}_2 \times_3 \mathbf{U}_3 \times_4 \mathbf{U}_4, \quad (6.25)$$

where $\mathbf{U}_1, \mathbf{U}_3 \in \mathbb{C}^{\bar{N} \times \bar{N}}$, and $\mathbf{U}_2, \mathbf{U}_4 \in \mathbb{C}^{N_c \times N_c}$ are orthonormal matrices, provided by the singular value decomposition of the i -dimension unfolding of tensor \mathcal{T} :

$$\mathcal{T}_{(i)} = \mathbf{U}_i \boldsymbol{\Lambda}_i \mathbf{U}_i^H. \quad (6.26)$$

$\mathcal{K} \in \mathbb{C}^{\bar{N} \times N_c \times \bar{N} \times N_c}$ is the core tensor. Since \mathcal{T} is an Hermitian tensor, i.e., $t_{i_1, i_2, i_3, i_4} = t_{i_3, i_4, i_1, i_2}^*$, $\forall i_1, i_2, i_3, i_4$, the HOSVD of \mathcal{T} can be written as

$$\mathcal{T} = \mathcal{K} \times_1 \mathbf{U}_1 \times_2 \mathbf{U}_2 \times_3 \mathbf{U}_1^* \times_4 \mathbf{U}_2^*. \quad (6.27)$$

6.3.3 Source number detection using SORTE

For source number detection, we use the sample interspectral tensor, calculated from the measurements:

$$\hat{\mathcal{R}} = \frac{1}{T} \sum_{t=1}^T \mathbf{Y}(t) \circ \mathbf{Y}(t)^*, \quad (6.28)$$

where T is the number of snapshots. Based on $\hat{\mathcal{R}}$, following (6.16), (6.18), and (6.22)-(6.24), we will obtain the sample spatially smoothed interspectral tensor $\hat{\mathcal{T}}$. Further, we get the sample matrices $\hat{\Lambda}_i$ and $\hat{\mathbf{U}}_i$, and we write

$$\hat{\Lambda}_1 = \text{diag}(\hat{\lambda}_1, \hat{\lambda}_2, \dots, \hat{\lambda}_{\bar{N}}). \quad (6.29)$$

Suppose the eigenvalues are sorted decreasingly:

$$\hat{\lambda}_1 \geq \hat{\lambda}_2 \geq \dots \geq \hat{\lambda}_K > \hat{\lambda}_{K+1} = \dots = \hat{\lambda}_{\bar{N}}.$$

Based on the eigenvalues, we apply the SORTE algorithm in Section 2.1.2.

The algorithm for source number detection using SORTE based on a 2-level nested vector-sensor array is shown in Table 6.1.

6.3.4 DOA estimation using tensor-MUSIC

DOA estimation is based on the condition that we already know, or have already estimated, the source number. MUSIC is one of the earliest proposed subspace-based algorithms for DOA estimation.

Suppose we know the source number is K . Based on $\hat{\mathbf{U}}_1$ and $\hat{\mathbf{U}}_2$, we obtain the approximation matrices $\tilde{\hat{\mathbf{U}}}_1$ and $\tilde{\hat{\mathbf{U}}}_2$ by truncating the first r_1 and r_2 columns respectively. Here r_1 and r_2 are the number of important values in the SVD of $\hat{\mathcal{R}}_{(1)}$ and $\hat{\mathcal{R}}_{(2)}$, where r_1 is equal to the source number K .

Table 6.1: Algorithm for Source Number Detection Using SORTE with a 2-level Nested Vector-sensor Array

```

begin
    Obtain  $T, \mathbf{Y}$ ;
    Calculate the sample interspectral tensor  $\hat{\mathcal{R}}$  using (6.28);
    Obtain the mode-2 matricization  $\hat{\mathbf{Q}}$  according to (6.16);
    Obtain the spatial smoothing interspectral tensor  $\hat{\mathcal{T}}$  in (6.24);
    Conduct HOSVD with (6.27) on  $\hat{\mathcal{T}}$  and obtain  $\hat{\Lambda}_1$  in (6.29);
    Calculate SORTE( $k$ ),  $k = 1, \dots, \bar{N} - 2$  following (2.23);
    Decide the source number  $\hat{K}$  following (2.25).
end

```

Thus, we can construct the tensor-MUSIC (TM) estimator as

$$\text{TM}(\theta, \phi) = \frac{1}{\mathbf{A}(\theta, \phi) \times_1 \tilde{\hat{\mathbf{U}}}_1 \tilde{\hat{\mathbf{U}}}_1^H \times_2 \tilde{\hat{\mathbf{U}}}_2 \tilde{\hat{\mathbf{U}}}_2^H} \quad (6.30)$$

with the steering matrix

$$\mathbf{A}(\theta, \phi) = \mathbf{d}(\theta) \circ \mathbf{p}(\theta, \phi), \quad (6.31)$$

where

$$\mathbf{d}(\theta) = [1, e^{j\pi\sin\theta}, e^{j2\pi\sin\theta}, \dots, e^{j(\bar{N}-1)\pi\sin\theta}]. \quad (6.32)$$

Then, to obtain the DOA estimates, we conduct an exhaustive search over the impinging direction space, compute the MUSIC spectrum for all direction angles, and find the K largest peaks. As for the polarized sources using EM vector sensors, the steering matrix in (6.31) will also be related to the polarization parameters. We can use similar strategies to estimate them.

The algorithm is shown in Table 6.2.

Table 6.2: Algorithm for DOA Estimation Using Tensor MUSIC with a 2-level Nested Vector-sensor Array

```

begin
    Obtain  $T$ ,  $\mathbf{Y}$ ;
    Calculate the sample interspectral tensor  $\hat{\mathcal{R}}$  using (6.28);
    Obtain the mode-2 matricization  $\hat{\mathbf{Q}}$  according to (6.16);
    Obtain the spatial smoothing interspectral tensor  $\hat{\mathcal{T}}$  in (6.24);
    Conduct HOSVD with (6.27) on  $\hat{\mathcal{T}}$  and obtain  $\hat{\mathbf{U}}_1$  and  $\hat{\mathbf{U}}_2$ ;
    Calculate the TM (6.30);
    Find the largest  $K$  peaks in TM as the source directions.
end

```

6.4 Numerical examples

In this section, we use numerical examples for both EM and acoustic cases to show the effectiveness of our strategies based on the proposed nested vector-sensor array signal model. The nested array we use contains $N = 6$ vector sensors, with $N_1 = 3$, $N_2 = 3$. As mentioned in the former sections, we have N_c sets of horizontal slices. Without loss of generality, we use the first set of horizontal slices. Note that any set of the horizontal slices is the manipulated results of all the original N_c components' received information. Since the 2-level nested array has 12 DOFs, we also consider the corresponding performance of a ULA with $N = 12$ EM or acoustic vector sensors, with sensor positions $[0 \ 1 \ 2 \ 3 \ 4 \ 5 \ 6 \ 7 \ 8 \ 9 \ 10 \ 11]d_l$. We will use the 12-sensor ULA as a benchmark at high SNRs.

Note that, in this chapter, the ULA-based method exploits the interspectral tensor \mathcal{R}_{ULA} which is similar to equation (6.12), rather than the spatially smoothed interspectral tensor \mathcal{T} in (6.24). Note that the tensor \mathcal{R}_{ULA} is achieved by using a ULA of vector sensors. Based on \mathcal{R}_{ULA} , we can conduct the estimation or detection using the proposed strategy in Section IV.D. Since the NA-based strategy increases the degrees of freedom by considering the difference co-array, the NA-based approach can resolve more sources than the ULA-based approach when the number of sensors is the same. We will verify this through the following numerical examples.

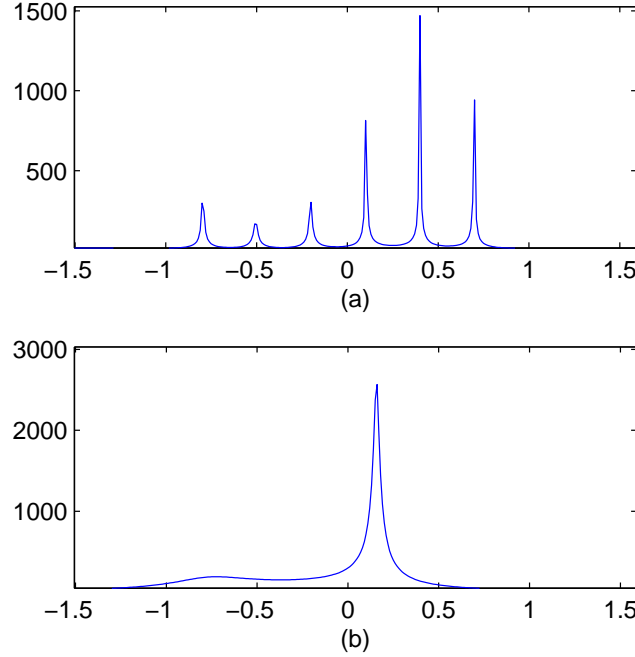


Figure 6.2: MUSIC spectrum using a nested EM vector-sensor array with 6 sensors, as a function of elevation angle θ , $K = 6$, $T = 1000$, SNR = 21.97dB. The horizontal axis is the elevation angle, whereas the vertical axis is the MUSIC spectrum. (a) 6-sensor nested array, (b) 6-sensor ULA.

6.4.1 MUSIC spectral for the EM case

We provide numerical examples for MUSIC spectral analysis corresponding to the following three cases.

- Case 1: $K = 6$ sources, with impinging directions $\boldsymbol{\theta} = [-0.8, -0.5, -0.2, 0.1, 0.4, 0.7]$ rad, $\phi_k = 0.3$ rad, for $k = 1, \dots, 6$, and polarization parameters $\gamma_k = \pi/6$, $\eta_k = \pi/6$, for $k = 1, \dots, 6$.

We use this scenario to illustrate the superior performance of the nested EM vector-sensor array in terms of degrees of freedom for 1-dimensional DOA estimation.

Suppose we know the azimuth angles of all the six sources. Fig. 6.2 shows the MUSIC spectrum with respect to different elevation angles using both a 6-sensor nested array and a

6-sensor ULA. In this example, we use $T = 1000$ snapshots at an SNR of 21.97dB. Here, we assume all sources are of equal power. As can be seen from Fig. 6.2(a), our method resolves the 6 sources well with the nested array. However, for the given number of sources ($K = 6$), since $K \geq N$, the presented tensor-MUSIC method could not have been applied on a ULA having $N = 6$ EM vector sensors. This is verified by Fig. 6.2(b). Note that we assume all sources have the same polarization parameters in this example, but our algorithm also works for cases with unequal polarization parameters.

- Case 2: $K = 2$ sources, with impinging directions $\boldsymbol{\theta} = [0.18, 0.26]$ rad, $\boldsymbol{\phi} = [0.3, 0.5]$ rad, and polarization parameters $\boldsymbol{\gamma} = [\pi/6, \pi/6]$ and $\boldsymbol{\eta} = [\pi/6, \pi/6]$.

Now, we consider 2-dimensional DOA estimation with two close sources in the surveillance region. For the purpose of intuitive demonstration, the polarization parameters are assumed to be known. The 2-dimensional MUSIC spectrum with respect to azimuth and elevation angles using the nested array is shown in Fig. 6.3. We can see that the two sources are well estimated. One thing to note is that the peaks are a little sharper along the direction of θ than along ϕ . This is reasonable because the sensors are aligned along the z -axis. As a comparison, we also plot the case of the ULA with 6 vector sensors in Fig. 6.4. We can see that the estimation performance is poor, and we can not tell where the sources are located. To show the superiority of our proposed algorithm, we also consider the estimation performance of the HOEVD-based strategy proposed in [71], which is plotted in Fig. 6.5. We can see that our algorithm outperforms the HOEVD-based method.

- Case 3: $K = 1$ source, with impinging directions $\theta = 0.12$ rad, $\phi = 0.3$ rad, and polarization parameters $\gamma = \pi/6$ and $\eta = \pi/6$.

We consider only one source in this example, but here we study the estimation performance of the polarization parameters. We represent the estimator values in the polarization (γ, η) plane in Fig. 6.6, from which we can see the polarization parameters are estimated well.

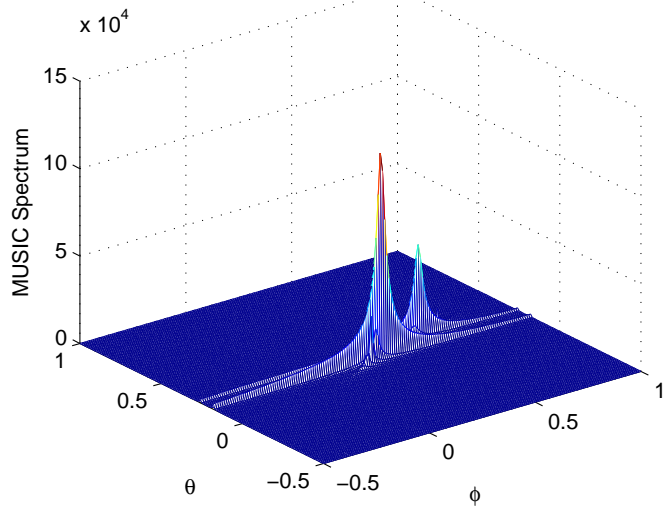


Figure 6.3: MUSIC spectrum using a nested EM vector-sensor array with 6 sensors using the proposed algorithm, as a function of azimuth ϕ and elevation angles θ , $K = 2$, $T = 1000$, SNR = 21.97dB, and true directions $\boldsymbol{\theta} = [0.18, 0.26]$, $\boldsymbol{\phi} = [0.3, 0.5]$.

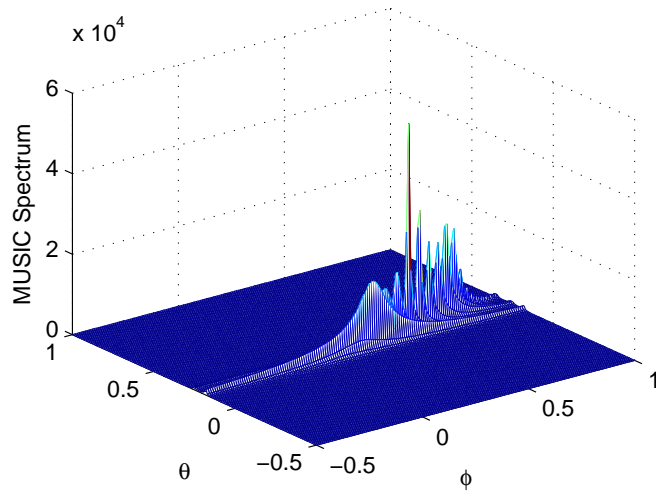


Figure 6.4: MUSIC spectrum using a ULA with 6 EM vector sensors, as a function of azimuth ϕ and elevation angles θ , $K = 2$, $T = 1000$, SNR = 21.97dB, and true directions $\boldsymbol{\theta} = [0.18, 0.26]$, $\boldsymbol{\phi} = [0.3, 0.5]$.

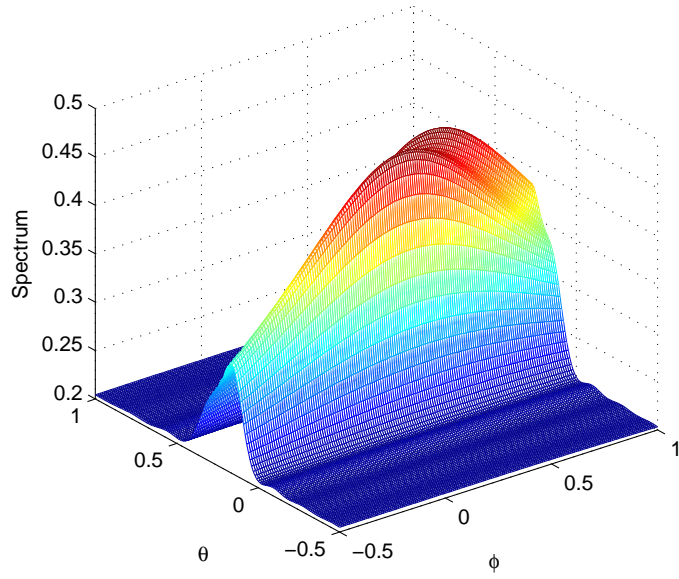


Figure 6.5: MUSIC spectrum using a nested EM vector-sensor array with 6 sensors using the HOEVD-based algorithm, as a function of azimuth ϕ and elevation angles θ , $K = 2$, $T = 1000$, SNR = 21.97dB, and true directions $\boldsymbol{\theta} = [0.18, 0.26]$, $\boldsymbol{\phi} = [0.3, 0.5]$.

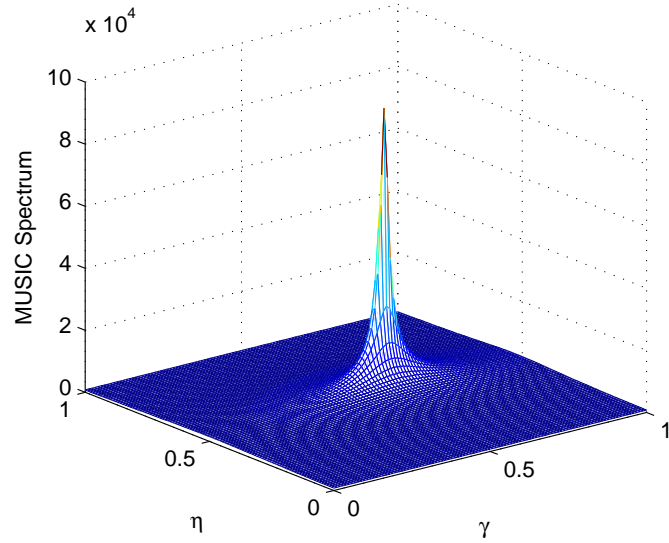


Figure 6.6: MUSIC spectrum using a nested EM vector-sensor array with 6 sensors, as a function of polarization parameters γ and η , $K = 1$, $T = 1000$, SNR = 0dB, and true polarization parameters $\eta = \pi/6$, $\gamma = \pi/6$.

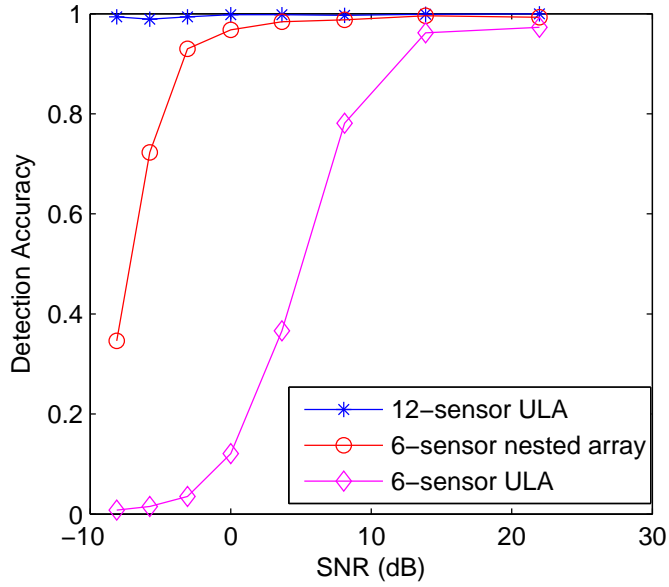


Figure 6.7: Probability of detection versus SNR using a nested array with 6 EM vector sensors and ULAs with 6 and 12 EM vector sensors, $K = 2$, $T = 1000$, and true directions $\boldsymbol{\theta} = [0.18, 0.26]$, $\boldsymbol{\phi} = [0.3, 0.7]$.

6.4.2 Detection performance for the EM case

In the previous examples, we assumed the number of sources to be known. However, in practical situations, we need to determine the source number first, before conducting estimation. Using the SORTE method presented in Section III, we investigate the detection performance of the proposed nested EM vector-sensor array.

We consider $K = 2$ sources, with impinging directions $\boldsymbol{\theta} = [0.18, 0.26]$ rad, $\boldsymbol{\phi} = [0.3, 0.5]$ rad, and polarization parameters $\gamma_k = \pi/6$, $\eta_k = \pi/6$, for $k = 1, 2$. The probability of detection of the proposed method using $T = 1000$ as a function of SNRs is plotted in Fig. 6.7. For comparison, we also plot the corresponding performance of the 6-sensor and 12-sensor ULAs. We define the probability of detection as F_K/F , where F is the trial number, and F_K is the number of times that K is detected. In this example, $F = 1000$. We can see that the detection performance of all the three arrays improves with increasing SNRs. In addition, the nested array outperforms the corresponding ULA with same number of sensors and performs close to the much longer ULA.

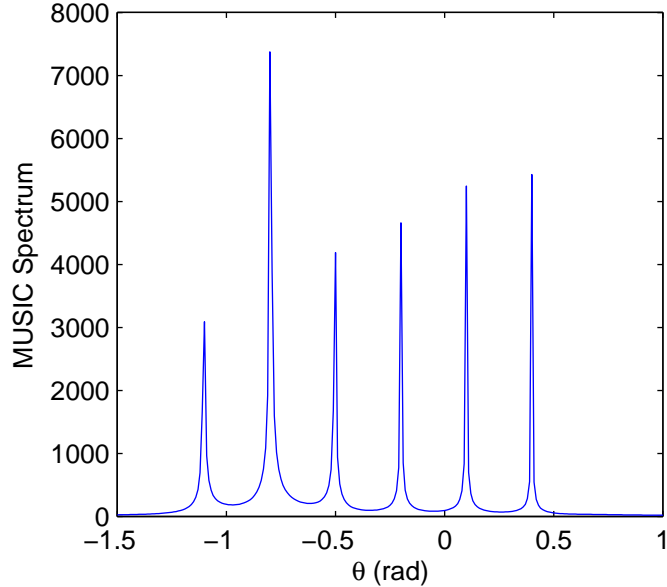


Figure 6.8: MUSIC spectrum using a nested vector-sensor array with 6 acoustic sensors, as a function of elevation angle θ , $K = 6$, $T = 1000$, SNR = 0dB.

6.4.3 Nested acoustic vector-sensor array

The performance results of the nested acoustic vector-sensor array, including DOA estimation and source number detection, are similar to the case of the EM vector-sensor array.

We first consider $K = 6$ sources, with impinging directions $\boldsymbol{\theta} = [-0.8, -0.5, -0.2, 0.1, 0.4, 0.7]$ rad, and $\phi_k = 0.3$ rad, for $k = 1, \dots, 6$. Fig. 6.8 shows the MUSIC spectrum with respect to different elevation angles, using $T = 1000$ snapshots at an SNR of 0 dB. We can see all the six sources are resolved.

Next, considering two close sources with $\boldsymbol{\theta} = [-0.05, -0.1]$ rad and $\boldsymbol{\phi} = [0.05, 0.15]$ rad, we investigate the estimation resolution using both a 6-sensor nested array and a 6-sensor ULA. The estimation results are shown in Fig. 6.9 and Fig. 6.10. We can see that the nested array resolves the two sources well, but the ULA with the same sensor number fails.

In the end, we consider the source number detection using acoustic sensors. Suppose we have $K = 2$ sources, with impinging directions $\boldsymbol{\theta} = [0.18, 0.26]$ rad and $\boldsymbol{\phi} = [0.3, 0.5]$ rad. The probability of detection of the proposed method using $T = 1000$ as a function of SNRs

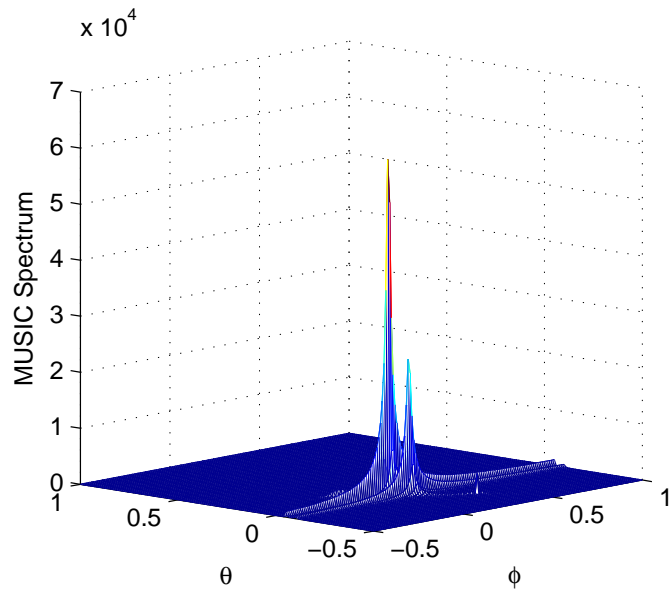


Figure 6.9: MUSIC spectrum using a nested acoustic vector-sensor array with 6 sensors, as a function of azimuth ϕ and elevation angles θ , $K = 2$, $T = 1000$, SNR = 21.97dB, and true directions $\boldsymbol{\theta} = [-0.05, -0.1]$, $\boldsymbol{\phi} = [0.08, 0.15]$.

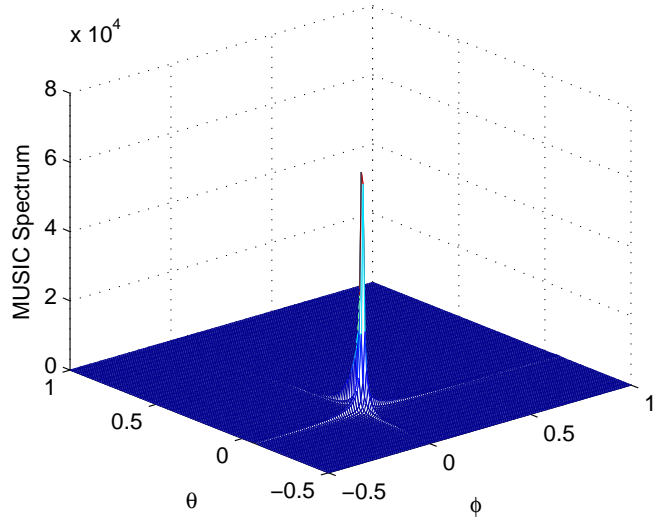


Figure 6.10: MUSIC spectrum using a ULA with 6 acoustic vector sensors, as a function of azimuth ϕ and elevation angles θ , $K = 2$, $T = 1000$, SNR = 21.97dB, and true directions $\boldsymbol{\theta} = [-0.05, -0.1]$, $\boldsymbol{\phi} = [0.08, 0.15]$.

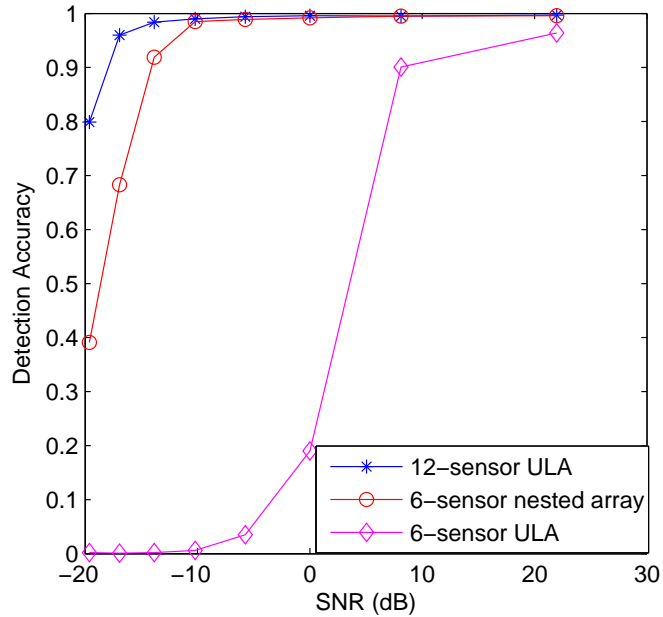


Figure 6.11: Probability of detection versus SNR using a nested array with 6 acoustic vector sensors and ULAs with 6 and 12 acoustic vector sensors, $K = 2$, $T = 1000$, and true directions $\boldsymbol{\theta} = [0.18, 0.26]$, $\boldsymbol{\phi} = [0.3, 0.7]$.

is plotted in Fig. 6.11, where we consider three arrays. We can see that the detection performance is similar to that of the EM case.

6.5 Summary

In this chapter [86], we proposed a novel sensor array model: a nested vector-sensor array. By exploiting multilinear algebra, we constructed the analytical foundation of the proposed model for signal processing. The number of elements in the co-array, namely the DOFs, was increased to $O(N^2)$ with only N sensors. Based on one set of horizontal slices of the matricized interspectral tensor, which corresponds to one component of the vector-sensor array, we proposed a novel spatial smoothing algorithm to exploit the increased DOFs. HOSVD was used to conduct the tensor decomposition, based on which we detected the source number and estimated the DOAs of sources. Numerical examples demonstrated the

effectiveness of the proposed strategy. The nested array with vector sensors also outperforms the ULA with vector sensors in terms of estimation resolution.

Chapter 7

Improved Detection and Estimation Using Jackknifing

In this chapter, we provide a novel strategy, based on jackknifing, to further improve the detection and estimation performance of nested arrays.⁵

7.1 Introduction

All the existing strategies, for both source number detection and DOA estimation, exploit all the available data together to calculate the whole sample covariance matrix. However, this fails to make full use of the available limited information. Here, we apply jackknifing, a general data-resampling method used in statistical analysis, to the measurement data under any scenario. Jackknifing replaces theoretical derivations in statistical analysis by repeatedly resampling the original data and making inferences from the resamples. Quenouille [87] invented this method with the intention of reducing the bias of the sample estimate. Tukey [88] extended this method to construct variance estimators. Without resting on a theoretical formula that is derived under any model assumption, jackknifing shows better robustness, making it less susceptible to violation of the model assumptions. The performance of jackknifing is dependent on the independence of the data. However, extensions of jackknifing to allow for dependence of the data have been proposed as well [89].

⁵This chapter is based on K. Han and A. Nehorai, “Improved source number detection and direction estimation with nested arrays and ULAs using jackknifing,” IEEE Trans. on Signal Processing, Vol. 61, pp. 6118-6128, Dec. 2013. © IEEE 2013.

The basic idea behind jackknifing lies in systematically recomputing the statistics, leaving out one or more observations at a time from the sample set. From this newly generated set of replicates of the statistics, more accurate estimates of the variables can be calculated. Jackknifing helps fully exploit the received data to improve the detection and estimation performance. Since we exploit numbers of data subsets, and conduct the detection and estimation for each of them, the extra computation would be the cost.

In this chapter, we will apply the idea of jackknifing to source number detection and DOA estimation for both ULAs and nested arrays. Specifically, rather than employing various detection and estimation algorithms on the covariance matrix of the whole data set, we choose to operate on a series of subsets, generated randomly from the whole set of measurements. Combining the results of all the subsets, we choose the value that occurs most frequently as the final estimated value. We can show that this strategy helps improve the accuracy of detection and estimation. As far as we know, our work here is the first attempt to apply jackknifing to source number detection and DOA estimation. In this chapter, we will propose a sufficient condition for the improvement of jackknifing.

7.2 Source number detection

In Section 2.1.2, we have introduced one source number detection approach SORTE. Now, based on eigenvalues and eigenvectors, we introduce three more approaches.

- VTRS [11]

Suppose \mathbf{E}_s is the combined signal eigenvectors of \mathbf{R}_y , and \mathbf{E}_x and \mathbf{E}_y are the first $N - 1$ rows and last $N - 1$ rows of \mathbf{E}_s respectively. Solving $\mathbf{E}_y = \mathbf{E}_x \Phi$ based on the least square criterion, we get matrix Φ . Define $\Delta_K = \{\Phi(i, j)\}_{(N-K-1) \times K}$, $i = K + 1, \dots, N - 1, j = 1, \dots, K$. Then the source number is

$$\hat{K} = \arg \min_K \frac{\|\Delta_K\|_F^2}{(N - K - 1)K}, \quad K = 1, \dots, N - 2.$$

- ET [10]

Define the eigen-threshold

$$\bar{\lambda}_{N-m} = [(m+1) \frac{1+t(T(m+1))^{-1/2}}{1-t(Tm)^{-1/2}} - m] l_{N-m+1}, \quad (7.1)$$

where t is a pre-set parameter, and

$$l_i = \frac{1}{N-i+1} \sum_{j=i}^N \lambda_j, \quad i = K+1, \dots, N.$$

Based on this, we keep testing the binary hypothesis: $H_0 : K < N - m$ and $H_1 : K = N - m$. Accept H_1 or H_0 according to $\lambda_{N-m} \leq_{H_1}^{H_0} \bar{\lambda}_{N-m}$. If H_0 is accepted, then we set $m = m + 1$, and continue. Otherwise, if H_1 is accepted, stop testing, and assign $\hat{K} = N - m$.

- AIC [6]

Define

$$L(K) = \frac{T}{2} \log \left(\frac{\prod_{i=K+1}^N \lambda_i^{1/(N-K)}}{\frac{1}{N-K} \sum_{i=K+1}^N \lambda_i} \right)^{N-K},$$

and $P(K) = 1 + NK - 1/2K(K-1)$. Then the source number is determined as

$$\hat{K} = \arg \min_K -2L(K) + 2P(K).$$

7.3 Jackknifing array processing

All the existing methods for array processing, including source number detection and DOA estimation, are based on the eigenvalues or eigenvectors of the sample covariance matrix $\hat{\mathbf{R}}_y$, which is calculated over the entire sample data set. However, the received data can tell us more.

Researchers have been using all the measurements as a whole to get the sample covariance, then proceeding further based on this covariance matrix. Here, we will make full use of the received data, achieving more accurate detection and estimation. Jackknifing is an effective strategy used in the statistical area to estimate sample statistics [89]. The idea is to use

subsets of available data to improve the estimation performance. For both source number detection and DOA estimation, we propose a novel array signal processing strategy based on the idea of jackknifing. Our basic belief is that a large proportion of the available data contains approximately the same amount of information as the whole available data set does.

7.3.1 Source number detection using jackknifing

Suppose we have T snapshots in total:

$$\mathbf{Y} = [\mathbf{y}(1), \mathbf{y}(2), \dots, \mathbf{y}(T)].$$

First, we take a subset \mathbf{Y}_J of size T_J from the T snapshots matrix \mathbf{Y} :

$$\mathbf{Y}_J = [\bar{\mathbf{y}}(1), \bar{\mathbf{y}}(2), \dots, \bar{\mathbf{y}}(T_J)],$$

where $\mathbf{Y}_J \subset \mathbf{Y}$, $\bar{\mathbf{y}}(t) \in \mathbf{Y}$, and $T_J = rT$, with r expressed as a percentage and satisfying $0.5 < r < 1$. The low constraint for r helps to guarantee our basic belief that the subsets contain enough information, whereas the high constraint guarantees that the subsets will not make exactly the same decision as the whole data set does. Specifically, we randomly pick T_J elements from \mathbf{Y} , without replacement, to form \mathbf{Y}_J . The sample covariance based on \mathbf{Y}_J is

$$\begin{aligned}\hat{\mathbf{R}}_{\mathbf{Y}_J} &= \frac{1}{T_J} \mathbf{Y}_J \mathbf{Y}_J^H \\ &= \frac{1}{T_J} \sum_{t=1}^{T_J} \bar{\mathbf{y}}(t) \bar{\mathbf{y}}(t)^H.\end{aligned}$$

Then we do eigenvalue decomposition for $\hat{\mathbf{R}}_{\mathbf{Y}_J}$:

$$\text{EVD}(\hat{\mathbf{R}}_{\mathbf{Y}_J}) = \mathbf{U}_J \boldsymbol{\Lambda}_J \mathbf{U}_J^H, \quad (7.2)$$

where $\boldsymbol{\Lambda}_J = \text{diag}(\hat{\lambda}_1, \dots, \hat{\lambda}_{T_J})$, sorted non-increasingly. Using $\boldsymbol{\Lambda}_J$ and \mathbf{U}_J , we conduct source detection using the existing methods. Suppose we obtain the source number \hat{K} . We continue the above two procedures for Z iterations, obtaining Z estimated source numbers,

Table 7.1: Algorithm for Source Detection Using Jackknifing

```

begin
    ite = 0; % Iteration counter
    Obtain  $r$ ,  $T_J$ ,  $\mathbf{Y}$ 
    do
        Randomly pick  $T_J^{ite}$  measurements from  $\mathbf{Y}$ , get  $\mathbf{Y}_{T_J}^{ite}$ ;
        Obtain the covariance  $\hat{\mathbf{R}}_{\mathbf{Y}_J}^{ite}$  of  $\mathbf{Y}_{T_J}^{ite}$ ;
        Conduct source detection using  $\hat{\mathbf{R}}_{\mathbf{Y}_J}^{ite}$ ;
        Obtain the estimated number  $K^{ite}$ ;
         $ite := ite + 1$ ;
    until  $ite = Z$  %  $Z$  is a pre-set threshold;
    Count the number of occurrences of different  $K^{ite}$ :  $Z_K$ ;
    Decide the source number as  $\hat{K} = \max_K Z_K$ .
end

```

\hat{K}_z , $z = 1, \dots, Z$. Before making the decision of the final source number, we need one more step, counting the occurrence of each estimated number, denoted as Z_1, Z_2, \dots, Z_{N-1} , with summation Z . The final source number is chosen as the one that occurs most frequently:

$$\hat{K} = \max_K Z_K.$$

The algorithm is shown in Table 7.1.

When the detection accuracy is greater than 50%, the improvement using jackknifing is guaranteed by the following theorem.

Theorem 7.1. *If the source number detection accuracy using the whole data set is $p \geq 0.5$, then the detection accuracy p_j , after applied jackknifing, will be greater than or equal to p :*

$$p_j \geq p.$$

Proof. Please see Appendix G. □

Remark 7.1. *When $Z = 2n$, there are $n + 1$ terms in (G.1), which can be split into $2n + 1$ terms according to (G.2). Note that the last term is transformed into one element. However the expansion of $(p + q)^{2n-1}$ just has $2n$ elements, thus there is an extra term, resulting in the strict ' $>$ ' in (G.3). As for the case $Z = 2n + 1$, we have $n + 1$ elements in (G.4), which*

can be split into $2n+1$ terms. This is exactly the number of the expansion terms of $(p+q)^{2n}$, leading to ' \geq ' for odd iteration numbers.

Remark 7.2. Equation (G.3) provides a lower bound for the improvement of jackknifing when the iteration number is even:

$$p_j - p \geq \binom{2n-1}{n} p^n q^n.$$

However, when the iteration number is odd, it is not obvious to find a lower bound because of the result " $p_j \geq p$ ".

Remark 7.3. Theoretically, when the detection accuracy is higher than 50%, the detection performance with jackknifing will definitely be improved. With over 50% accuracy, the correct number should be detected more frequently than other numbers. This assumption is based on the condition that the jackknifing sample subset contains enough information to guarantee over 50% accuracy. Otherwise, the jackknifing will lose its power.

Remark 7.4. For methods that are sensitive to the sample number, we need to increase the sample number to guarantee the efficiency of jackknifing. For example, one method might perform well with the whole T samples. However, when applying jackknifing, we just use rT samples, in which case this method may achieve an accuracy lower than 50%. Consequently, jackknifing provides no improvement. Alternatively, we can adjust the value of r to guarantee the accuracy.

Remark 7.5. When there is a low SNR, namely a high noise level, the detection methods may fail to detect the source number correctly, with accuracy lower than 50%. This will cause jackknifing to perform badly, as discussed in the second remark.

Remark 7.6. One thing to note is that we choose the value that occurs most frequently as the final source number. One problem in this process is that ties may exist. However, the greater the SNR or the larger the sample number, the less frequently ties happen. Equivalently, when the detection accuracy is greater than 0.5, the probability that ties happen will be relatively low. Therefore, based on the assumption that $p \geq 0.5$, we expect the ties rarely happen, and will verify this through our numerical examples. When ties happen, we just choose the first one after arranging them in a descending order. Even if the choice is wrong, this can be ignored because of our assumption that $p \geq 0.5$.

7.3.2 DOA estimation using jackknifing

Similar to the previous discussion for source number detection using jackknifing, we choose the subset \mathbf{Y}_J of size T_J from the T snapshots matrix \mathbf{Y} , and obtain the sample covariance matrix $\hat{\mathbf{R}}_{\mathbf{Y}_J}$. According to (7.2), we get the sample noise subspace

$$\mathbf{U}_{J_e} = [\hat{\mathbf{u}}_{K+1}, \hat{\mathbf{u}}_{K+2}, \dots, \hat{\mathbf{u}}_N],$$

which consists of the last $N-K$ eigenvectors corresponding to the smallest $N-K$ eigenvalues.

The impinging direction of the signal is a continuous variable, so it is impossible for us to conduct an exhaustive search over all the direction space for the sample spectrum:

$$\hat{S}_{\text{MUSIC}}(\theta) = \frac{1}{\mathbf{a}(\theta)^H \mathbf{U}_{J_e} \mathbf{U}_{J_e}^H \mathbf{a}(\theta)}. \quad (7.3)$$

Consequently, we will not be able to apply jackknifing to DOA estimation. To circumvent this problem, we discretize the direction space into D grid points:

$$\Theta = [-90^\circ, -90^\circ + \frac{180^\circ}{D-1}, \dots, 90^\circ - \frac{180^\circ}{D-1}, 90^\circ].$$

Then the estimated DOA is

$$\hat{\theta} = \max_{\theta} \hat{S}_{\text{MUSIC}}(\theta), \quad \theta \in \Theta. \quad (7.4)$$

Since we can have at most D different estimated DOAs, jackknifing is suitable for DOA estimation. We iteratively choose Z subsets from the whole data set, and employ MUSIC based on the sub-covariance matrices. Based on the Z estimated directions, we count the occurrence of different entries, and consider the DOA to be the one that has the largest frequency. The MUSIC algorithm, applied with jackknifing, is shown in Table 7.2.

Similar to source number detection, we have the comparative theorem for DOA estimation.

Theorem 7.2. *If the DOA estimation accuracy using the whole data set is $p \geq 0.5$, then the DOA estimation accuracy p_j , after applied jackknifing, will be greater than or equal to p : $p_j \geq p$.*

Table 7.2: MUSIC for DOA Estimation Using Jackknifing

```

begin
    ite = 0; % Iteration counter
    Obtain  $r$ ,  $T_J$ ,  $\mathbf{Y}$ 
    do
        Randomly pick  $T_J^{ite}$  measurements from  $\mathbf{Y}$ , get  $\mathbf{Y}_{T_J}^{ite}$ ;
        Obtain the covariance  $\hat{\mathbf{R}}_{\mathbf{Y}_J}^{ite}$  of  $\mathbf{Y}_{T_J}^{ite}$ ;
        Conduct eigenvalue decomposition, get noise sample
        space  $\mathbf{U}_{J_e}^{ite}$ ;
        Calculate the sample spectrum  $\hat{S}_{\text{MUSIC}}(\theta)$ , according
        to (7.3),  $\theta \in \Theta$ ;
        Obtain the DOA estimation  $\hat{\theta}^{ite}$ , according to (7.4);
         $ite := ite + 1$ ;
    until  $ite = Z$  %  $Z$  is a pre-set threshold;
    Count the number of occurrences of different  $\hat{\theta}^{ite}$ :  $Z_\theta$ ;
    Decide the DOA estimation as  $\hat{\theta} = \max_\theta Z_\theta$ .
end

```

Proof. The proof is similar to that for Theorem 7.1. Just note that the DOA estimation accuracy is defined as the probability of the event that the estimated direction $\hat{\theta}$ is equal to the true direction over the direction space Θ . \square

For ULAs, we simply apply the sample covariance matrix, whereas for nested arrays, we need to construct the spatially smoothed matrix \mathbf{R}_{ss} in (2.41) for each iteration when using jackknifing.

7.4 Numerical examples

In this section, we use numerical examples to show the superiority of our proposed strategy, considering source number detection and DOA estimation, for both ULAs and nested arrays.

We consider the following three scenarios:

Scenario 1: We consider a ULA with $N = 8$ sensors and a nested array with $N = 6$ sensors.

- For the 8-sensor ULA:

- Sensor position $[0 \ 1 \ 2 \ 3 \ 4 \ 5 \ 6 \ 7]d$, with spacing $d = \lambda/2$.
- Source number $K = 3$.
- Impinging directions $\theta_1 = [-60^0, 0^0, 30^0]$.
- Impinging directions $\theta_2 = [10^0, 20^0, 35^0]$.
- Source power $\sigma_1^2 = \sigma_2^2 = \sigma_3^2 = 9$.

- For the 6-sensor nested array:

- Sensor position $[1 \ 2 \ 3 \ 4 \ 8 \ 12]d$, with spacing $d = \lambda/2$, and $N_1 = N_2 = 3$.
- Source number $K = 8$.
- Impinging directions $\theta = [-60^0, -45^0, -15^0, 0^0, 15^0, 30^0, 45^0, 60^0]$.
- Source power $\sigma_1^2 = \sigma_2^2 = \dots = \sigma_8^2 = 9$.

Scenario 2: We consider a ULA with $N = 6$ sensors and a nested array with $N = 6$ sensors. For both arrays, we suppose there is only one source, with impinging direction $\theta = 40^0$, and power $\sigma^2 = 9$.

- For the 6-sensor ULA:

- Sensor position $[0 \ 1 \ 2 \ 3 \ 4 \ 5]d$, with spacing $d = \lambda/2$.

- For the 6-sensor nested array:

- Sensor position $[1 \ 2 \ 3 \ 4 \ 8 \ 12]d$, with spacing $d = \lambda/2$, and $N_1 = N_2 = 3$.

Scenario 3: We consider a ULA with $N = 6$ sensors, a nested array with $N = 6$ sensors, and a ULA with $N = 12$ sensors. For all the three arrays, we suppose there are two sources, with impinging direction $\theta_1 = [-60^0, 0^0]$ or $\theta_2 = [0^0, 10^0]$, and power $\sigma_1^2 = \sigma_2^2 = 9$.

- For the 6-sensor ULA:

- Sensor position $[0 \ 1 \ 2 \ 3 \ 4 \ 5]d$, with spacing $d = \lambda/2$.

- For the 6-sensor nested array:
 - Sensor position $[1 2 3 4 8 12]d$, with spacing $d = \lambda/2$, and $N_1 = N_2 = 3$.
- For the 12-sensor ULA:
 - Sensor position $[0 1 2 3 4 5 6 7 8 9 10 11]d$, with spacing $d = \lambda/2$.

7.4.1 Source number detection

We consider four cases for source number detection: two cases for scenario 1, one case for scenario 3, and one case for scenario 4.

- The ULA in scenario 1.

We choose a jackknifing iteration number $Z = 20$, the percentage of $r = 0.85$, and the Monte Carlo simulation number $T = 1000$. Fig. 7.1 shows the detection results of the aforementioned four different methods: SORTE, VTRS, ET, and AIC, with impinging direction $\boldsymbol{\theta}_1$. It describes the detection accuracy with respect to different SNRs. We take the detection accuracy as

$$\text{Accuracy} = F_K/F,$$

where F is the trial number, and F_K is the number of times that K is detected. In this example, we use $F = 1000$ trials.

In Fig. 7.1, all four methods achieve different levels of improvement by applying jackknifing. SORTE improves the most, and performs even better when the SNR is low. Note that the detection accuracy is always above 0.5 without jackknifing, which guarantees the improvement of jackknifing. For ET, the performance is highly related to the appropriate choice of parameter t in (7.1). The decision of this value depends on *a priori* information, such as the probability density function of false alarm, SNR level, etc. In many applications some of the information is not available, in which case the parameter must be chosen based on empirical decision. In our example, $t = 1.2$.

The computation time with jackknifing is highly related to the number of iterations Z . The larger Z is, the longer it takes using jackknifing. When we use jackknifing, another

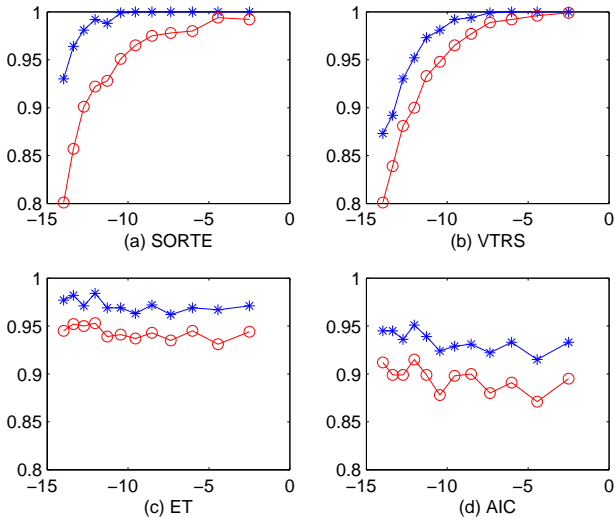


Figure 7.1: Performance comparison of four methods with ULA using 1000 samples for $\theta_1 = [-60^0, 0^0, 30^0]$: the blue-star line is the performance with jackknifing, and the red-circle line without jackknifing. The vertical axis represents the detection accuracy, while the horizontal axis represents the SNR.

Table 7.3: Computation time ($\times 10^{-4}s$) for various methods based on an 8-sensor ULA with or without jackknifing, where $T = 1000$, $Z = 20$.

| | SORTE | VTRS | ET | AIC |
|---------------------|-------|------|------|------|
| Without Jackknifing | 2.43 | 2.05 | 1.78 | 1.25 |
| With Jackknifing | 56 | 65 | 55 | 54 |

part that consumes time is randomly picking a subset from the whole data set iteratively. Therefore, it may take more than Z times the computation cost of the original algorithm. The computation burdens of the four methods are shown in Table 7.3, with $T = 1000$ and $Z = 20$. We can see that, as a computer-intensive method, jackknifing does cost much more time than the case without jackknifing. However, because of the availability of inexpensive and fast computing, jackknifing is still appreciated by current researchers.

We also calculated the detection accuracy for impinging direction θ_2 , which has smaller source spacing. Fig. 7.2 shows the results of the four methods using $T = 1000$ samples. We can see that jackknifing improves the detection performance much as in Fig. 7.1 for SORTE, ET, and AIC. However, VTRS loses its detection ability at small SNRs. One thing to note

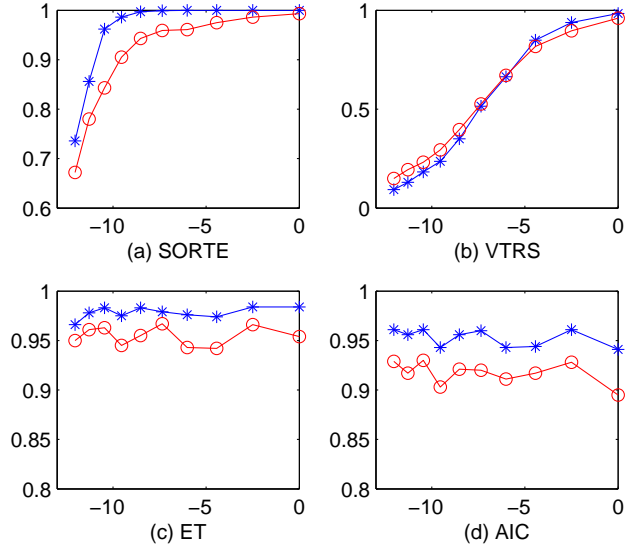


Figure 7.2: Performance comparison of four methods with ULA using 1000 samples for $\theta_2 = [10^0, 20^0, 35^0]$: the blue-star line is the performance with jackknifing, and the red-circle line without jackknifing. The vertical axis represents the detection accuracy, while the horizontal axis represents the SNR.

is that, once VTRS works, namely the detection accuracy is greater than 0.5, jackknifing works as well. We can see this through the high SNR points.

- The 2-level nested array in scenario 1.

The spacings are $d_I = \lambda/2$ and $d_O = 4d_I$. It is impossible for us to use a 6-element ULA to detect 8 sources. However the spatial matrix \mathbf{R}_{ss} in (2.41) helps a nested array obtain this goal. We choose jackknifing iteration number $Z = 20$, and the percentage $r = 0.85$. We use $F = 1000$ trials. From Fig. 7.1, we can see that SORTE and VTRS perform a little better, thus we consider only these two methods for the nested array.

Fig. 7.3 shows the performance of SORTE and VTRS, with and without jackknifing, using $T = 2000$ Monte Carlo simulations. We can see that at high SNR both methods can detect the source number correctly with high probability. Moreover, with jackknifing, both methods' detection accuracy increases. In this example, we can see that, at high SNRs, the improvement is greater than that at low SNRs. That jackknifing's performance degrades

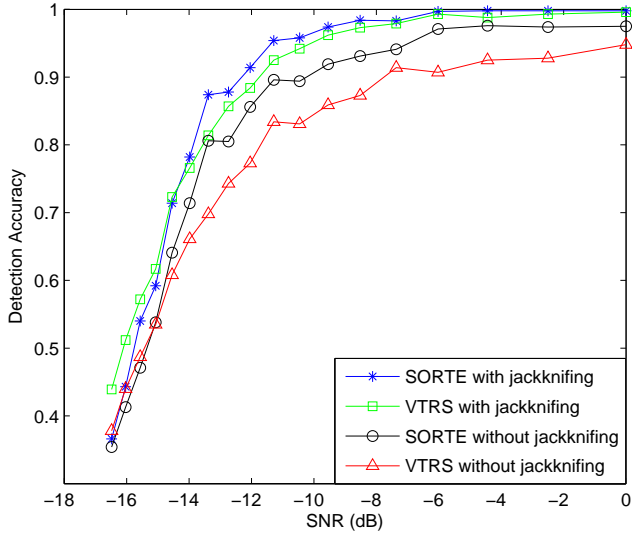


Figure 7.3: Performance comparison of SORTE and VTRS with a nested array using 2000 samples.

Table 7.4: Computation time ($\times 10^{-4}s$) for SORTE and VTRS based on a 6-sensor nested array with or without jackknifing, where $T = 1000$, $Z = 20$.

| | SORTE | VTRS |
|---------------------|-------|------|
| Without Jackknifing | 2.84 | 3.38 |
| With Jackknifing | 79 | 89 |

at low SNRs is in accordance with our previous analysis. Additionally, SORTE slightly outperforms VTRS.

In Table 7.4, we tabulate the computation time for SORTE and VTRS with and without jackknifing, where $T = 2000$ and $Z = 20$. The results are similar to the case of ULA.

Note that, for jackknifing, we choose the percentage $r = 0.85$. However, this may not be the best value. In Fig. 7.4, we plot the detection accuracy with respect to different percentage values for both SORTE and VTRS, at an SNR of -24 dB using $T = 1000$ snapshots. We can see $r = 0.65$ is the best choice for both VTRS and SORTE, which confirms our statement that r should be moderate, neither too big nor too small. To have a clearer picture of how the percentage value affects the detection performance, we list the best r for different numbers of snapshots in Table 7.5, where we consider just SORTE. We can see that when the snapshot

Table 7.5: Best percentage values for different number of snapshots using SORTE with a nested array, at an SNR of -24 dB.

| Snapshot(T) | 500 | 600 | 700 | 8000 | 900 |
|-----------------|------|------|------|------|------|
| Best r | 0.75 | 0.7 | 0.65 | 0.65 | 0.7 |
| Snapshot(T) | 1000 | 1100 | 1200 | 1300 | 1400 |
| Best r | 0.65 | 0.65 | 0.65 | 0.6 | 0.5 |

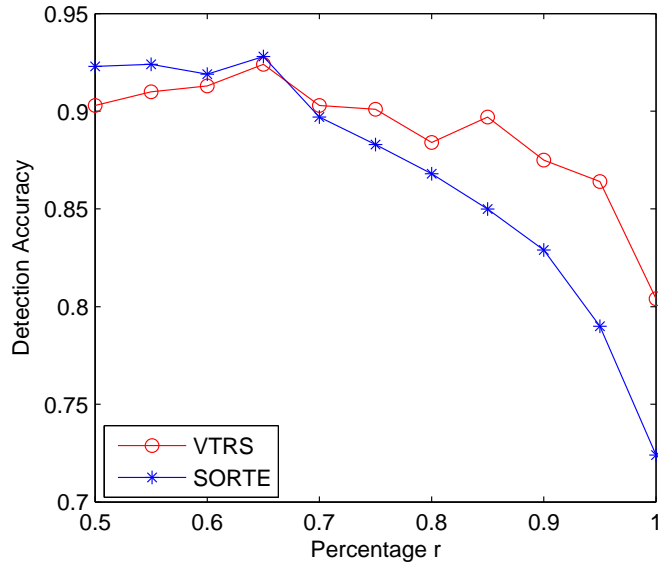


Figure 7.4: Detection accuracy of SORTE and VTRS for different percentage values, with a nested array at an SNR of -24 dB using $T = 1000$ snapshots.

number increases, the best r decreases, which means that larger size of subset may result in worse performance. Therefore, to achieve good performance using jackknifing given a certain number of samples, we should be careful when choosing the percentage parameter.

- Scenario 3.

Since a nested array takes advantage of the increased DOFs provided by the co-array, we expect its detection accuracy to improve greatly. Similar to the aforementioned examples, we plot the detection accuracy versus SNR for θ_1 , shown in Fig. 7.5 using $T = 1000$ snapshots. The trial number is 1000, the percentage $r = 0.85$, and the jackknifing iteration number is set as $Z = 50$. Clearly, the two-level nested array outperforms the corresponding ULA with

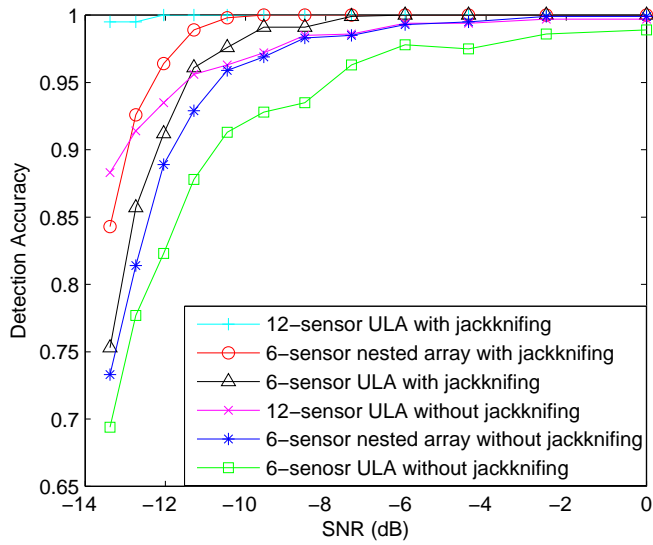


Figure 7.5: SORTE performance comparison of a 6-sensor nested array, a 6-sensor ULA, and a 12-sensor ULA using 1000 samples for $\boldsymbol{\theta}_1 = [-60^0, 0^0]$, with and without jackknifing.

same number of sensors and performs close to the much longer ULA. Moreover, jackknifing helps all three arrays achieve substantial improvement.

We also calculated the detection accuracy for impinging direction $\boldsymbol{\theta}_2 = [0^0, 10^0]$, which has smaller source spacing. Fig. 7.6 shows the results using $T = 1000$ samples. We can see that the 6-sensor nested array and 12-sensor ULA work the same as the wide spacing case. As for the 6-sensor ULA, the performance degrades at low SNRs. However, once the detection accuracy without jackknifing is greater than 0.5, jackknifing works well. The result is similar to the aforementioned VTRS in the case of ULA.

7.4.2 DOA estimation

Considering scenario 2, we split the direction space by choosing $D = 181$, namely $\Theta = [-90^0, -89^0, \dots, 90^0]$. By applying the algorithm in Table 7.2, we get the results for both a nested array in Fig. 7.7. Besides the estimation accuracy, we also plot the root mean square error (RMSE) versus SNR.

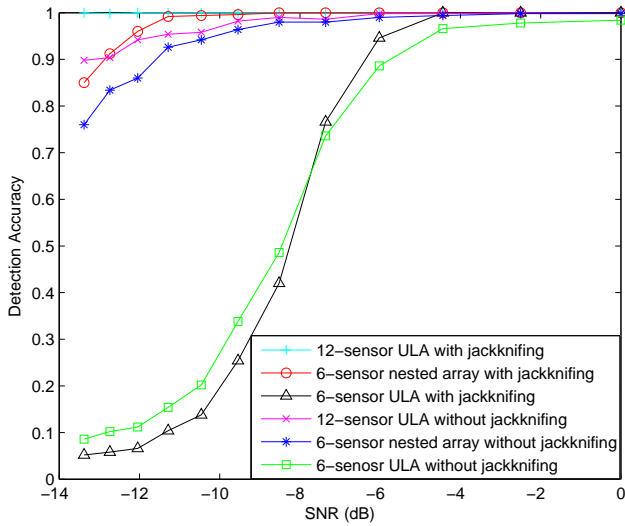


Figure 7.6: SORTE performance comparison of a 6-sensor nested array, a 6-sensor ULA, and a 12-sensor ULA using 1000 samples for $\theta_2 = [0^0, 10^0]$, with and without jackknifing.

We can see that the performance is slightly improved with jackknifing. The improvements in DOA estimation using jackknifing are less apparent than those for source number detection. The reasons, we believe, are mainly owing to the following issues. First, the size of the result space of DOA estimation is much larger than that of source number detection, with $D = 181$ for DOA estimation versus, at most, $N = 12$ for source number detection. Second, the DOA estimation may be more sensitive to the sample number: with rT snapshots, the estimation accuracy may degrade more than the source number detection does. Another possible explanation is that the the nested or ULA array may provide small DOA estimation errors which are already close to the CRB. Thus the improvement obtained from jackknifing cannot be very significant.

7.5 Summary

In this chapter [39], by applying the resampling strategy jackknifing, we proposed a novel strategy for source number detection and DOA estimation. Iteratively employing subsets of the whole data set, the strategy greatly improves the performance of the existing detection and estimation by making full use of the limited available data. Using jackknifing, we

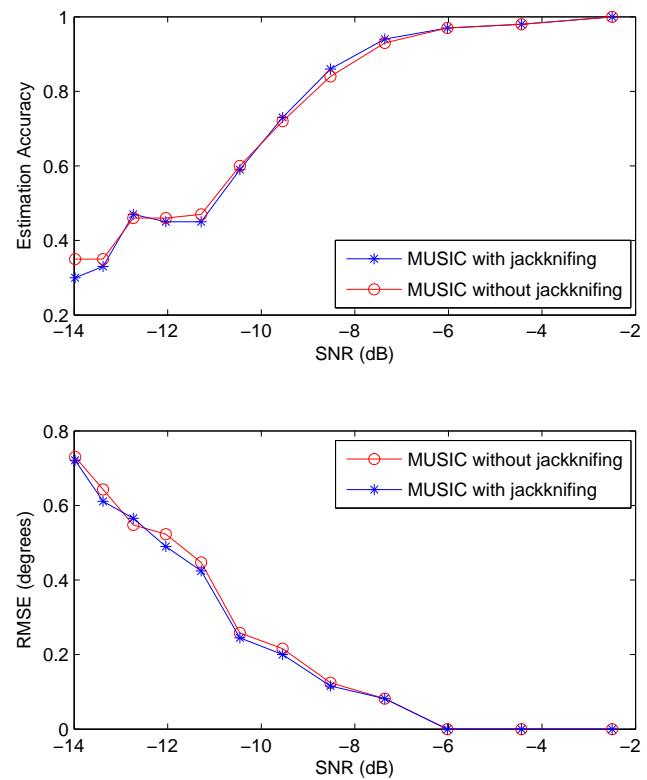


Figure 7.7: DOA estimation using a nested array with 6 sensors: the top figure is the estimation accuracy versus SNR, and the bottom figure shows the RMSE versus SNR.

investigated four source number detection approaches based on different principles, as well as the MUSIC algorithm for DOA estimation. All achieve different levels of improvement. With the assumption that the subsets of the data set contain enough information, we analytically proved that the improvement is guaranteed when the detection or estimation accuracy is greater than or equal to 50%. Both ULAs and the newly developed nested arrays are considered. The advantage of our strategy was verified through simulations. The expense for using jackknifing is the higher computation burden, more than Z times that of the case without jackknifing. Additionally, we investigated the performance effect of the percentage parameter we choose when doing jackknifing, finding that a moderate value is the best choice, and either a larger or smaller subset will degrade the performance.

Chapter 8

Conclusions and Future Work

8.1 Summary and conclusions

In this dissertation we studied statistical signal processing with nested arrays. We first reviewed the background about array signal processing, and basic schemes for nested arrays. Then we investigated mainly five interesting but important topics.

We extended the point and narrowband sources to more general wideband and distributed sources. Specifically, we established the nested array model for both kinds of sources. Then for wideband topic, we succeeded to decompose the wideband sources into multiple narrowband frequencies, and constructed corresponding strategies to combine all the results to achieve accurate detection and estimation performance. As for distributed sources, we proposed an improved spatial smoothing strategy based on *a priori* knowledge of the spreading parameter, and analytically proved its effectiveness. The results were verified through numerical examples for both cases.

Nested arrays with model errors were discussed next. We investigated the practical problem of direction-of-arrival estimation with model errors for nested arrays, and then extended the proposed strategies to the general case of nonuniform linear arrays. We provided detailed analysis of the error effect on nested arrays, and proposed robust self-calibration algorithms to estimate the model errors and the DOAs as well. The CRB was also derived to analyze the estimation performance of the proposed strategies. The general case of nonuniform linear arrays, including co-prime arrays, has also been considered. Numerical examples

demonstrated the effectiveness of our strategies. Additionally, the nested array showed more robust performance than the ULA with the same number of sensors.

We next studied the case of vector sensors, which is not a straightforward extension from the scalar case. We proposed a novel sensor array model: a nested vector-sensor array. By exploiting multilinear algebra, we constructed the analytical foundation of the proposed model for signal processing. The number of elements in the co-array, namely the DOFs, was increased to $O(N^2)$ with only N sensors. Based on one set of horizontal slices of the matricized interspectral tensor, which corresponds to one component of the vector-sensor array, we proposed a novel spatial smoothing algorithm to exploit the increased DOFs. HOSVD was used to conduct the tensor decomposition, based on which we detected the source number and estimated the DOAs of sources. Numerical examples demonstrated the effectiveness of the proposed strategy. The nested array with vector sensors also outperforms the ULA with vector sensors in terms of estimation resolution.

Finally, we proposed a novel improved strategy for source number detection and DOA estimation by applying jackknifing. Iteratively employing subsets of the whole data set, the strategy greatly improves the performance of the existing detection and estimation by making full use of the limited available data. Using jackknifing, we investigated four source number detection approaches based on different principles, as well as the MUSIC algorithm for DOA estimation. All achieved different levels of improvement. Both ULAs and nested arrays were considered. The advantage of our strategy was verified through simulations. We investigated the performance effect of the percentage parameter we choose when doing jackknifing, finding that a moderate value is the best choice, and either a larger or smaller subset will degrade the performance.

8.2 Future directions

In the future, we plan to extend the work in several directions.

Correlated sources: In this dissertation we focused on uncorrelated sources, which is a strict assumption made by most works regarding nested arrays. Methods that can handle correlated sources generally require more antennas than sources. Recently, DOA estimation

for more correlated sources than active sensors was first investigated [90]. Though fewer active sensors are required, more real sensors are necessary. It would be of great interest to work on correlated sources with fewer real sensors.

Higher dimensional nested arrays via tensor modeling: Two-dimensional nested arrays have been proposed in [22][23]. However the strategies are based on matrix framework, thus losing valuable higher-dimensional information. The tensor modeling scheme proposed in our vector sensor topic [86] provides a potential research direction to further improve the estimation performance of two-dimensional nested arrays, by employing the higher dimensional information.

Multiple co-prime arrays: Multiple co-prime arrays in a distributed configuration would enhance the spatial observability of the targets/sources. These distributed arrays will overcome the endfire DOA ambiguity experienced by ULAs [91]. Further, they provide a uniform spatial response and facilitate the joint estimation of azimuth and elevation angles. Target scattering coefficients typically vary rapidly with the angle of view. Therefore, by viewing the target from different, widely separated angles, the effect of target scintillations is significantly mitigated [92]. This approach is similar to distributed MIMO radar in its exploitation of the spatial diversity of the targets. However, here each antenna in MIMO radar will be replaced by a co-prime array, providing an increase in the degrees of freedom in addition to improved spatial observability.

Multi-modal sensing: We propose to formulate a new framework for performing statistical inference from the fusion of multi-modal and multi-sensor data obtained by employing co-prime arrays jointly with various other sensing modalities. Our proposed framework for multi-sensor data fusion and sensor selection is inspired by the trading behavior in a commercial society [93]. The additional modality dimensions will provide the system with more information about the parameters of interest and hence will improve the overall performance of the system.

References

- [1] S. Haykin, *Array Signal Processing*. New Jersey: Prentice-Hall, 1985.
- [2] H. L. V. Trees, *Optimum Array Processing: Part IV of Detection, Estimation and Modulation Theory*. New York: Wiley Intersci., 2002.
- [3] A. Di and L. Tian, “Matrix decomposition and multiple source location,” in *Acoustics, Speech, and Signal Processing, IEEE International Conference on ICASSP*, Mar. 1984, pp. 722–725.
- [4] A. P. Liavas and P. A. Regalia, “On the behavior of information theoretic criteria for model order selection,” *IEEE Trans. Signal Process.*, vol. 49, pp. 1689–1695, Aug 2001.
- [5] J. F. Gu, P. Wei, and H. M. Tai, “Detection of the number of sources at low signal-to-noise ratio,” *Signal Processing, IET*, vol. 1, pp. 2–8, Mar 2007.
- [6] H. Akaike, “A new look at the statistical model identification,” *IEEE Trans. Autom. Control*, vol. 19, pp. 716–723, Dec. 1974.
- [7] J. E. Cavanaugh, “A large-sample model selection criterion based on Kullback’s symmetric divergence,” *Stat. Probab. Lett.*, vol. 44, pp. 333–344, 1999.
- [8] M. Wax and I. Ziskind, “Detection of the number of coherent signals by the MDL principle,” *IEEE Trans. Acoust., Speech, Signal Process.*, vol. 37, pp. 1190–1196, Aug 1989.
- [9] Z. He, A. Cichocke, S. Xie, and K. Choi, “Detecting the number of clusters in n-way probabilistic clustering,” *IEEE Trans. Pattern Anal. Mach. Intell.*, vol. 32, pp. 2006–2021, Nov 2010.
- [10] W. Chen, K. M. Wong, and J. P. Reilly, “Detection of the number of signals: a predicted eigen-threshold approach,” *IEEE Trans. Signal Process.*, vol. 39, pp. 1088–1098, May 1991.
- [11] J. S. Jiang and M. A. Ingram, “Robust detection of number of sources using the transformed rotational matrix,” in *Wireless Communications and Networking Conference*, Mar. 2004, pp. 501–506.

- [12] Z. Chen, G. K. Gokeda, and Y. Yu, *Introduction to Direction-Of-Arrival Estimation*. Artech House, 2010.
- [13] H. Krim and M. Viberg, “Two decades of array signal processing research: the parametric approach,” *IEEE Signal Process. Mag.*, vol. 13, pp. 67–94, Jul. 1996.
- [14] B. D. Van Veen and K. M. Buckley, “Beamforming: a versatile approach to spatial filtering,” *IEEE ASSP Mag.*, vol. 5, pp. 4–24, Apr. 1988.
- [15] R. O. Schmidt, “Multiple emitter location and signal parameter estimation,” *IEEE Trans. Antennas Propag.*, vol. 34, pp. 276–280, Mar. 1986.
- [16] M. Haardt, *One-, Two-, and Multidimensional High-Resolution Array Signal Processing*. New York: Shaker Verlag, 1997.
- [17] J. J. Fuchs, “On the application of the global matched filter to DOA estimation with uniform circular arrays,” *IEEE Trans. Signal Process.*, vol. 49, pp. 702–729, Apr. 2001.
- [18] D. Malioutov, M. Çetin, and A. S. Willsky, “A sparse signal reconstruction perspective for source localization with sensor arrays,” *IEEE Trans. Signal Process.*, vol. 53, pp. 3010–3022, Aug. 2005.
- [19] H. Zhu, G. Leus, and G. B. Giannakis, “Sparsity-cognizant total least-squares for perturbed compressive sampling,” *IEEE Trans. Signal Process.*, vol. 59, pp. 2002–2016, May 2011.
- [20] P. Stoica, P. Babu, and J. Li, “SPICE: A sparse covariance-based estimation method for array processing,” *IEEE Trans. Signal Process.*, vol. 59, pp. 629–638, Feb. 2011.
- [21] P. Pal and P. P. Vaidyanathan, “Nested array: A novel approach to array processing with enhanced degrees of freedom,” *IEEE Trans. Signal Process.*, vol. 58, pp. 4167–4181, Aug. 2010.
- [22] ——, “Nested arrays in two dimensions, part I: geometrical considerations,” *IEEE Trans. Signal Process.*, vol. 60, pp. 4694–4705, Sep. 2012.
- [23] ——, “Nested arrays in two dimensions, part II: application in two dimensional array processing,” *IEEE Trans. Signal Process.*, vol. 60, pp. 4706–4718, Sep. 2012.
- [24] ——, “Coprime sampling and the MUSIC algorithm,” in *14th IEEE DSP/SPE workshop*, Sedona, AZ, Jan 2011, pp. 289–294.
- [25] P. P. Vaidyanathan and P. Pal, “Theory of sparse coprime sensing in multiple dimensions,” *IEEE Trans. Signal Process.*, vol. 59, pp. 3592–3608, Aug. 2011.

- [26] ——, “System identification with sparse coprime sensing,” *IEEE Signal Process. Lett.*, vol. 17, pp. 823–826, Oct. 2010.
- [27] Y. D. Zhang, M. G. Amin, , and B. Himed, “Sparsity-based doa estimation using co-prime arrays,” in *IEEE Int. Conf. Acoustics, Speech, and Signal Processing*, Vancouver, Canada, May 2013.
- [28] P. Pal and P. Vaidyanathan, “correlation-aware techniques for sparse support recovery,” in *2012 IEEE Statistical Signal Processing Workshop (SSP)*, Ann Arbor, MI, Aug. 2012, pp. 53–56.
- [29] Z. Tan and A. Nehorai, “Sparse direction of arrival estimation using co-prime arrays with off-grid targets,” *IEEE Signal Process. Lett.*, vol. 21, pp. 26–29, Jan. 2014.
- [30] P. Stoica and R. L. Moses, *Introduction to Spectral Analysis*. New Jersey: Prentice Hall, 1997.
- [31] R. R. Hooton and S. A. Kassam, “The unifying role of the coarray in aperture synthesis for coherent and incoherent imaging,” *Proc. IEEE*, vol. 78, pp. 735–752, Apr. 1990.
- [32] M. Dogan and J. Mendel, “Applications of cumulants to array processing .i. aperture extension and array calibration,” *IEEE Trans. Signal Process.*, vol. 43, pp. 1200–1216, May. 1995.
- [33] P. Chevalier, L. Albera, A. Ferreol, and P. Comon, “On the virtual array concept for higher order array processing,” *IEEE Trans. Signal Process.*, vol. 53, pp. 1254–1271, Apr. 2005.
- [34] M. Wax, T.-J. Shan, and T. Kailath, “Spatio-temporal spectral analysis by eigenstructure methods,” *IEEE Trans. Acoust., Speech, Signal Process.*, vol. 32, pp. 817–827, Aug. 1984.
- [35] H. Wang and M. Kaveh, “Coherent signal-subspace processing for the detection and estimation of angles of arrival of multiple wide-band sources,” *IEEE Trans. Acoust., Speech, Signal Process.*, vol. 33, pp. 823–831, Aug. 1985.
- [36] Y. R. Zheng, R. A. Goubran, and M. El-Tanany, “Experimental evaluation of a nested microphone array with adaptive noise cancellers,” *IEEE Trans. Instrum. Meas.*, vol. 53, pp. 777–786, Jun. 2004.
- [37] D. Opitz and R. Maclin, “Popular ensemble methods: an empirical study,” *Journal of Artificial Intelligence Research*, vol. 11, pp. 169–198, 1999.
- [38] J. Li, D. Zheng, and P. Stoica, “Angle and waveform estimation via RELAX,” *IEEE Trans. Aerosp. Electron. Syst.*, vol. 33, pp. 1077–1087, Jul. 1997.

- [39] K. Han and A. Nehorai, “Improved source number detection and direction estimation with nested arrays and ULAs using jackknifing,” *IEEE Trans. Signal Process.*, vol. 61, pp. 6118–6128, Dec. 2013.
- [40] ———, “Wideband Gaussian source processing using a linear nested array,” *IEEE Signal Process. Lett.*, vol. 20, pp. 1110–1113, Nov 2013.
- [41] S. Valaee, B. Champagne, and P. Kabal, “Parametric localization of distributed sources,” *IEEE Trans. Signal Process.*, vol. 43, pp. 2144–2153, Sep. 1995.
- [42] Y. U. Lee, J. Choi, I. Song, and S.-R. Lee, “Distributed source modeling and direction-of-arrival estimation techniques,” *IEEE Trans. Signal Process.*, vol. 45, pp. 960–969, Apr. 1997.
- [43] A. Gershman, C. Mecklenbrauker, and J. F. Bhme, “Matrix fitting approach to direction of arrival estimation with imperfect spatial coherence of wavefronts,” *IEEE Trans. Signal Process.*, vol. 45, pp. 1894–1899, Jul. 1997.
- [44] O. Besson, F. Vincent, P. Stoica, and A. Gershman, “Approximate maximum likelihood estimators for array processing in multiplicative noise environments,” *IEEE Trans. Signal Process.*, vol. 48, pp. 2506–2518, Sep. 2000.
- [45] S. Shahbazpanahi, S. Valaee, and M. Bastani, “Distributed source localization using ESPRIT algorithm,” *IEEE Trans. Signal Process.*, vol. 49, pp. 2169–2178, Oct. 2001.
- [46] J. Lee, J. Joung, and J. D. Kim, “A method for the direction-of-arrival estimation of incoherently distributed sources,” *IEEE Trans. Veh. Technol.*, vol. 57, pp. 2885–2893, Sep. 2008.
- [47] K. Han and A. Nehorai, “Nested array processing for distributed sources,” *IEEE Signal Process. Lett.*, vol. 21, pp. 1111–1114, Sep. 2014.
- [48] B. Friedlander and A. Weiss, “Eigenstructure methods for direction finding with sensor gain and phase uncertainties,” in *Proc. IEEE ICASSP*, Apr. 1988, pp. 2681–2684.
- [49] A. Swindlehurst and T. Kailath, “A performance analysis of subspace-based methods in the presence of model errors. I. the MUSIC algorithm,” *IEEE Trans. Signal Process.*, vol. 40, pp. 1758–1774, Jul. 1992.
- [50] ———, “A performance analysis of subspace-based methods in the presence of model errors. II. Multidimensional algorithms,” *IEEE Trans. Signal Process.*, vol. 41, pp. 2882–2890, Sep. 1993.
- [51] A. Paulraj and T. Kailath, “Direction of arrival estimation by eigenstructure methods with unknown sensor gain and phase,” in *Proc. IEEE ICASSP*, Apr. 1985, pp. 640–643.

- [52] A. Ferreol, P. Larzabal, and M. Viberg, “On the asymptotic performance analysis of subspace DOA estimation in the presence of modeling errors: case of MUSIC,” *IEEE Trans. Signal Process.*, vol. 54, pp. 907–920, Mar. 2006.
- [53] A. Liu, G. Liao, C. Zeng, Z. Yang, and Q. Xu, “An eigenstructure method for estimating DOA and sensor gain-phase errors,” *IEEE Trans. Signal Process.*, vol. 59, pp. 5944–5956, Dec. 2011.
- [54] Y. Bresler, “Maximum likelihood estimation of a linearly structured covariance with application to antenna array processing,,” in *Spectrum Estimation and Modeling, Fourth Annual ASSP Workshop on*, Minneapolis,MN, Aug. 1988, pp. 172–175.
- [55] P. Stoica and A. Nehorai, “Performance study of conditional and unconditional direction-of-arrival estimation,” *IEEE Trans. Acoust., Speech, Signal Process.*, vol. 38, pp. 1783–1795, Oct. 1990.
- [56] K. Han, P. Yang, and A. Nehorai, “Calibrating nested sensor arrays with model errors,,” in *Proc. 48th Asilomar Conf. Signals, Syst. Comput.*, Pacific Grove,CA, Nov. 2014.
- [57] A. Nehorai and E. Paldi, “Vector-sensor array processing for electromagnetic source localization,” *IEEE Trans. Signal Process.*, vol. 42, pp. 376–398, Feb. 1994.
- [58] K. T. Wong and M. D. Zoltowski, “Self-initiating music-based direction finding and polarization estimation in spatio-polarizational beamspace,” *IEEE Trans. Antennas Propag.*, vol. 48, pp. 1235–1245, Aug. 2000.
- [59] ——, “Diversely polarized root-music for azimuth-elevation angle-of-arrival estimation,” in *Proc. IEEE Antennas and Propagation Society International Symposium*, Baltimore, Md, July 1996, pp. 1352–1355.
- [60] J. Li, “Direction and polarization estimation using arrays with small loops and short dipoles,” *IEEE Trans. Antennas Propag.*, vol. 41, pp. 379–387, Mar. 1993.
- [61] K.-C. Ho, K.-C. Tan, and A. Nehorai, “Estimating directions of arrivals of completely and incompletely polarized signals with electromagnetic vector sensors,” *IEEE Trans. Signal Process.*, vol. 47, pp. 2845–2852, Oct. 1999.
- [62] K.-C. Ho, K.-C. Tan, and B. T. G. Tan, “Estimation of directions-of-arrival of partially polarized signals with electromagnetic vector sensors,” in *Proc. ICASSP*, May 1996, pp. 2900–2903.
- [63] K.-C. Ho, K.-C. Tan, and W. Ser, “An investigation on number of signals whose directions-of-arrival are uniquely determinable with an electromagnetic vector sensor,” *Signal Processing*, vol. 47, pp. 41–54, Nov. 1995.

- [64] B. Hochwald and A. Nehorai, “Identifiability in array processing models with vector-sensor applications,” *IEEE Trans. Signal Process.*, vol. 44, pp. 83–95, jan. 1996.
- [65] A. Nehorai and E. Paldi, “Acoustic vector-sensor array processing,” *IEEE Trans. Signal Process.*, vol. 42, pp. 2481–2491, Sep. 1994.
- [66] M. Hawkes and A. Nehorai, “Acoustic vector-sensor beamforming and Capon direction estimation,” *IEEE Trans. Signal Process.*, vol. 46, pp. 2291–2304, Sep. 1998.
- [67] K. T. Wong and M. D. Zoltowski, “Self-initiating beamspace MUSIC for underwater acoustic direction-finding with irregularly spaced vectorhydrophones,” in *Proc. IEEE Int. Symp. Circ. Syst.* Hong Kong, June. 1997, pp. 2553–2556.
- [68] ——, “Closed-form underwater acoustic direction-finding with arbitrarily spaced vector hydrophones at unknown locations,” *IEEE J. Ocean. Eng.*, vol. 22, pp. 566–575, Jul. 1997.
- [69] M. Hawkes and A. Nehorai, “Acoustic vector-sensor processing in the presence of a reflecting boundary,” *IEEE Trans. Signal Process.*, vol. 48, pp. 2981–2993, Nov. 2000.
- [70] ——, “Wideband source localization using a distributed acoustic vector-sensor array,” *IEEE Trans. Signal Process.*, vol. 51, pp. 1479–1491, Jun. 2003.
- [71] S. Miron, N. L. Bihan, and J. Mars, “Vector-sensor MUSIC for polarized seismic sources localization,” *EURASIP Journal on Applied Signal Processing*, pp. 74–84, Jan. 2005.
- [72] T. Kolda and B. Bader, “Tensor decompositions and applications,” *SIAM Review*, vol. 51, pp. 455–500, 2009.
- [73] L. De Lathauwer, “Signal processing based on multilinear algebra,” Ph.D. thesis, Katholieke Universiteit Leuven, Leuven, Belgium, 1997.
- [74] N. Sidiropoulos, R. Bro, and G. Giannakis, “Parallel factor analysis in sensor array processing,” *IEEE Trans. Signal Process.*, vol. 48, pp. 2377–2388, Aug. 2000.
- [75] D. Muti and S. Bourennane, “Multidimensional filtering based on a tensor approach,” *Signal Processing*, vol. 85, pp. 2338–2353, Dec. 2005.
- [76] L. D. Lathauwer and J. Castaing, “Fourth-order cumulant based blind identification of underdetermined mixtures,” *IEEE Trans. Signal Process.*, vol. 55, pp. 2965–2973, May. 2007.
- [77] L. D. Lathauwer and A. D. Baynast, “Blind deconvolution of DS-CDMA signals by means of decomposition in rank-(1,L,L) terms,” *IEEE Trans. Signal Process.*, vol. 56, pp. 1562–1571, April. 2008.

- [78] S. Miron, X. Guo, and D. Brie, “DOA estimation for polarized sources on a vector-sensor array by PARAFAC decomposition of the fourth-order covariance tensor,” in *EUSIPCO 2008*, Lausanne, Switzerland, Aug. 2008.
- [79] M. Boizard, G. Ginolhac, F. Pascal, S. Miron, and P. Forster, “Numerical performance of a tensor MUSIC algorithm based on HOSVD for a mixture of polarized sources,” in *EUSIPCO 2013*, Marrakech, Morocco, Sep. 2013.
- [80] J. D. Carroll and J. J. Chang, “Analysis of individual differences in multidimensional scaling via an N-way generalization of ”Eckart-Young” decomposition,” *Psychometrika*, vol. 35, pp. 283–319, 1970.
- [81] R. A. Harshman, “Foundation of the parafac procedure: Model and conditions for an explanatory multi-mode factor analysis,” *UCLA Working Papers in Phonetics*, vol. 16, pp. 1–84, Dec. 1970.
- [82] L. De Lathauwer, B. De Moor, and J. Vandewalle, “A multilinear singular value decomposition,” *SIAM J. Matrix Anal. Appl.*, vol. 24, pp. 1253–1278, 2000.
- [83] M. Haardt, F. Roemer, and G. Del Galdo, “Higher-order SVD-based subspace estimation to improve the parameter estimation accuracy in multidimensional harmonic retrieval problems,” *IEEE Trans. Signal Process.*, vol. 56, pp. 3198–3213, Jul. 2008.
- [84] X. Gong, Y. Xu, and Z. Liu, “On the equivalence of tensor-MUSIC and matrix-MUSIC,” in *Antennas, Propagation & EM Theory, 2006. ISAPE ’06. 7th International Symposium on*, Guilin, China, Oct. 2006.
- [85] R. T. Hoctor and S. A. kassam, “The unifying role of the coarray in aperture synthesis for coherent and incoherent imaging,” *Proc. IEEE*, vol. 78, pp. 735–752, Apr. 1990.
- [86] K. Han and A. Nehorai, “Nested vector-sensor array processing via tensor modeling,” *IEEE Trans. Signal Process.*, vol. 62, pp. 2542–2553, May 2014.
- [87] M. Quenouille, “Approximation tests of correlation in time series,” *J. R. Statist. Soc. B*, vol. 11, pp. 18–84, 1949.
- [88] J. Tukey, “Bias and confidence in not quite large samples,” *Ann. Math. Statist.*, vol. 29, p. 614, 1958.
- [89] J. Shao and D. S. Tu, *The Jackknifing and Bootstrap*. New York: Springer, 1995.
- [90] D. D. Ariananda and G. Leus, “Direction of arrival estimation for more correlated sources than active sensors,” *Elsevier Signal Processing*, vol. 93, pp. 3435–3448, Dec. 2013.

- [91] M. Hawkes and A. Nehorai, “Acoustic vector-sensor beamforming and capon direction estimation,” *IEEE Trans. Signal Process.*, vol. 46, pp. 2291–2303, Sep. 1998.
- [92] A. M. Haimovich, R. S. Blum, and L. J. Cimini, “Mimo radar with widely separated antennas,” *IEEE Signal Process. Mag.*, vol. 25, pp. 116–129, Jan. 2008.
- [93] P. Mariano, A. Pereira, L. Correia, R. Ribeiro, V. Abramov, N. Szirbik, J. Goosse-naerts, T. Marwala, and P. D. Wilde, “Simulation of a trading multi-agent system,” in *Intl. Conf. on Systems, Man, and Cybernetics*, Tucson, AZ, Oct. 2001, pp. 3378–3384.
- [94] S. Pillai, F. Haber, and Y. Bar-Ness, “A new approach to array geometry for improved spatial spectrum estimation,” in *Proc. ICASSP*, Oct 1985, pp. 1522–1524.
- [95] Y. I. Abramovich, D. A. Gray, A. Y. Gorokhov, and N. K. Spencer, “Positive-definite Toeplitz completion in DOA estimation for nonuniform linear antenna arrays. I. fully angularly arrays,” *IEEE Trans. Signal Process.*, vol. 46, pp. 2458–2471, Sep. 1998.
- [96] Q.-K. Ma, T.-H. Hsieh, and C.-Y. Chi, “DOA estimation of quasistationary signals via Khatri-Rao subspace,” in *Proc. ICASSP*, Apr. 2009, pp. 2165–2168.
- [97] K.-C. Tan, K.-C. Ho, and A. Nehorai, “Uniqueness study of measurements obtainable with arrays of electromagnetic vector sensors,” *IEEE Trans. Signal Process.*, vol. 44, pp. 1036–1039, Apr. 1996.
- [98] B. Hochwald and A. Nehorai, “Polarimetric modeling and parameter estimation with application to remote sensing,” *IEEE Trans. Signal Process.*, vol. 43, pp. 1923–1935, Aug. 1995.
- [99] T. Kah-Chye, H. Kwok-Chiang, and A. Nehorai, “Linear independence of steering vectors of an electromagnetic vector sensor,” *IEEE Trans. Signal Process.*, vol. 44, pp. 3099–3107, Dec. 1996.
- [100] K. T. Wong and M. D. Zoltowski, “High accuracy 2D angle estimation with extended aperture vector sensor arrays,” in *Proc. ICASSP*, May 1996, pp. 2789–2792.

Appendix A

Derivation of (5.40)

With the assumption of one source, we have

$$\mathbf{a}(\omega) = \{e^{jd_i\omega} | i = 1, \dots, N\}. \quad (\text{A.1})$$

Thus, we have

$$\bar{\mathbf{a}}(\omega) = \Psi \Phi \mathbf{a}(\omega). \quad (\text{A.2})$$

According to the definition of \mathbf{d}_k in (5.39), we can get

$$\mathbf{d} = j\Psi \Phi \mathbf{B} \mathbf{a}. \quad (\text{A.3})$$

Since all Ψ , Φ and \mathbf{B} are diagonal, we can obtain

$$\mathbf{d} = j\mathbf{B}\Psi\Phi\mathbf{a} = j\mathbf{B}\bar{\mathbf{a}}. \quad (\text{A.4})$$

Thus,

$$\mathbf{H} = \mathbf{d}^H [\mathbf{I} - \bar{\mathbf{a}}(\bar{\mathbf{a}}^H \bar{\mathbf{a}})^{-1} \bar{\mathbf{a}}^H] \mathbf{d} \quad (\text{A.5})$$

$$= \bar{\mathbf{a}}^H \mathbf{B}^H [\mathbf{I} - \bar{\mathbf{a}}(\bar{\mathbf{a}}^H \bar{\mathbf{a}})^{-1} \bar{\mathbf{a}}^H] \mathbf{B} \bar{\mathbf{a}} \quad (\text{A.6})$$

$$= \bar{\mathbf{a}}^H \mathbf{B}^H \mathbf{B} \bar{\mathbf{a}} - (\bar{\mathbf{a}}^H \bar{\mathbf{a}})^{-1} \bar{\mathbf{a}}^H \mathbf{B}^H \bar{\mathbf{a}} \bar{\mathbf{a}}^H \mathbf{B} \bar{\mathbf{a}}. \quad (\text{A.7})$$

On the other hand, model (5.4) can be written as

$$\mathbf{R}_y = \sigma_s^2 \bar{\mathbf{a}} \bar{\mathbf{a}}^H + \sigma_e^2 \mathbf{I}. \quad (\text{A.8})$$

According to the matrix inversion Lemma, we have

$$\mathbf{R}_y^{-1} = \frac{1}{\sigma_e^2} \mathbf{I} - \frac{\sigma_s^2 \bar{\mathbf{a}} \bar{\mathbf{a}}^H}{(\sigma_e^2 + \bar{\mathbf{a}}^H \bar{\mathbf{a}} \sigma_s^2) \sigma_e^2}. \quad (\text{A.9})$$

Hence, the right part of \bullet in (5.35) can be computed as

$$\sigma_s^4 \bar{\mathbf{a}}^H \mathbf{R}_y^{-1} \bar{\mathbf{a}} \quad (\text{A.10})$$

$$= \frac{\sigma_s^4 \bar{\mathbf{a}}^H \bar{\mathbf{a}}}{\sigma_e^2} - \frac{\sigma_s^6 \bar{\mathbf{a}}^H \bar{\mathbf{a}} \bar{\mathbf{a}}^H \bar{\mathbf{a}}}{(\sigma_e^2 + \bar{\mathbf{a}}^H \bar{\mathbf{a}} \sigma_s^2) \sigma_e^2} \quad (\text{A.11})$$

$$= \frac{\sigma_s^4 \bar{\mathbf{a}}^H \bar{\mathbf{a}}}{\sigma_e^2 + \bar{\mathbf{a}}^H \bar{\mathbf{a}} \sigma_s^2}, \quad (\text{A.12})$$

which is a scalar. Further we can compute

$$\text{CRB}(\omega) = \frac{\sigma_e^2 (\sigma_e^2 + \bar{\mathbf{a}}^H \bar{\mathbf{a}} \sigma_s^2)}{2T \sigma_s^4 [\bar{\mathbf{a}}^H \bar{\mathbf{a}} \bar{\mathbf{a}}^H \mathbf{B}^H \mathbf{B} \bar{\mathbf{a}} - (\bar{\mathbf{a}}^H \mathbf{B}^H \bar{\mathbf{a}})^2]}. \quad (\text{A.13})$$

Appendix B

Derivation of (6.15)

We define two new tensors \mathcal{W} and \mathcal{U} as

$$\mathcal{W} = \text{E}[(\mathcal{A} \times_3 \mathbf{x}) \circ (\mathcal{A} \times_3 \mathbf{x})^*], \quad (\text{B.1})$$

and

$$\mathcal{U} = \mathcal{A} \times_3 \text{E}[\mathbf{x} \circ \mathbf{x}^*] \dot{\times}_3 \mathcal{A}^*. \quad (\text{B.2})$$

They are both $N \times N_c \times N \times N_c$ tensors. We consider each element of \mathcal{W} :

$$\begin{aligned} w_{i_1 i_2 i_3 i_4} &= \text{E}[(\mathcal{A} \times_3 \mathbf{x})_{i_1 i_2} (\mathcal{A} \times_3 \mathbf{x})_{i_3 i_4}^*] \\ &= \text{E}\left[\sum_{k_1=1}^K a_{i_1 i_2 k_1} x_{k_1} \left(\sum_{k_2=1}^K a_{i_3 i_4 k_2} x_{k_2} \right)^* \right] \\ &= \text{E}\left[\sum_{k=1}^K a_{i_1 i_2 k} x_k a_{i_3 i_4 k}^* x_k^* \right] \\ &= \sum_{k=1}^K a_{i_1 i_2 k} \text{E}[x_k x_k^*] a_{i_3 i_4 k}^*. \end{aligned} \quad (\text{B.3})$$

The second to the last step is due to the independence assumption between sources, and to the zero mean assumption. Similarly, we get the elements of \mathcal{U} :

$$\begin{aligned}
u_{i_1 i_2 i_3 i_4} &= \sum_{k_1=1}^K (\mathcal{A} \times_3 \text{E}[\mathbf{x} \circ \mathbf{x}^*])_{i_1 i_2 k_1} a_{i_3 i_4 k_1}^* \\
&= \sum_{k_1=1}^K \left(\sum_{k_2=1}^K a_{i_1 i_2 k_2} (\text{E}[\mathbf{x} \circ \mathbf{x}^*])_{k_1 k_2} \right) a_{i_3 i_4 k_1}^* \\
&= \sum_{k=1}^K a_{i_1 i_2 k} \sigma_k^2 a_{i_3 i_4 k}^*
\end{aligned} \tag{B.4}$$

Obviously, $w_{i_1 i_2 i_3 i_4} = u_{i_1 i_2 i_3 i_4}$, so $\mathcal{W} = \mathcal{U}$.

Appendix C

Derivation of Equation (6.16)

We use the following notations:

$$\mathcal{A} = \{a_{i_1, i_2, k}, 1 \leq i_1 \leq I_1, 1 \leq i_2 \leq I_2, 1 \leq k \leq K\},$$

$$\mathcal{A}_{(3)}^H = \{\bar{a}_{l, k}^*, 1 \leq l \leq I_1 I_2, 1 \leq k \leq K\},$$

$$\begin{aligned} \mathcal{R}' &= \mathcal{A} \times_3 \text{E}[\mathbf{x} \circ \mathbf{x}^*] \times_3 \mathcal{A}^* \\ &= \{r'_{i_1, i_2, i_3, i_4}, 1 \leq i_1 \leq I_1, 1 \leq i_2 \leq I_2, \\ &\quad 1 \leq i_3 \leq I_3, 1 \leq i_4 \leq I_4\}, \end{aligned}$$

$$\begin{aligned} \mathcal{E} &= \{e_{i_1, i_2, i_3, i_4}, 1 \leq i_1 \leq I_1, 1 \leq i_2 \leq I_2, \\ &\quad 1 \leq i_3 \leq I_3, 1 \leq i_4 \leq I_4\}, \end{aligned}$$

$$\mathbf{Q} = \mathcal{R}_{(2)}^T = \{q_{j, i_2}, 1 \leq j \leq I_1^2 I_2, 1 \leq i_2 \leq I_2\},$$

where $I_1 = I_3 = N, I_2 = I_4 = N_c$.

We derive (6.16) through two steps. First we show that the mode-2 matricization of $\mathcal{A} \times_3 \text{E}[\mathbf{x} \circ \mathbf{x}^*] \times_3 \mathcal{A}^*$, denoted as $\bar{\mathbf{R}}^T$, is equal to $(\mathcal{A}_{(3)}^H \odot \mathcal{A}) \times_3 \mathbf{s}$, denoted as $\bar{\mathbf{Q}}^T$:

$$\bar{\mathbf{R}} = \{\bar{r}_{j, i_2}, 1 \leq j \leq I_1^2 I_2, 1 \leq i_2 \leq I_2\}, \text{ and}$$

$$\bar{\mathbf{Q}} = \{\bar{q}_{j, i_2}, 1 \leq j \leq I_1^2 I_2, 1 \leq i_2 \leq I_2\}.$$

Considering any element r'_{i_1, i_2, i_3, i_4} in tensor \mathcal{R}' , there is a corresponding element in $\bar{\mathbf{R}}$ such that

$$\begin{aligned}\bar{r}_{(i_1+(i_3-1)I_1+(i_4-1)I_1I_3),i_2} &= r'_{i_1, i_2, i_3, i_4} \\ &= \sum_{k=1}^K a_{i_1 i_2 k} \sigma_k^2 a_{i_3 i_4 k}^*. \end{aligned}\quad (\text{C.1})$$

The second step is shown in Appendix B. Now, we consider the corresponding element in $\bar{\mathbf{Q}}$:

$$\begin{aligned}&\bar{q}_{(i_1+(i_3-1)I_1+(i_4-1)I_1I_3),i_2} \\ &= \sum_{k=1}^K (\mathcal{A}_{(3)}^H \odot \mathcal{A})_{(i_1+(i_3-1)I_1+(i_4-1)I_1I_3),i_2,k} \sigma_k^2 \\ &= \sum_{k=1}^K (\mathcal{A}_{(3)}^H \odot \mathcal{A})_{(i_1+[i_3+(i_4-1)I_3-1]I_1),i_2,k} \sigma_k^2 \\ &= \sum_{k=1}^K \bar{a}_{(i_3+(i_4-1)I_3),k}^* a_{i_1, i_2, k} \sigma_k^2 \\ &= \sum_{k=1}^K a_{i_3, i_4, k}^* a_{i_1, i_2, k} \sigma_k^2 \end{aligned}\quad (\text{C.2})$$

The last two steps are due to the definitions of extended Khatri-Rao product and matricization. From (C.1) and (C.2), it is obvious that

$$\bar{r}_{(i_1+(i_3-1)I_1+(i_4-1)I_1I_3),i_2} = \bar{q}_{(i_1+(i_3-1)I_1+(i_4-1)I_1I_3),i_2}. \quad (\text{C.3})$$

So now we have $\bar{\mathbf{R}} = \bar{\mathbf{Q}}$.

Next, we show that the mode-2 matricization of $E[\mathbf{E} \circ \mathbf{E}^*]$, denoted as $\bar{\mathbf{E}}^T$, is equal to $\sigma_e^2 \vec{\mathbf{I}}$, denoted as \mathbf{G} :

$$\bar{\mathbf{E}} = \{\bar{e}_{j,i_2}, 1 \leq j \leq I_1^2 I_2, 1 \leq i_2 \leq I_2\}, \text{ and}$$

$$\mathbf{G} = \{g_{j,i_2}, 1 \leq j \leq I_1^2 I_2, 1 \leq i_2 \leq I_2\}.$$

Based on the white Gaussian noise assumption, we have

$$e_{i_1 i_2 i_3 i_4} = \begin{cases} \sigma_e^2, & \text{if } i_1 = i_3, i_2 = i_4, \\ 0, & \text{otherwise.} \end{cases} \quad (\text{C.4})$$

Since

$$\bar{e}_{(i_1 + (i_3 - 1)I_1 + (i_4 - 1)I_1 I_3), i_2} = e_{i_1, i_2, i_3, i_4}, \quad (\text{C.5})$$

we have

$$\bar{e}_{(i_1 + (i_3 - 1)I_1 + (i_4 - 1)I_1 I_3), i_2} = \begin{cases} \sigma_e^2, & \text{if } i_1 = i_3, i_2 = i_4, \\ 0, & \text{otherwise.} \end{cases} \quad (\text{C.6})$$

According to the definition of $\vec{\mathbf{I}}$, we can see that

$$g_{(i_1 + (i_3 - 1)I_1 + (i_4 - 1)I_1 I_3), i_2} = \begin{cases} \sigma_e^2, & \text{if } i_1 = i_3, i_2 = i_4, \\ 0, & \text{otherwise.} \end{cases} \quad (\text{C.7})$$

Therefore, we have $\bar{\mathbf{E}} = \mathbf{G}$.

Based on the above analysis, we can conclude that

$$\begin{aligned} \mathbf{Q} &= \mathbf{R}_{(2)}^T \\ &= (\mathcal{A}_{(3)}^H \odot \mathcal{A}) \times_3 \mathbf{s} + \sigma_e^2 \vec{\mathbf{I}}. \end{aligned} \quad (\text{C.8})$$

Appendix D

Internal analysis of $\mathcal{A}_{(3)}^H \odot \mathcal{A}$

The mode-3 unfolding of tensor \mathcal{A}^* , $\mathcal{A}_{(3)}^*$ can be written as

$$\mathcal{A}_{(3)}^* = [\tilde{\mathbf{A}}_1^H, \tilde{\mathbf{A}}_2^H, \dots, \tilde{\mathbf{A}}_{N_c}^H], \quad (\text{D.1})$$

where

$$\tilde{\mathbf{A}}_i^* = \begin{pmatrix} p_{1i}^* e^{-jd_1\pi\sin\theta_1} & \dots & p_{Ki}^* e^{-jd_1\pi\sin\theta_K} \\ p_{1i}^* e^{-jd_2\pi\sin\theta_1} & \dots & p_{Ki}^* e^{-jd_2\pi\sin\theta_K} \\ \vdots & \ddots & \vdots \\ p_{1i}^* e^{-jd_N\pi\sin\theta_1} & \dots & p_{Ki}^* e^{-jd_N\pi\sin\theta_K} \end{pmatrix}, \quad (\text{D.2})$$

with

$$\begin{aligned} \mathbf{d} &= [d_1, d_2, \dots, d_N]^T \\ &= [1, 2, \dots, N_1, N_1 + 1, \dots, N_2(N_1 + 1)]^T. \end{aligned} \quad (\text{D.3})$$

Then we can write

$$\mathcal{A}_{(3)}^H \odot \mathcal{A} = \begin{pmatrix} \tilde{\mathbf{A}}_1^* \odot \mathcal{A} \\ \tilde{\mathbf{A}}_2^* \odot \mathcal{A} \\ \dots \\ \tilde{\mathbf{A}}_{N_c}^* \odot \mathcal{A} \end{pmatrix}, \quad (\text{D.4})$$

where we have N_c sets of horizontal slices, each corresponding to one component. Let the i th set be

$$\mathcal{B}^i = \tilde{\mathbf{A}}_i^* \odot \mathcal{A}, \quad (\text{D.5})$$

with element

$$\{b_{l,m,k}^i, 1 \leq i \leq N_c, 1 \leq l \leq N^2, 1 \leq m \leq N_c, 1 \leq k \leq K\}.$$

We can see that there are N^2 slices in \mathbf{B}^i . Following the definition of the extended Khatri-Rao product, we have

$$b_{l,m,k}^i = p_{k,i}^* p_{k,m} e^{j\tilde{d}_l \pi \sin \theta_k}, \quad (\text{D.6})$$

with

$$\begin{aligned} \tilde{\mathbf{d}} &= \mathbf{d} \ominus \mathbf{d} \\ &= [\tilde{d}_1, \tilde{d}_2, \dots, \tilde{d}_{N^2}]^T, \end{aligned} \quad (\text{D.7})$$

where we define the Khatri-Rao minus \ominus as $\tilde{d}_{(i-1)N+j} = d_i - d_j$. Now, we have provided the closed form of each element of $\mathcal{A}_{(3)}^H \odot \mathcal{A}$, and can easily see that there are N_c parallel sets of horizontal slices in $\mathcal{A}_{(3)}^H \odot \mathcal{A}$. Over the N_c sets, the exponential terms of the corresponding elements are the same.

Appendix E

Generating $\bar{\mathcal{A}}$

Following the analysis in Appendix D, we can see that there are N_C parallel sets of horizontal slices in (D.4). We consider the $N^2 \times N_c \times K$ dimensional i th set \mathcal{B}^i , as defined in (D.5).

Looking at the element $b_{l,m,k}^i$ in (D.6), we can see that the first dimensional index l affects only \tilde{d}_l in the exponential term. Since there are many repeated values in the virtual sensor position vector $\tilde{\mathbf{d}}$ in (D.7), we get the corresponding repeated horizontal slices in \mathcal{B}^i .

By removing the repeated horizontal slices and sorting the remaining ones so that the i th slice corresponds to the virtual sensor position $(-\bar{N} + i)d_I$ in the difference co-array of the 2-level nested array, we can construct a new $(2\bar{N} - 1) \times N_c \times K$ tensor $\bar{\mathcal{A}}$.

To make it clearer, we consider the case by fixing the second and third indexes in \mathcal{B}^i :

$$\mathbf{b}_{m,k}^i = [p_{k,i}^* p_{k,m} e^{j\tilde{d}_1 \pi \sin \theta_k}, \dots, p_{k,i}^* p_{k,m} e^{j\tilde{d}_{N^2} \pi \sin \theta_k}]^T. \quad (\text{E.1})$$

After we remove the repeated elements and sort them according to the above strategy, we will have

$$\bar{\mathbf{b}}_{m,k}^i \triangleq [p_{k,i}^* p_{k,m} e^{j\bar{d}_1 \pi \sin \theta_k}, \dots, p_{k,i}^* p_{k,m} e^{j\bar{d}_{2\bar{N}-1} \pi \sin \theta_k}]^T. \quad (\text{E.2})$$

with

$$\begin{aligned} \bar{d} &\triangleq [\bar{d}_1, \bar{d}_2, \dots, \bar{d}_{2\bar{N}-1}] \\ &= [-\bar{N} + 1, \dots, -1, 0, 1, \dots, \bar{N} - 1]. \end{aligned} \quad (\text{E.3})$$

Based on (E.2), we can easily obtain $\bar{\mathcal{A}}$ by extending the m and k indexes.

Appendix F

Derivation of Equation (6.20)

We consider the i th set \mathcal{B}^i in (D.5). Following (E.2) we can write any element $a_{i,m,k}^{(1)}$ of the first subarray tensor $\bar{\mathcal{A}}_1$ as

$$a_{i,m,k}^{(1)} = p_{k,i}^* p_{k,m} e^{j\bar{d}_{(i-1+\bar{N})}\pi \sin \theta_k}, \quad (\text{F.1})$$

where $i = 1, \dots, \bar{N}$, $m = 1, \dots, N_c$, and $k = 1, \dots, K$. Similarly, for the l th subarray tensor $\bar{\mathcal{A}}_l$, its element can be written as

$$a_{i,m,k}^{(l)} = p_{k,i}^* p_{k,m} e^{j\bar{d}_{(i-1-(l-1)+\bar{N})}\pi \sin \theta_k}. \quad (\text{F.2})$$

According to (E.3), we can easily get that

$$a_{j,m,k}^{(l)} = a_{j,m,k}^{(1)} e^{-j(l-1)\pi \sin \theta_k}. \quad (\text{F.3})$$

Thus, in the tensor form, we can get

$$\bar{\mathcal{A}}_l = \bar{\mathcal{A}}_1 \times_3 \Phi^{l-1}, \quad (\text{F.4})$$

where

$$\Phi = \begin{pmatrix} e^{-j\pi \sin \theta_1} & & & \\ & e^{-j\pi \sin \theta_2} & & \\ & & \ddots & \\ & & & e^{-j\pi \sin \theta_K} \end{pmatrix}. \quad (\text{F.5})$$

Appendix G

Proof of Theorem 7.1

Proof. Recall our basic assumption that the jackknifing subset contains almost the same information as the original whole data set. Therefore the detection accuracy based on a jackknifing subset is assumed to be p , satisfying $p \geq 0.5$.

Suppose we conduct Z iterations, and the detected source number is \hat{K} . Then the probability of correct detection for any independent iteration is

$$p(\hat{K} = K) = p.$$

The false detection probability is denoted as

$$q = p(\hat{K} \neq K) = 1 - p.$$

Let Z_K denote the occurrence times of the number K , and $\bar{Z}_K = Z - Z_K$ denote the occurrence times of other numbers except K . We consider the proof through two cases: $Z = 2n$ or $Z = 2n + 1$; namely, the iteration number is even or odd.

Case 1 : $Z = 2n$

According to the jackknifing algorithm in Table 7.1, we can obtain the detection accuracy after applying jackknifing:

$$\begin{aligned} p_j &= p(Z_K \geq \bar{Z}_K) \\ &= \binom{2n}{n} p^n q^n + \binom{2n}{n+1} p^{n+1} q^{n-1} + \dots \\ &\quad + \binom{2n}{2n-1} p^{2n-1} q + \binom{2n}{2n} p^{2n} q^0. \end{aligned} \quad (\text{G.1})$$

Considering

$$\binom{n}{m} = \binom{n-1}{m} + \binom{n-1}{m-1}, \quad (\text{G.2})$$

we get

$$\begin{aligned} p_j &= p \cdot \left\{ \binom{2n-1}{n} p^{n-1} q^n + \binom{2n-1}{n-1} p^{n-1} q^n + \right. \\ &\quad \binom{2n-1}{n+1} p^n q^{n-1} + \binom{2n-1}{n} p^n q^{n-1} + \dots + \\ &\quad + \binom{2n-1}{2n-1} p^{2n-2} q + \binom{2n-1}{2n-2} p^{2n-2} q + \\ &\quad \left. + \binom{2n-1}{2n-1} p^{2n-1} q^0 \right\}. \end{aligned}$$

Applying

$$\binom{n}{m} = \binom{n}{n-m},$$

we get

$$\begin{aligned} p_j &= p \cdot \left\{ \binom{2n-1}{n} p^{n-1} q^n + \binom{2n-1}{n-1} p^{n-1} q^n + \right. \\ &\quad \binom{2n-1}{n-2} p^n q^{n-1} + \binom{2n-1}{n} p^n q^{n-1} + \dots + \\ &\quad + \binom{2n-1}{0} p^{2n-2} q + \binom{2n-1}{2n-2} p^{2n-2} q + \\ &\quad \left. + \binom{2n-1}{2n-1} p^{2n-1} q^0 \right\}. \end{aligned}$$

Since $p \geq 0.5$, namely $p \geq q$, we have

$$\begin{aligned}
p_j &\geq p \cdot \left\{ \binom{2n-1}{n} p^{n-1} q^n + \binom{2n-1}{n-1} p^{n-1} q^n + \right. \\
&\quad \binom{2n-1}{n-2} p^{n-2} q^{n+1} + \binom{2n-1}{n} p^n q^{n-1} + \cdots + \\
&\quad + \binom{2n-1}{0} p^0 q^{2n-1} + \binom{2n-1}{2n-2} p^{2n-2} q + \\
&\quad \left. + \binom{2n-1}{2n-1} p^{2n-1} q^0 \right\} \\
&= p \cdot \left\{ \binom{2n-1}{n} p^{n-1} q^n + (p+q)^{2n-1} \right\} \\
&= p \cdot \left\{ \binom{2n-1}{n} p^{n-1} q^n + 1 \right\} \\
&> p.
\end{aligned} \tag{G.3}$$

Case 2 : $Z = 2n + 1$

Similarly, we can calculate the detection accuracy after applying jackknifing as

$$\begin{aligned}
p_j &= p(Z_K \geq \bar{Z}_K) \\
&= \binom{2n+1}{n+1} p^{n+1} q^n + \binom{2n+1}{n+2} p^{n+2} q^{n-1} + \dots \\
&\quad + \binom{2n+1}{2n} p^{2n} q + \binom{2n+1}{2n+1} p^{2n+1} q^0 \\
&= p \cdot \left\{ \binom{2n}{n+1} p^n q^n + \binom{2n}{n} p^n q^n + \right. \\
&\quad \left(\binom{2n}{n+2} p^{n+1} q^{n-1} + \binom{2n}{n+1} p^{n+1} q^{n-1} + \dots + \right. \\
&\quad \left. + \binom{2n}{2n} p^{2n-1} q + \binom{2n}{2n-1} p^{2n-1} q + \binom{2n}{2n} p^{2n} q^0 \right\} \\
&\geq p \cdot \left\{ \binom{2n}{n-1} p^{n-1} q^{n+1} + \binom{2n}{n} p^n q^n + \right. \\
&\quad \left(\binom{2n}{n-2} p^{n-2} q^{n+2} + \binom{2n}{n+1} p^{n+1} q^{n-1} + \dots + \right. \\
&\quad \left. + \binom{2n}{0} p^0 q^{2n} + \binom{2n}{2n-1} p^{2n-1} q + \binom{2n}{2n} p^{2n} q^0 \right\} \\
&= p \cdot (p+q)^{2n} \\
&= p.
\end{aligned} \tag{G.4}$$

The above two cases together prove the theorem: for any number of iterations n , after applied jackknifing, the source detection accuracy $p_j \geq p$. \square

Vita

Keyong Han

| | |
|------------------------|--|
| Degrees | Ph.D., Electrical Engineering, Washington University in St. Louis, Missouri, USA, May 2015 M.S., Electrical Engineering, Washington University in St. Louis, Missouri, USA, May 2012 B.S., Electrical Engineering, University of Science and Technology of China, Anhui, China, June 2010 |
| Professional Societies | The Institute of Electrical and Electronics Engineers (IEEE) IEEE Signal Processing Society |
| Publications | <u>Journal Publications:</u> K. Han and A. Nehorai, “Jointly optimal design for MIMO radar frequency-hopping waveforms using game theory”, in revision for <i>IEEE Trans. on Aerospace and Electronic Systems</i> . K. Han , P. Yang, and A. Nehorai, “Calibrating nested sensor arrays with model errors,” in revision for <i>IEEE Trans. on Antennas Propagat.</i> K. Han and A. Nehorai, “Nested array processing for distributed sources,” <i>IEEE Signal Processing Letters</i> , Vol 21, No. 1, pp. 1111-1114, Sep. 2014. K. Han and A. Nehorai, “Nested vector-sensor array processing via tensor modeling,” <i>IEEE Trans. on Signal Processing</i> , Vol 62, pp. 2542-2553, May 2014. K. Han and A. Nehorai, “Improved source number detection and direction estimation with nested arrays and ULAs using jackknifing,” <i>IEEE Trans. on Signal Processing</i> , Vol 61, pp. 6118-6128, Dec. 2013. |

K. Han and A. Nehorai, “Wideband Gaussian source processing using a linear nested array,” *IEEE Signal Processing Letters*, Vol. 20, pp. 1110-1113, Nov. 2013.

Conference Publications:

K. Han, P. Yang, and A. Nehorai, “Calibrating nested sensor arrays with model errors,” in Proc. *48th Asilomar Conf. Signals, Syst. Comput.*, Pacific Grove, CA, Nov. 2014, 5 pages.

K. Han and A. Nehorai, “Direction of arrival estimation using nested vector-sensor arrays via tensor modeling,” in Proc. *8th IEEE Sensor Array and Multichannel Signal Processing (SAM) Workshop*, A Coruña, Spain, Jun. 22-25, 2014, pp. 429-432.

K. Han and A. Nehorai, “Distributed source processing with linear nested arrays,” in Proc. *8th IEEE Sensor Array and Multichannel Signal Processing (SAM) Workshop*, A Coruña, Spain, Jun. 22-25, 2014, pp. 521-524.

K. Han and A. Nehorai, “Source number detection with nested arrays and ULAs using jackknifing,” in Proc. *Fifth Intl. Workshop on Computational Advances in Multi-Sensor Adaptive Processing (CAMSAP)*, Saint Martin, 4 pages, Dec. 15-18, 2013, pp. 57-60.

K. Han and A. Nehorai, “Wideband direction of arrival estimation using nested arrays,” in Proc. *Fifth Intl. Workshop on Computational Advances in Multi-Sensor Adaptive Processing (CAMSAP)*, Saint Martin, Dec. 15-18, 2013, pp. 188-191.

K. Han and A. Nehorai, “Joint frequency-hopping waveform design for MIMO radar estimation using game theory,” in Proc. *2013 IEEE Radar Conference (RADAR)*, Ottawa, Canada, Apr. 2013, 4 pages.

May 2015